RESEARCH AND DEVELOPMENT ON RESISTIVE PLATE CHAMBER BASED MUON TOMOGRAPHY SYSTEM

A DISSERTATION

SUBMITTED IN PARTIAL FULFILLMENT OF THE REQUIREMENTS FOR THE AWARD OF THE DEGREE OF

MASTER OF TECHNOLOGY
IN
NUCLEAR SCIENCE AND ENGINEERING

SUBMITTED BY

CHANDAN BARAI

2K16/NSE/01

UNDER THE SUPERVISION OF

PROF. RINKU SHARMA

APPLIED PHYSICS DEPARTMENT, DTU

&

DR. SUBHASIS CHATTOPADHYAY

HEAD, EXPERIMENTAL HIGH ENERGY PHYSICS & APPLICATION GROUP
VECC, KOLKATA

DEPARTMENT OF APPLIED PHYSICS

DELHI TECHNOLOGICAL UNIVERSITY

(FORMERLY DELHI COLLEGE OF ENGINEERING)

BAWANA ROAD, DELHI- 110042

MAY, 2018

DELHI TECHNOLOGICAL UNIVERSITY

(Formerly Delhi College of Engineering)

Bawana Road, Delhi-110042

CANDIDATE'S DECLARATION

I, Chandan Barai, Roll No 2K16/NSE/01, student of M.Tech NUCLEAR SCIENCE AND ENGINEERING, hereby declare that the project dissertation titled "RESEARCH AND DEVELOPMENT ON RESISTIVE PLATE CHAMBER BASED MUON TOMOGRAPHY SYSTEM" which is submitted by me to the Department of Applied Physics, Delhi Technological University, Delhi in partial fulfillment of the requirement for the award of the degree of Master of Technology is original and not copied from any source without proper citation. The work has not previously formed the basis for the award of any Degree, Diploma Associateship, Fellowship or other similar title or recognition.

Chandan Barai

Place: Delhi

Date: 10.7.18 (CHANDAN BARAI)

DEPARTMENT OF APPLIED PHYSICS

DELHI TECHNOLOGICAL UNIVERSITY

(Formerly Delhi College of Engineering)

Bawana Road, Delhi-110042

CERTIFICATE

I hereby certify that the Project Dissertation titled "RESEARCH AND DEVELOPMENT ON RESISTIVE PLATE CHAMBER BASED MUON TOMOGRAPHY SYSTEM" which is submitted by CHANDAN BARAI, Roll No. 2K16/NSE/01 , Department of Applied Physics, Delhi Technological University, Delhi in partial fulfillment of the requirement for the award of the degree of Master in Technology , is a record of the project work carried out by the student under my supervision. To the best of my knowledge this work has not been submitted in part or full for any Degree or Diploma to this University or elsewhere.

Place : Delhi

Prof. RINKU SHARMA

(Department of Applied Physics, DTU)

Date:10.07.18

SUPERVISOR

GOVERNMENT OF INDIA
DEPARTMENT OF ATOMIC ENERGY
VARIABLE ENERGY CYCLOTRON CENTRE

सत्यमेव जयते

भारत सरकार
परमाणु ऊर्जा विभाग
परिवर्ती ऊर्जा साइक्लोट्रॉन केन्द्र

CERTIFICATE

This is to certify that the project report entitled as "Research and Development of Resistive Plate Chamber based Muon Tomography System" submitted for fulfillment of the requirements of 4th Semester of M.Tech in Nuclear Science & Engineering under Delhi Technological University, has been carried out by Mr. Chandan Barai (Roll No- 2K16/NSE/01), during 08.01.2018 to 22.06.2018, at Variable Energy Cyclotron Centre, Kolkata, under the guidance of Dr. Subhasis Chattopadhyay, Scientific Officer (H+), Head, Experimental High Energy Physics and Applications Group, Variable Energy Cyclotron Centre, Kolkata.

(Project guide)

डॉ. सुभाशीष चट्टोपाध्याय / Dr. Subhasis Chattopadhyay
वैज्ञानिक अधिकारी (एच+) / Scientific Officer (H+)
प्रमुख, प्रायोगिक उच्च ऊर्जा भौतिकी एवं अनुप्रयोग वर्ग
Head, Experimental High Energy Physics and Applications Group
वीईसीसी / पऊवि/ VECC / DAE
1/ए.एफ., बिधान नगर, कोलकाता
1/AF, Bidhan Nagar, Kolkata-700064
पश्चिम बंगाल, भारत / West Bengal, India

सेक्टर - I ब्लाक - ए एफ विधान नगर, कोलकाता-700 064 भारत
दूरभाष : (सीधा) २३३७१२३०, फैक्स : (९१) (०३३) २३३४६८७१
SECTOR - 1, BLOCK-AF, BIDHAN NAGAR, KOLKATA - 700 064, INDIA
Tel. : (Direct) 2337 1230 (4 Lines), Fax : +(91) (033) 2334-6871
Web : www.vecc.gov.in, e-mail : <user-id>@vecc.gov.in

ACKNOWLEDGEMENT

With immense pleasure, I am really thankful to my guide Dr. SUBHASISH CHATTOPADHYAY, head of the experimental high energy physics and application group at VECC for allowing me to work in VECC and for his constant motivation and guidance.

I want to express my heartiest thanks my supervisor Prof. RINKU SHARMA of applied physics department, DTU, .She was the one who motivated me to go for the work of my interest. Whenever I had a query I went to her and she was every time there for me. She is a kind of mentor who everyone wish to have.

I owe my deep sense of gratitude to Dr. ZUBAYER AHAMED of VECC for his valuable suggestions, and motivation during the whole period of my project work.

I am very much grateful to Dr. NITIN KUMAR PURI, coordinator of Nuclear Science and Engineering of applied physics department DTU, for his sumptuous guidance.

I want to thank the head of the department of applied physics of DTU, Dr. SURESH CH. SHARMA, for his valuable support and allowing me to go out and work at VECC.

I have no words to thank or to express my gratitude to Miss. MITALI MONDAL and Mr. TANAY DEY for their valuable time, support and hour long discussions which helped me clear my ideas on various topics. They have always encouraged me to take experiment and theory part hand in hand and to understand the things before implementing. Whenever needed they both were always there for supporting and encouraging me. I am very much indebted to them.

I am thankful to Mr. PARTHA BHASKAR for helping me by providing necessary electronic modules, whenever needed.

I am thankful to Mr. GANESH DAS of VECC who helped me out in the fabrication of the detectors.

CHANDAN BARAI

ABSTRACT

Cosmic ray muons are the particles which are continuously falling on earth's surface. It is observed that while travelling through materials having high atomic number , muons undergo the phenomenon called multiple Coulomb scattering. Using this property and detecting the unscattered and scattered muons their tracks can be reconstructed to get a image of the material through which muons have passed. It is possible by using particle detectors like Gas electron multiplier (GEM) ,drift tubes etc. In this dissertation , I have reported the process of fabrication of six resistive plate chambers (RPC) for this purpose. Six resistive plate chambers were fabricated using high resistive bakelite plates . These gaseous detectors were thoroughly tested to determine whether they are suitable or not for the purpose of muon tomography. The characterization reports, which have shown very successful results are given in details . It includes surface resistance measurement, I-V characterization, current stability test , efficiency measurement and calculation of noise rate in different voltages. A proper simulation study of the resistive plate chamber dynamics was also carried out by using the simulation toolkit GARFIELD++ , the study report is presented in chapter 3. The calculation of electrostatic field , generation of ionization in avalanche mode of RPC was done along with calculation of signal generation with the simulation toolkit. After completion of fabrication of the detectors, suitable front end electronics was selected by testing them with RPCs. Among conventional electronics , PADI-application specific integrated circuit (ASIC) and NINO-ASIC front end electronics. Among these, NINO-ASIC have shown the best result . Further testing was done using NINO-ASIC based front end electronics. A six bakelite resistive plate chamber based muon tomography prototype system was constructed and preliminary data was collected using cosmic ray muons . A MUCH-XYTER ASIC based data acquisition system was used for this purpose.

CONTENTS

LIST OF FIGURES

CHAPTER 1

INTRODUCTION

Muon tomography is a form of radio imaging where interaction of muons through matter is taken into account. The motivation for muon tomography is quite a lot. This type of imaging can help us to predict volcanic eruptions beforehand. In other fields like archeology cosmic ray imaging can determine the structural mapping of historical artifacts like pyramid. Muon tomography can be used in border security where shielded radioactive materials can be illegally transported. It is impossible for other type of scanning to scan through high Z materials like lead. But with the help of muon tomography it can be easily detected. The principle, construction of detectors, testing of detectors and data acquisition for muon tomography is described in details in the following chapters.

1.1Cosmic rays

It is required to briefly discuss about cosmic rays before reporting the details of the particle detector system and its characterization. This chapter will describe briefly the phenomenon related to cosmic ray, how it produce ionization in air, how it causes shower of particles to generate in the atmosphere in cascades and the production of muon in this process. Multiple coulomb scattering and the interaction of muon passing through matter will also be discussed in this chapter.

1.2 Origin of cosmic rays

A shower of extraterrestrial particles is falling on our earth all the time. These are mostly fragments of highly energized nucleus and particles which fall on the atmosphere. They are travelling with velocity nearly equal to speed of light & hitting our atmosphere from outer space. Their energies have a continuous distribution with a very broad range. These rays are known as cosmic rays. The origin is still unknown but it can be safely said that generation of these rays take place mostly outside the solar system, though some of them are found to be produced in the sun. As mentioned earlier he source of all the primary cosmic rays are unknown but a large portion of the ray are produced from supernova explosions from dying stars. Another portion comes from active galactic nuclei. Gamma ray bursts from collapsing stars also spread out highly energized particles in the space.

1.3 Discovery of cosmic ray

In the year of 1900, three scientists Elster , Gaitel and Wilson independently discovered that when pure gas is kept in a vessel the gas shows electrical conductivity. Even without having an apparent cause of ionization. To explain this phenomenon, Charles Tomson Wilson proposed that an invisible, highly penetrating ray coming from the outer space is responsible for it, however the idea was rejected by him letter. In 1909 Theodor Wulf, a germen physicist who was a Jesuit priest too developed an electrometer. Using the electrometer he measured the ionization variation of a gas in a closed container at the base and top of the Eifel tower. The result of the experiment showing variation in ionization and the conclusion by Wulf did not become popular in the scientific community at that time. The variation of ionization inside gas using electrometer was measured at a height of 5.3 kilometer using a balloon by Austrian turned American physicist named Victor Hess in the year 1912. Hess found that the variation in the altitude 5.3km showed three times more ionization in the gas than sea level. Conducting a similar experiment during total solar eclipse Hess then ruled out the general possibility of the source of this bizzare radiation to be coming from the sun only and concluded it to be extraterrestrial,
probably coming completely outside of the solar system. In 1914 Hess's experiment was repeated and the result was supported by a German physicist Werner Kolhorster enhancing the altitude to 9km. In the year 1936 Victor Hess won the Noble prize for the important discovery in physics, the cosmic ray.

1.4 **Classification of cosmic ray**

Cosmic ray can be divided in the following classification.

With respect to origin cosmic ray is divided into two categories

(i)Galactic Cosmic Rays (GCR)

Galactic cosmic rays originate in places beyond the solar system. The high energy particles and fragments of nucleus are generated due to astrophysical events like supernova explosions in different galaxies or because of active galactic nuclei.

(ii) Solar energetic particles

A portion of total cosmic ray flux is due to production of high energized protons in the sun due to different solar events.

Generally we consider the Galactic Cosmic Rays in calculations and experiments with cosmic rays.

With respect to impact on earth atmosphere the can be divided into two categories

(i)Primary cosmic rays

Primary cosmic rays are highly energized particles, antiparticles and nucleuses coming from outer space. They are composed of mainly protons (89%). Among other particles, 10% of them are alpha particles and only 1percent are heavier nucleus like from boron, carbon etc. to uranium. These primary cosmic rays fall on the earth's atmosphere and interacts, which is responsible for the production of a secondary stream of energized particles.

(ii)Secondary cosmic rays

When primary cosmic rays are fall on the earth's atmosphere they cause collisions with mainly N_2 and O_2 atoms and molecules. As a result they produce various other particles and those particles combined cause a new stream of cosmic ray which reach earth. This newly produced stream of particles are termed as secondary cosmic-rays. Secondary cosmic rays are made up of particles like neutron, neutrino, pion, kaon, muon etc.

1.5 Production of muons from primary cosmic rays

In 1936 Carl Anderson & Seth Neddermeyer discovered muon while they were busy in experimenting with cosmic rays. Electrons and neutrinos are lighter than muons but hadrons and other particles are heavier. Generally the largest section of the muons observed on Earth's surface are generated by the primary cosmic rays interacted at the upper Atmosphere. Cosmic ray protons re continuously bombarded on the atmosphere of the earth. With various interaction in the atmosphere these protons create many other particles. This is termed as "showers". In this process many hadronic particles like pions & kaons are

created. Highly energized cosmic ray nucleons interact mostly with the major component of the atmosphere which are nitrogen and oxygen to create these pions & kaons . Cosmic ray pions are charged particles with high energies. Sometimes their energy can be greater than 100GeV. These pions before decaying, interact with atmospheric nitrogen and oxygen and produces additional cascades of secondary particles. It is observed that relatively low energized particle, pions are more prone to undergo weak decay without interacting with the O2 and N2. They decay and produce muons . The decay schemes are as follows:

$$K^+ \rightarrow \mu^+ + \nu_\mu$$

$$\pi^+ \rightarrow \mu^+ + \nu_\mu$$

$$\pi^- \rightarrow \mu^- + \nu_\mu$$

$$K^- \rightarrow \mu^- + \nu_\mu$$

(1.1)

Muons are the highest number of energetic particles, which reaches the sea level, with a flux of about 1 muon per square centimeter per minute.

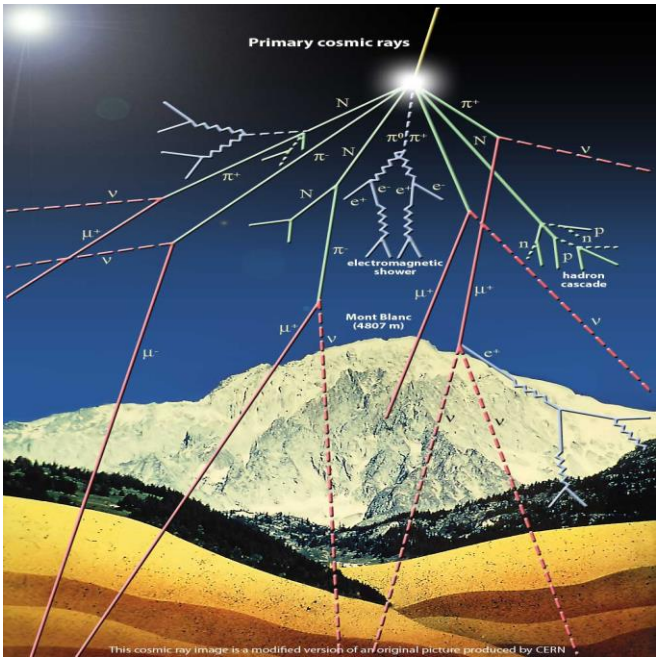

Figure 1.1 Primary cosmic ray producing secondary cosmic “showers” (Image courtesy: www.cern.ch)

The average energy of muons reaching the ground is approximately 4 GeV. As muons are charged particles, they interact with matter by ionization. The loss of energy while travelling inside the atmosphere is proportional to the amount of mass the particle is penetrating. It is found that the amount of energy decrease of muons is approximately 2 MeV per gram/ cm2. It can be inferred that the 4GeV muons which reach earth originally had 6 GeV energy. Muons are unstable with a mean life of of 2.2 μs. Detecting the muons at ground is an example of relativistic time dilatation. With muons having 4 GeV energy , the relativistic time dilatation factor is calculated to be around 38.8.

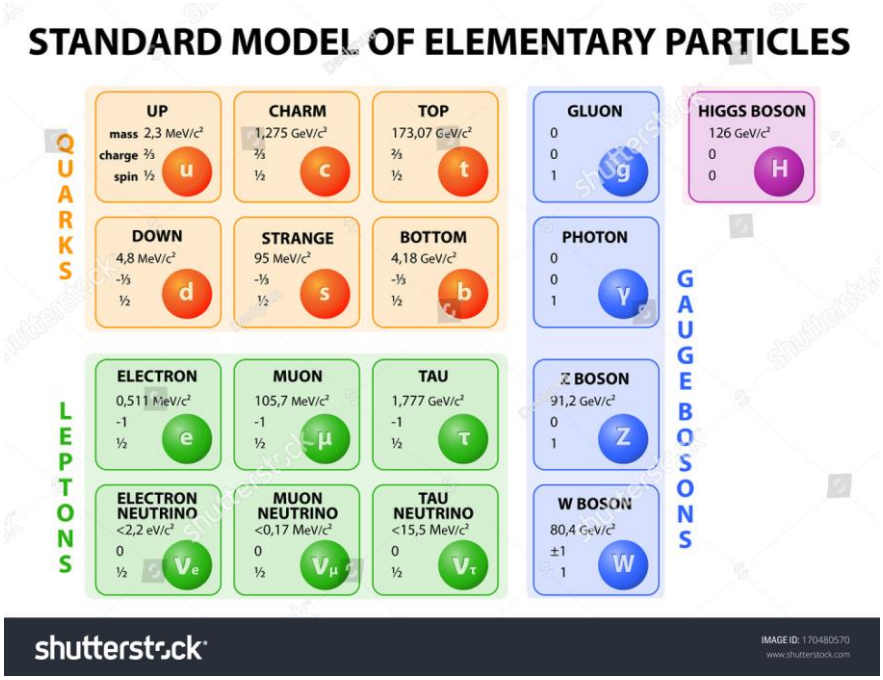

Figure 1.2 Elementary particles according to standard model (Picture courtesy :www.shutterstock.com)

The decay scheme of muons is through weak interaction. To conserve lepton number and charge muons decay produces one or more electron, along with two neutrinos. In some cases to balance the energy, no spin and no charge particles like photons or positronium are also produced in muon decay. The general muon decay reaction is as follows:

$$\mu^- \rightarrow e^- + \bar{\nu}_e + \nu_\mu$$
$$\mu^+ \rightarrow e^+ + \nu_e + \bar{\nu}_\mu$$

mass = $207m_e$ = 105.7 MeV/c^2 of μ

Figure 1.3 Decay reaction of muons

1.6 SPECTRUM OF MUONS

With a broad range of varying energy and angle muons come down to earth from the upper atmosphere. From the muon energy and angle distribution information indicates muon production spectrum, loss of energy by the muon in atmosphere & decay of muon . The spectrum calculated at sea level varies with change in geographical location, height and the solar wind. Solar wind is a solar phenomenon where magnetized plasma gets extended from the sun. Many experiments have been conducted regarding these variation. From the experimental data scientists have developed many models for muon generation. This theoretical models are the basic building stones of simulation packages. The intensity of the primary rays which produces muons is given by the formula below.

$$I_N(E) = 1.8 \times \left(\frac{E}{1\ \text{GeV}}\right)^{-\alpha} \frac{\text{nucleons}}{\text{m}^2\ \text{s}\ \text{sr}\ \text{GeV}} \qquad (1.2)$$

Where E is value of the each neucleons have and α = 2.7 (differential spectral index of cosmic ray flux).

CHAPTER 2

GASEOUS DETECTORS

In experimental high energy physics, particle detectors are used to identify the trace of incoming sub atomic particles. Particle detectors which are used for identifying and calculating radiations are called radiation detectors .Start of the particle detection techniques leads us back to 1890's when X-ray and radioactivity were discovered.

H. Becquerel discovered that photosensitive paper was blackened by the emitted radiations of the uranium salt, which possible made it the first documented particle detector. In the early years of 20^{th} century, E. Rutherford and E. Marsden used a scintillating to detect scattered alpha particles with the eye. After observing the final location of the particles, attempts to track and photograph the trajectory of the particles were made, which lead to the evolution of emulsion techniques and the spark-, cloud-, streamer- and bubble chambers. From that time until now they have been used with utmost success in various physics experiments. The wide variety of different applications of the detectors in many instruments can be seen today. The development is still going on today. The working principles or governing physical processes inside these particle detectors are mostly clear now a days. The computerized simulation techniques have helped us a lot in this. with the help of this simulation software, new design or configurations of detectors are at first tested, studied and optimized by changing different parameters. Afterwards they are fabricated and used in experiments.

The two type of detectors used in the experiments of this report are scintillators and gaseous detectors. Hence a very brief introduction of scintillator detectors is given below.

Scintillation detector was discovered earlier than most of the particle detectors. Scintillation is actually nothing but the property of giving away light or showing luminescence. Those materials which emit light or exhibit luminescence are termed as scintillators. When incoming particle strikes luminescent material, at first its energy is absorbed & then it is re-emitted by photons. The scintillation detector is one amongst those detectors which are widely used for particle detection in nuclear, particle or high-energy physics. There exist classification of scintillators, say, gaseous, liquid, solid, organic, or inorganic. Scintillation based detectors comprises a scintillator material coupled with a photodetector. A photodetector converts the light from the scintillator into electrical pulses. Among common

photodetectors there is the photomultiplier tubes composed of photocathodes. This photocathodes are followed by many dynodes.

The light photon when strikes the photocathode photo electric effect is occurred. In this process the emitting photoelectron is deliberately focused on the dynode present in the vicinity. After this the electrons which gets multiplied by the dynode present at first is again get multiplied by the next dynode present in the chain. This creates an amplified signal. This amplified signal is collected at the power source's positive terminal connected electrode or anode plate which thereafter is passed to the electronics present for signal processing.

2.1. HISTORY OF GASEOUS DETECTORS

In late 1960's, gaseous detectors like wire or drift chambers came into use. They exploited the radial electric field which is present because it is produced by wire-like anode electrodes (positively charged), where the field has very strong dependence on the distance r from the wire (the electric field E is proportional to $1/r$). It actually leads to the characteristics that the multiplication/amplification region and the radial discharge dimension as well are limited to a distance of the diameter wire order. Thus all electrons need to drift into this region before amplification and the signal generation sets in, which introduces a time jitter, limiting the time resolution of wire based detectors to few nanoseconds. The detector is very stable since the field intensity is very low on the cathode faces, allowing extremely good spatial resolution. Multiwire proportional chambers or drift chambers hence have good spatial resolution. So, gaseous detectors like drift chambers or wire chambers have replaced most scintillation counter in experiments demanding very high spatial resolution. Although scintillators are still used in particle physics experiments. To overcome the problem of this time jitter and allowing improvement in the time resolution, a strong uniform electric field could be used, where the avalanche amplification sets in instantly for all primary clusters right after primary ionization.

The intrinsic detector time resolution is then dominated by the spatial variation of the primary interaction leading to a temporal spread, avalanche statistics and noise induced triggering time fluctuations spread,

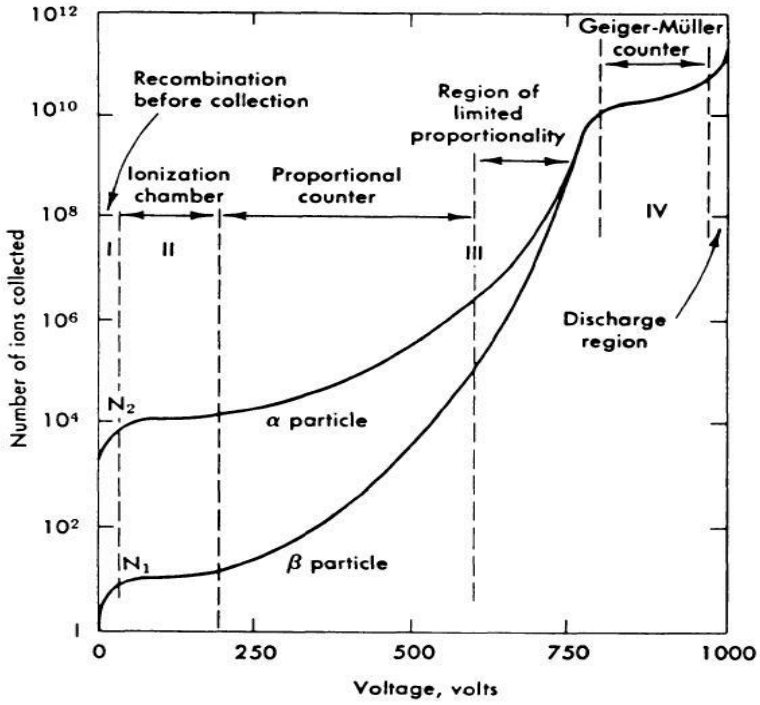

Figure 2.1 Different regions of gas detector operation depending on gas ionization(image courtesy :www.phyorg.co)

Avalanche statistics and noise induced triggering time fluctuations are thus minimized. In 1948, Keuffel Spark Counter was the first gas detector to use uniform electric field with parallel metal plate geometry.

It offered a time resolution of around 1 ns which was far better than any of the Geiger-Müller Counters that were commonly used at that time and had a timing resolution of around 100 ns. This development opened the possibility for the construction of accurate timing systems to measure the velocity of fast charged particles. Keuffel Spark Counter consists of two planar metal electrodes with a high voltage applied to them and a gas mixture filled between gap. When a charged particle passes through this gap, the particle leaves a trail of free charge carriers produced by primary ionization occured in the gas particles present in the gap which trigger avalanches of charge carriers in the electric field.

Due to the spark produced in the gas, a switching-off circuit is needed to prevent the metal electrodes from being short-circuited. This leads to a long dead time (~1 s), which poses limits on the maximum detection rate it could sustain. In addition, it worked with low-pressure gas and had a very short operating span.

Note that the standard spark chamber has an area of a few cm^2 only because with the increase in the area, the discharge energy in a spark increases to an extent that it can damage the electrode surface. The main problems which were observed in Keuffel Spark Counter were the excessive dead time and secondary ionizations. To overcome these problems, Pestov Spark Counter was introduced in 1971, with resistive plate electrodes & special gas mixtures for photon absorption. The resistivity of around 10^9 Ohm-cm of the electrodes limits the discharge at the area nearby to the occurance of primary avalanche. The energy in the sparks is observed to be much smaller than in the case of metallic electrodes and larger electrode surfaces can be used.

Moreover, if organic gases with high ultra violet absorption capability are used then charge diffusion in the gas will be prevented and the actual area of the detector which suffers from the voltage drop is localized around the primary ionization region. Using Pestov Spark Counter with a 0.1mm gap reaches time resolutions around 25 ps. However, the very thin gap (0.1 mm) combined with the high values of the electric field (500 kV/cm) demand a very good surface smoothness of the electrodes. Moreover, the detector has to be operated at a large overpressure of 12 bar. This ensures a large density of primary ionization in the thin gap to account for good detection efficiency.

The main problems which were observed in Keuffel Spark Counter were the excessive dead time and secondary ionizations. To overcome these problems, Pestov Spark Counter was introduced in 1971, with resistive plate electrodes and with special gas mixtures for photon absorption. The resistivity of around 10^9 ohm-cm of the electrodes limits the discharge to the local area around the primary avalanche and because the high voltage drops only locally, the remaining counter area is still sensitive to particles.

The energy in the sparks is much smaller than in the case of metallic electrodes and larger electrode surfaces can be used.

Moreover, if organic gases with high UV absorption capability are used then charge diffusion in the gas will be prevented & the actual area of the detector which suffers from the voltage drop is localized around the primary ionization region. The primary and important advantage of the use of resistive electrodes is that it was previously required to

use high voltage switching off electronic circuits which is found to be no longer necessary using resistive electrodes & consequently detection rate higher than the previous detectors can be seen.

Pestov Spark Counters with a 0.1mm gap reach time resolutions aroumd 25 ps. However, the very thin gap (0.1 mm) combined with the high values of the electric field (500 kV/cm) demand a very good surface smoothness of the electrodes. Moreover, the detector has to be operated at a large overpressure of 12 bar. This ensures a large density of primary ionization in the thin gap to account for good detection efficiency.

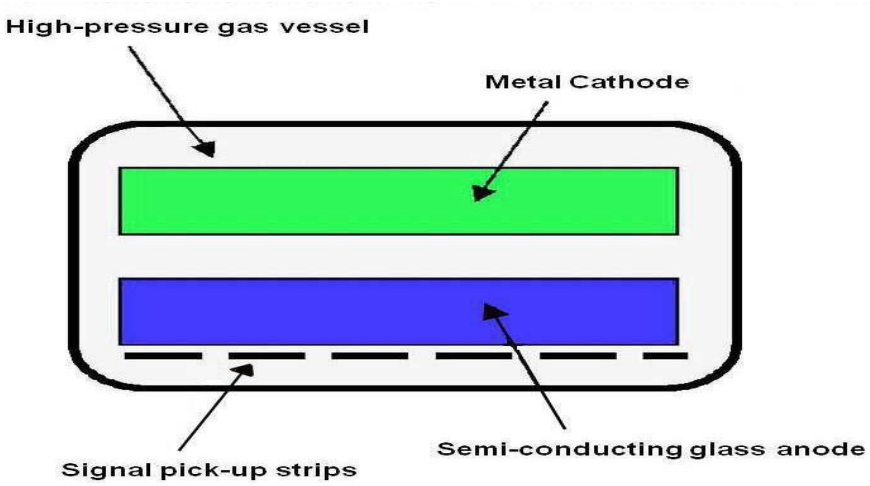

Figure:2.2 A schematic diagram of Pestov counter

Parallel Avalanche Chambers are gaseous detectors which are used in avalanche mode. They have a single gas gap & the electrode plates are similar to Spark Counter. It normally consists of two planar metal electrodes, or metalized ceramic or plastic, with a gap from 0.5 to 2 mm by precise spacers.The time resolution is around 100 to 250 ps. Depending on the gas filling, a gain of 10^3 to 10^4 can be reached with a very low discharge probability of 10^{-5} for minimum ionizing particles.

The PPAC signals are small (about 100 fC on an average) which gives a low value of ratio between signal and noise. To account for a good detection efficiency, the electronics has to be free form noise with a high precision & very sensitive, which collides with the fast rise time needed for timing purposes.

Formation of streamers and discharges are effects which are unwanted in PPAC . The posible feasibility of using this technology for large scale applications is questionable.

2.2 RESISTIVE PLATE CHAMBER

Resistive plate chambers can provide excellent time and position information which are desirable features of many high energy experiments dealing with triggering and particle tracking. The simplicity and robustness in this detector's design and from economical viewpoint its low budget construction, make it tremendously useful in many high energy & nuclear physics related experiments. The resistive plate chamber descended around 1980 from Parallel Plate Counter. Parallel plate chamber was invented in the decade of 1940.Parallel plate chambers improved the timing resolution of the contemporary gaseous detectors. The basic construction of PPC consists of a gas mixture kept in between a pair of metallic electrodes. RPC is almost like the detector named parallel plate chamber but made of highly resistive material. Having electrode resistivity of almost 10^{9}-10^{12} ohm-cm. Materials like glass or bakelite satisfy the criteria of having resistivity of the said order.

A suitable gas mixture is filled between the plates and the plates are sealed. Thus constructing the gas chamber. Polycarbonate made side spacers and button spacers, having higher order of resistance than glass and bakelite are used to keep a constant gap between the two resistive plates. A particle having charge and decent amount of energy, whenever enters the detector volume and passes through the gas mixture present inside the detector, it ionizes the gas molecules contained inside the detector volume. It is required to separate out the electron-ion pair created inside the gas volume due to ionization before they recombine and form neutral molecule again. In order to stop the process of recombination a uniform & constant electric field is applied in the electrodes. The electric field makes the electrons to move towards anode and the ions towards cathode. The position of ionization can be determined through pick-up strips which are the part of the detector to collect the signal.

This enable us to locate position of the detectable incoming charged particle. Pick up strips are placed throughout the length of the electrode for the purpose of picking up the signal. The primary ionization location of the particle is located by keeping the pick-up strips perpendicular to each other. It allows them to read out the x- & y-coordinate of position of the passing particle. An insulating layer keeps the strips separated from the conducting graphite coating. This insulating layer is actually like a dielectric in between graphite

coating and pickup strips both of which are conducting material. This makes the charge to travel from graphite to pick-up strips by the method of induction. Since the electrodes are made of insulators it's hard to obtain a constant or uniform electric field distribution. One of the surfaces of the of the electrodes which is kept outside is uniformly painted with a graphite coating giving a constant surface resistance ~1MegaOhm/cm and can be decided as per the need of the experiment. Note that graphite coating and its surface resistance goes inversely with each other. Time resolution measured for RPC having single gap is around 1-2 ns, which can be increased up to less than 50 ps by minimizing the existing gaps between the electrodes.

2.3 Classification of RPCs

RPCs can be divided or classified into different categories. The categories are based on their application and design. The no of gaps between the electrodes, use of oil and choice of material are the main criteria of classification.

RPCs are classified in two types based upon application

2.3.1 Trigger RPCs

There are many high energy physics experiments where particle strike is necessary to trigger further circuits present in the system. In many cases RPCs are used in mentioned cases. This type RPCs are called as Trigger RPCs. They are used in various HEP experiments for the purpose of triggering muons, which is an example of minimum ionizing particles. Single gap or double gap RPCs with gas gap of 2mm operated in either avalanche mode or streamer mode if shows efficiency ~98% with a time resolution of ~1-1.5ns then they are perfect to be used as Trigger RPCs.

2.3.2 Timing RPCs

The RPCs which can indicate preciously the timing information of an incoming particle is referred to as timing RPC.

Timing RPCs are mostly operated in avalanche mode to get better time resolution. The time resolution is ~50ps with an electric field of ~100kV/cm. These RPCs provides an efficiency of ~99%. The time resolution of timing RPC is better than trigger RPC. RPCs the gas gap of 0.2 - 0.3 mm wide are mostly used in multi-gap configurations for Time-of-Flight or TOF measurements.

The combination of different kinds of resistive electrodes and their materials, types of pick up panels used, types of spacers used, RPCs are generally classified in different categories depending on their design:

2.3.4 Single-gap RPCs

When the original RPC was fabricated in 1981, it was a single gap RPC with high resistive electrodes of bakelite.

Later on according to the need, Bakelite RPCs were fabricated which showed better resistivity and are in trend nowadays. The inherent advantage of this design is that high voltage capacitors are absent and thus the high voltage insulation of the strip is not required. Time resolution of ~1-1.5ns is obtained in a standard 2mm gap RPCs in either of the operating modes [6]. To obtain such results discriminators (for e.g. Leading Edge Discriminator or (LED) are used. In the conventional single gap RPC to maintain a constant gas-gap, gasmixture containing Argon, isobutane, tetrafluoroethane (R134a) is used and is operated at streamer mode.

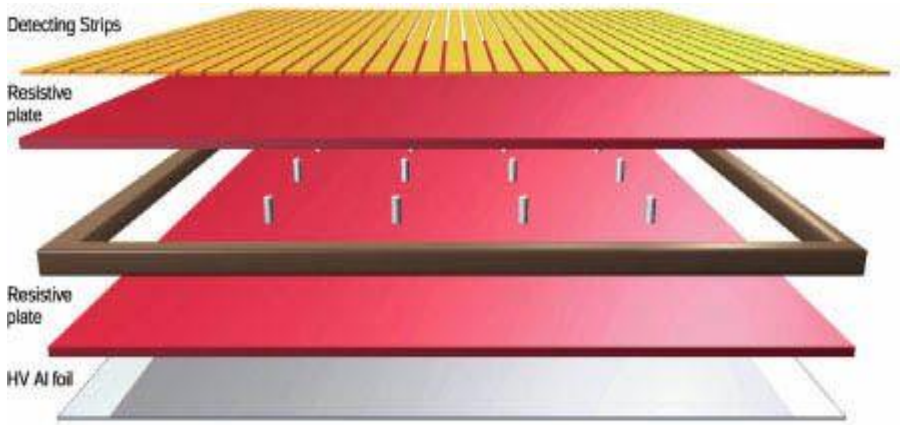

Figure2.3 Schematic diagram of single gap resistive plate chamber

2.3.5 Double gap RPCs

Double-gap design is almost the same as the signal-gap but with more number of elements involved in it. The main purpose to introduce the Double-gap design was to improve efficiency of detection by the detector while operating it in the avalanche mode [2].

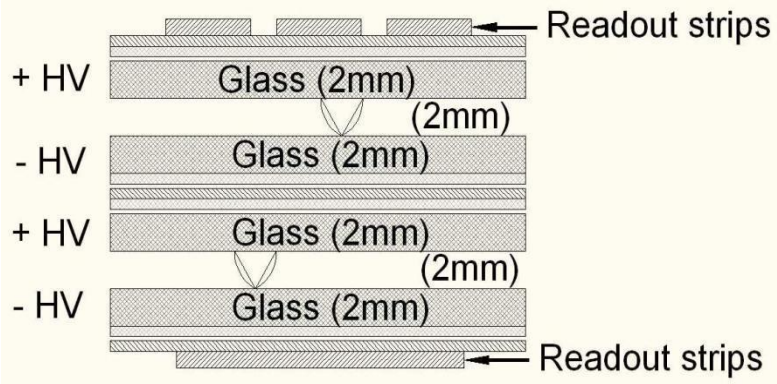

Figure 2.4 Schematic diagram of a double gap RPC

2.3.6 Multi-gap RPCs

Multigap Resistive Plate Chambers acronymed as MRPC, are nothing but the extended version of RPCs where the single gap of RPC is divided into many small sub-gaps to improve the value of time resolution provided by the detector. This is done by inserting highly resistive electrodes (~10^9-10^{12} Ω-cm) floating within the gas gap between the two outer electrodes. High voltage is applied on the two outer electrodes. When the charged particle enters & passes through the gas gap, formation of avalanche takes place in many of the gaps. The signals which are induced on the pick-up strips are the sum of individual signal of the avalanches produced in any gas gap. In case of MRPCs because of the small gaps time jitter should be less. The attractive and important feature of MRPCs is that they are robust, easy to fabricate, can be fabricated in any size and have simple electronics associated.

RPC utilizes a constant and high uniform electric field (~50-100 kV/cm) produced between highly resistive electrodes (10^{10} -10^{12} Ω-cm). A single-gap configuration provides time resolutions down to ~1ns and position resolution of micrometers, whereas a multi-gap configuration can give time resolutions down to 20ps [8]. This makes RPCs well-suited for TOF (Time Of Flight) applications, medical imaging and triggering purposes.

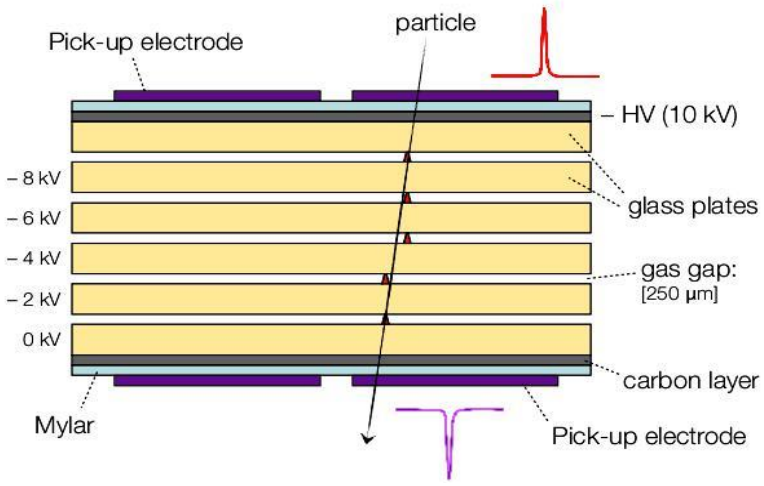

Figure 2.5 Schematic diagram of a multi gap resistive plate chamber

2.3.7 Hybrid RPCs

Hybrid RPCs are made of both type of materials, resistive & metallic electrodes. A schematic of hybrid RPC is shown in figure 2.4 below. The electrodes connected to high voltage are metallic where as the floating electrodes are made of highly resistive material. The anodes by connecting together, kept at the potential same as ground. These detectors are simple & easy to construct and have a very good time resolution <50 ps and detection efficiency >95%.

These types of RPCs can also be used for ToF-PET imaging [6].But these RPCs give very poor timing resolution because of conducting electrodes. That's why Multi-gap RPCs are preferred over Hybrid RPCs for their excellent timing resolution because of the presence of resistive plates.

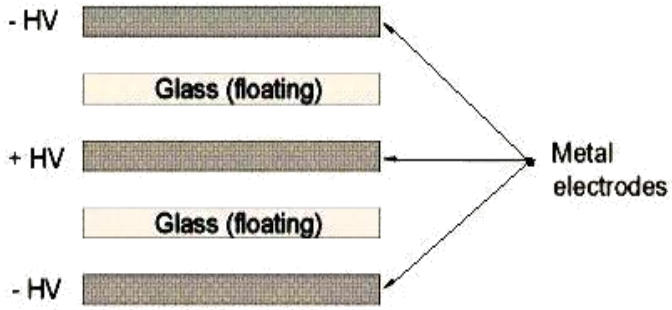

Figure 2.6 Schematic diagram of a hybrid gap resistive plate chamber

2.4 BASIC OPERATIONAL PRINCIPLE

The basic principle on which most gaseous detectors work on is **gas ionization**. As the particle enters the chamber if the particle has sufficient energy then it ionizes gas atoms and makes electron-ion pairs. If the electric field/energy of the incoming particle applied is high enough, electrons produced from primary ionization interact with the other neutral gas atoms and further ionizations take place which makes secondary, tertiary and so on electron-ion pairs. As electric field is always maintained across the chamber, ions & electrons produced tend to move to the electrodes. Note that the drift velocity in case of electrons (10^7 cm s^{-1}) is greater than ions (10^5 cm s^{-1}).

Ions have less freedom of movement inside the gas volume, hence they move relatively slower than the electrons. Hence the tip like shape is formed by the ions and the shape looking like cluster is created by electrons. this gives the conical or teardrop like characteristic shape of the avalanche.

The effect of avalanche between electrodes: The first ionization frees one electron from the gas atom. Then the particle undergoes more collisions and liberates electrons in each collision. Each collision process gives away two electrons , one from ionization and another one is liberated electron. The time when chamber gain becomes high there emerges a local electric field due to avalanche. This field creates space charge effect which interferes with the existing electric field maintained inside the gas gap.

In the regions above and below the avalanche (with electric field E1 and E3 respectively), the net field is more than the applied electric field (E0) (The reason is the same direction of the both fields).

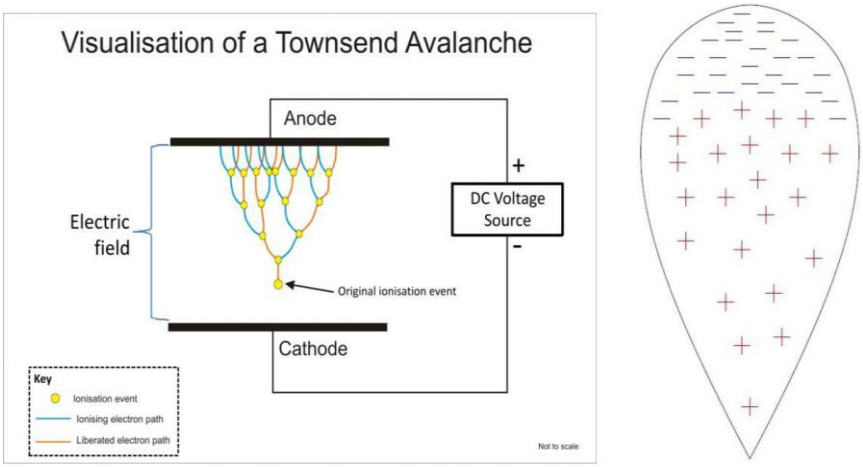

Figure 2.7 Formation of Townsend avalanche

But in the region where the avalanche is present (region of highest electron density), the local induced field which is expressed by (E2) and applied field which is also shown in figure as (E0) cancel each other.

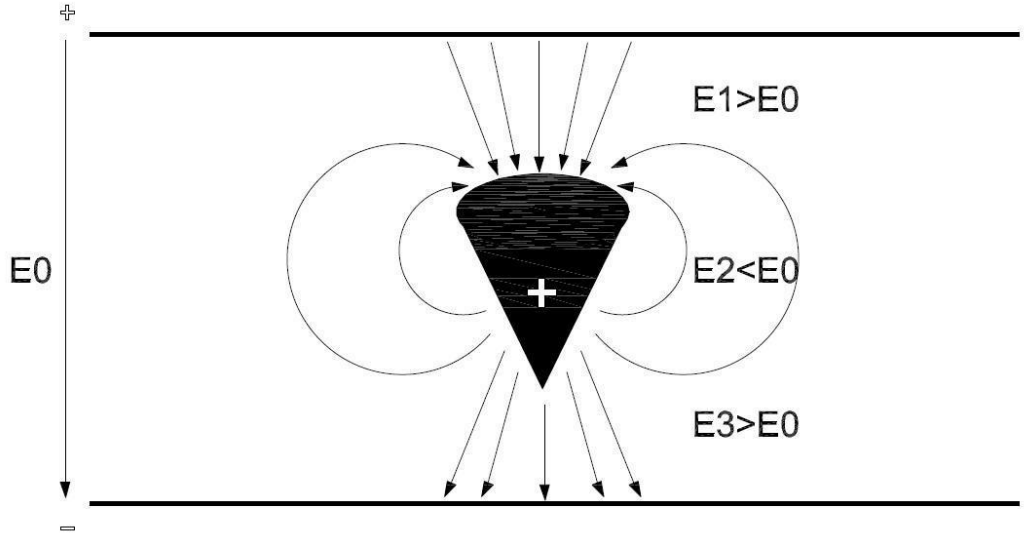

Figure 2.8 Schematic of an avalanche and the electric field variations caused by the avalanche charge carriers inside the RPC.

2.5 OPERATIONAL MODES

RPCs are generally operated in two different modes: (i) Avalanche & (ii) Streamer Mode. Avalanche mode includes the formation of an avalanche and multiplication of electrons formed by many ionizations followed by primary ionization. The growth of this avalanche is controlled by Townsend equation. With the increase in the chamber gain, the space charge effects start influencing the applied electric field, and the electrons & ions from the avalanche. Then they move and the direction of movement is in the direction of their respective electrodes. The charges in the electrode layers influence the field in a small area around the region where the avalanche is developed.

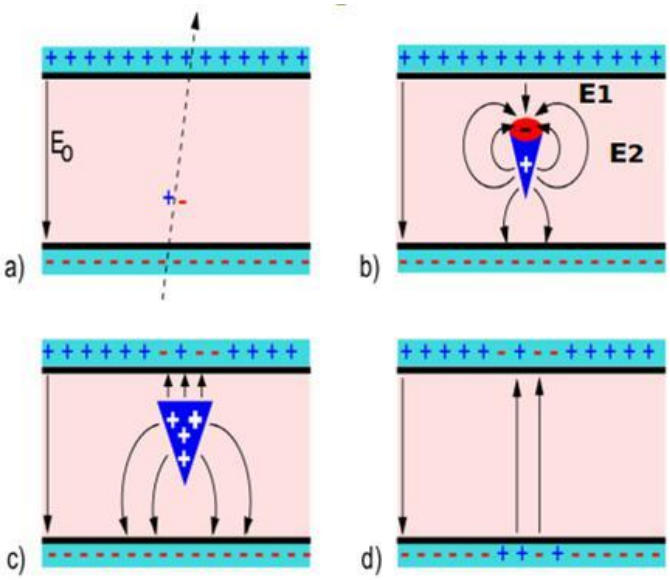

Figure 2.9 Schematic diagram showing the development of avalanche in an RPC

The streamer mode can be taken as advancement in the avalanche mode. After the space charge effect, when the gas gain is increased further, discharge photons start to contribute to the avalanche propagation and streamers appear. Then, a conductive channel is formed in between the electrodes, through which the local electrode surfaces are discharged and a weak spark is created. The discharge area is localized due to high bulk resistivity of the electrode material. The electric field is strongly decreased around the spot where avalanche is formed, thus the detector develops a blind spot. The pulse produced in streamer mode would be of some 100 mV. Since the pulse amplitude is large (~200 mV) so no pre-amplifier is required in this mode which reduces the electronics used in processing of the detector signal.

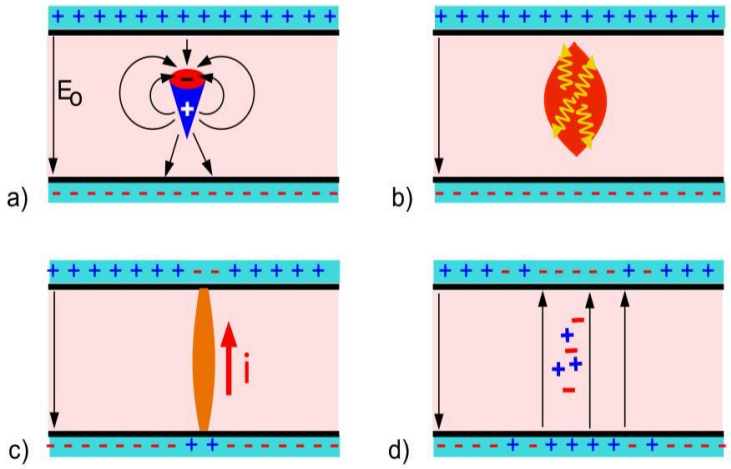

Figure 2.10 Schematic images of the development of streamer in an RPC

2.5.1 Raether limit

In an experiment the avalanche mode and streamer mode are differentiated on the basis of Raether limit.

If at some particular point, there are “n” number of electrons inside the gas-gap the rise in the number of electrons during the unit path length is given by Townsend equation:

$$dn = n \alpha dx \quad (2.1)$$

where,

α = first townsend coefficient

The total number of electrons created in path x is given by the equation

$$n = n_0 e^{\alpha x} \quad (2.2)$$

where,

n_0 = Total number of primary electrons

If n_0 be the total number of electrons then multiplication factor given by

$$M = n/ n_0 = e^{\alpha x} \quad (2.3)$$

where;

n = Total number of the electron reaching the anode

n_0 = Total number of primary electron

α = First Townsend coefficient

x = The distance between the anode and the point where primary ionization created.

The mode of operation of RPCs is decided by the multiplication factor, M. If the multiplication factor $M << 10^8$, the operating mode will be the avalanche mode and if $M >> 10^8$, the operating mode w1ill be the streamer mode. This is known as the **Raether limit**.

2.5.2 Avalanche mode versus streamer mode for RPCs[11]

Avalanche Mode	Streamer Mode
1. Gas mixture used is Freon:Isobutane:SF6 in the ratio 95:4.5:0.5.	Gas mixture used is Argon:Freon:Isobutane in the ratio 55:40:05.
2. Small pulse amplitude (~5mV), sophisticated front-end electronics is required.	large pulse amplitude (~200mV), no amplifier is required.
3. Reduces the aging of RPCs.	Increases aging in RPCs.
4. Operating voltage is ~15 kV.	Operating voltage is ~9 kV.
5. MRPCs are generally operated in this mode.	RPCs are generally operated in this mode.

2.6 GAS COMPOSITION

As discussed in previous sections, avalanche multiplication must occur at low electric fields. Noble gases show the aforementioned property better than other gases. Since argon is comparatively cheap and readily available than other noble gases like krypton and xenon, it is used as the primary constituent of the gas mixture.

After the formation of an avalanche, photons are emitted from the process of radiative decay as the gas molecules get excited and this can lead to further development of secondary avalanches. This will result in unwanted streamer formation. So further gases are needed that can absorb these emitted photons and can then dissipate the energy without emitting any further radiations and ionizations. This quenching process requires a polyatomic gas like isobutene that has many vibrational and rotational degrees of freedoms and excited states. Therefore, it can absorb the photons without emitting further photons or radiations.

The peripheral electrons around the main avalanche body accounts for the lateral spread of the discharge area on the electrodes' surface. So, for clearing these electrons and limiting the avalanche size, a highly electronegative gas such as R-134a is used.

R-134A ($C_2H_2F_4$) : It is a variant of freon, however, is comparatively less prone to cause hazzard to the environment. Along with a large primary ionization cross-section, it has a property of controlling the avalanche generation due to its slightly electronegative nature.

Iso-butane (i-C4H10) : It is used as a quencher that can absorb the energy of the photons in its vibrational states. Since it is a combustible gas, its concentration in the gas mixture is always kept below the flammability limit.

Sulpher hexaflouride (SF6) : It is a strongly electro-negative gas that helps in arresting the avalanche development through electron attachment. This leads to an effective reduction in the creation of streamers.

Gas is being provided to the RPC used by a gas system. There are three main components of the gas system. Which are briefly explained as below.

Figure 2.11 The gas supply system for RPC

i) **Read outs for gas outlet:** It tells us about the amount of gas being applied by the system.

Figure 2.12 Gas read out

ii) **Leak indication bubbler or Safety bubbler:** As it is clear from the name itself that safely bubblers indicates bubbling in the bubbler when there is some leak inside the detector. It protects RPCs from the over pressure and takes care of back pressure which may damage RPCs. These bubblers are made of a material named borosilicate Bakelite and with the help of a flexible Tygon Tube they are attached to a stainless steel tube. Each of the bubblers has nearly 5ml (~25 mm) of silicon diffusion pump oil having density of 1.08 g/cc at low vapour pressure at the room temperature. So when the proper inlet and outlet connections are made to the detectors, then there should not be any bubbling through the safety bubblers. The outlets of all the bubblers are connected to a vent which is common to them all.

Figure 2.13 Safety bubbler showing no bubbles

iii) Isolation Bubbler Isolation bubblers having their working similar to that of the safety bubblers instead the bubbling in the isolation bubblers indicates the proper gas flow in the detector. This means that there is no leakage in RPCs. They help to prevent the back diffusion process of gas in the RPCs. Through each isolation bubbler gas mixture for each RPCs flows. If no bubble is seen in isolation bubbler it indicates that some leak in gas is there or there is malfunctioning of the channel. All the bubblers output is fed into an exhaust manifold and then it is vented out.

Figure 2.14 Bubbling in the isolation bubbler can be seen in the picture.

CHAPTER 3

SIMULATION OF RPC DYNAMICS USING GARFIELD++

3.1GARFIELD++

Garfield++ is an object oriented toolkit that is used by high energy physicists and nuclear physicists to make simulation of radiation detectors. This toolkit creates simulation of those particle detectors which have gas mixture or semiconductor material inside them as sensitive medium. Various properties like electrical field, transport properties, electron inside gas and ionization pattern can be calculated with great precision using Garfield++. Electric field created the detector can be calculated by finite element programs and Synopsis device simulation program. Magboltz program is interfaced with Garfield++ to calculate the transport properties of electrons inside gas mixture. The ionization pattern produced by high & low energy particles are calculated by Heed (Hybrid Energy Efficient Distribution cluster) and SRIM (the Stopping and Range of Ions in Matter) software package respectively.

Garfield classes are heavily depended on graphic classes of ROOT framework while plotting data in a graph.

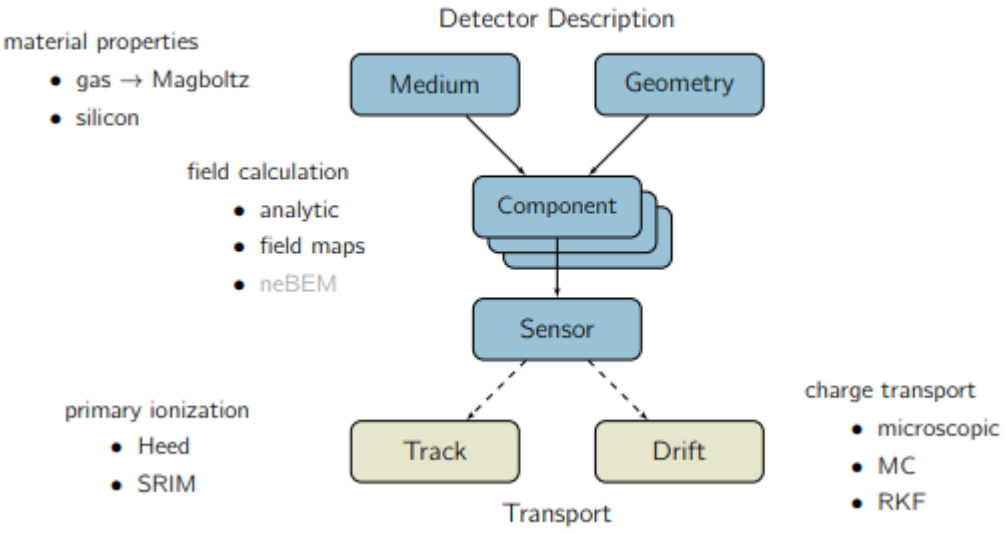

Figure 3.1 GERFIELD++ and its classes

3.2 ASSUMPTIONS AND APPROXIMATIONS

The physical process inside a gaseous detector is well studied and established, however it is an onerous task to entirely model those inside a single framework. The reason behind it is the complexity of modeling and requirement of heavy computational resources. To make the arduous work achievable, a set of assumptions and predefined conditions are taken into account during the simulation. They are listed below.

1. The temperature and pressure inside the detector was assumed to be 300K and 1atm respectively.

2. The gas volume is considered to be completely dry,i.e. humidity was considered to be 0%. Which is to keep the properties of the detectors and the gas mixture unaffected.

3.All the solid materials used in defining the geometry of the detector are assumed to be perfectly-smooth.

4. It is considered that the gas mixture which are flowed inside the gas chamber of the RPC detector has similar chemical properties in all region of the detector.

5. The gas is taken to be uniformly distributed everywhere inside the detector volume.

6. The resistive nature of the electrodes was not considered as it does not have any significant effect for the present studies [6].

7. The incident muons did not follow any special spectrum and their energy varied between 0.5 GeV to 10 GeV randomly. The angle of acceptance was restricted to $\theta = 10^{\circ}$ to match the present experimental arrangement.

8. The produced positive ions were assumed to move with a constant mobility (= $1.33 \times 10{-}6$ cm2/μs V) which sets a constant ion velocity for a fixed value of applied field. Also the positive ions were assumed not to produce any secondary ionization owing to their slow movement.

9. The physics of streamer generation is a topic which in not very much clearly understood till now and was completely ignored in the present calculations.

3.3 GEOMETRY MODELLING

The Garfield provides an sophisticated 2D and 3D geometry modeler. Different 2D (infinite equipotential plane, tube) and 3D (box with right angles, box with a cylindrical hole in center, cylinder, thin-wire, sphere etc.) elements are defined inside the software. A specific detector geometry can be modeled with the help of these elements.

The description of the specified chamber can either be in polar or in Cartesian coordinates and consists of a listing of the position, dimension and the boundary conditions in the form of potentials. In the COMSOL , the geometry was built using its built-in basic 3D blocks like box, cylinder etc.

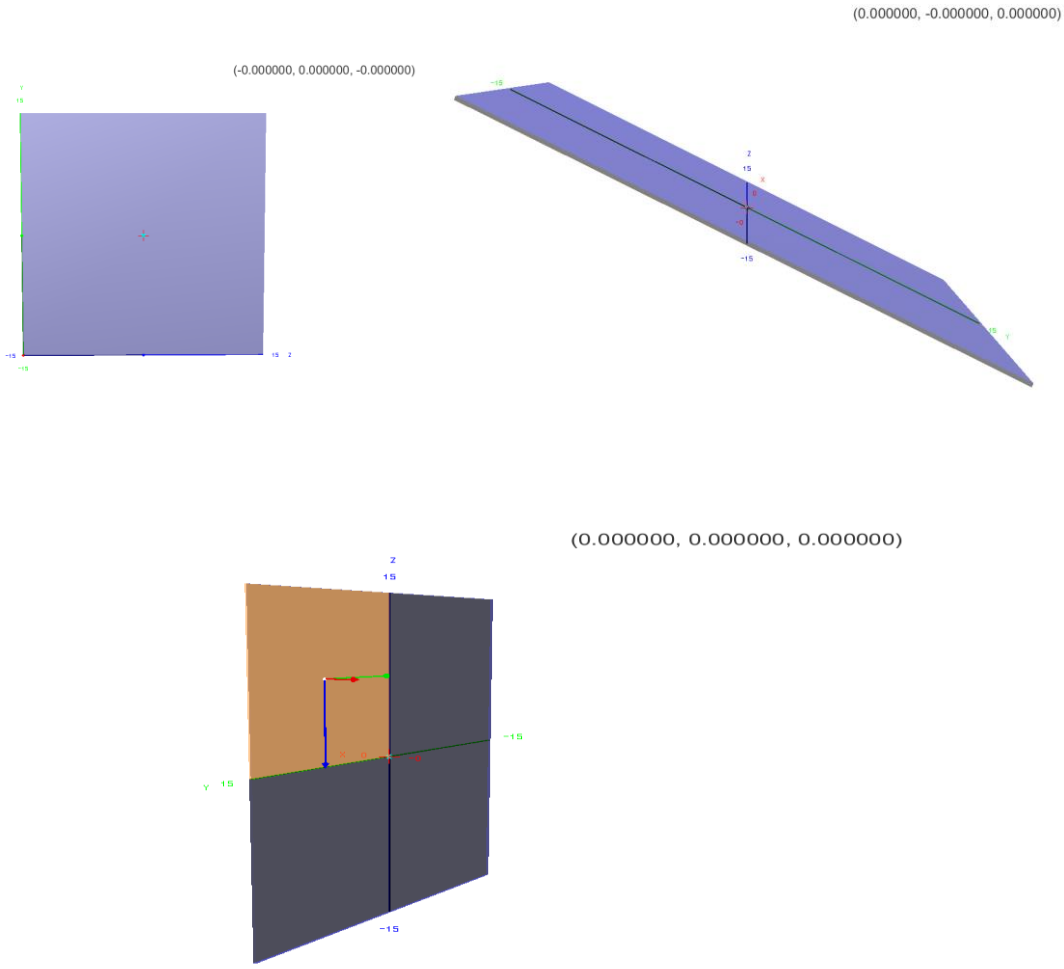

Figure 3.2 The blue boxes showing the effective gas volume of the detector from different angles.. The brown and black box is showing the detector geometry

3.4 CALCULATION OF ELECTRIC FIELD

The mapping of electrostatic field inside the gas volume of a single gap RPC requires solving of Poission equation. Poission equation for this electrostatic field is solved by applying finite element method (FEM) & along with Boundary Element Method (BEM). There are some common general steps which is applied in both the method to solve a problem.

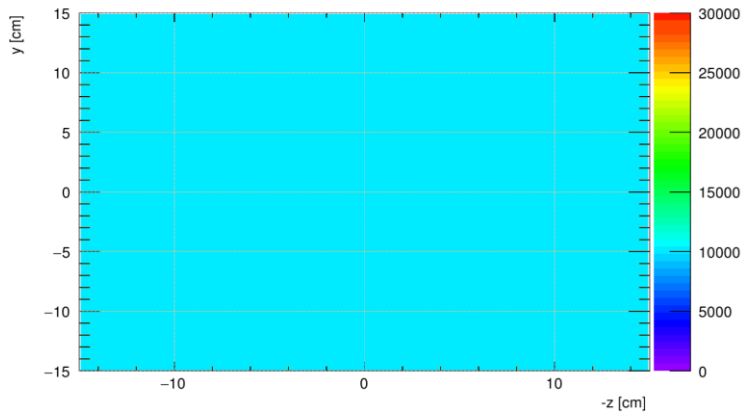

Figure 3.3 Electrostatic field map inside RPC at 10kV

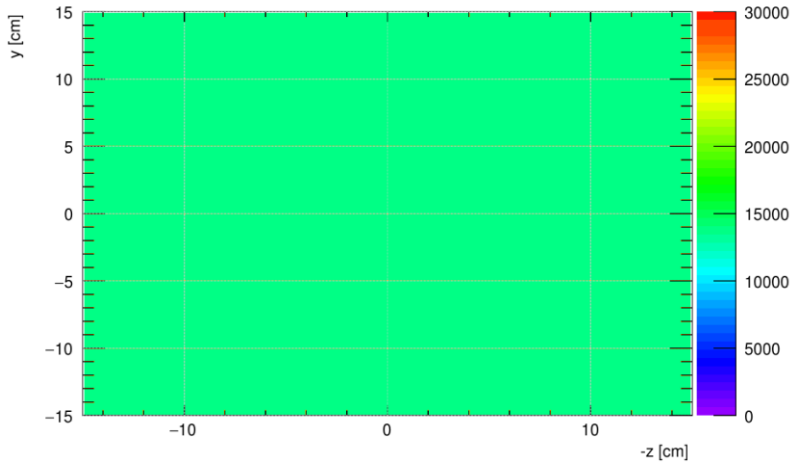

Figure 3.4 Electrostatic field map inside RPC at 13 kV

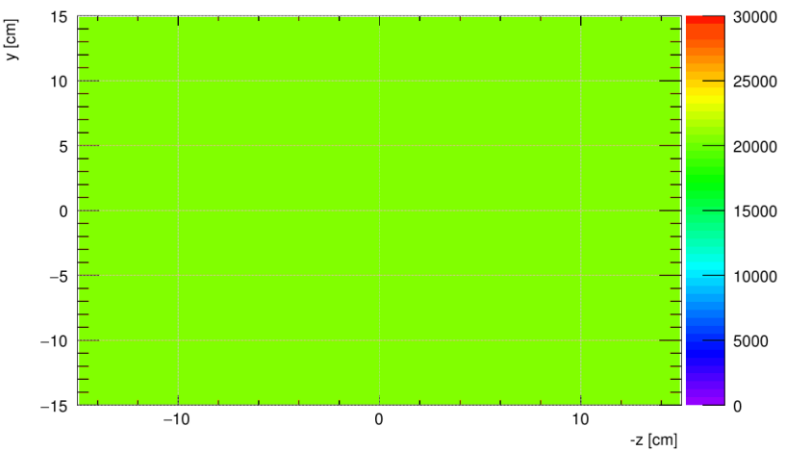

Figure 3.5 Electrostatic field map inside RPC at 17kV

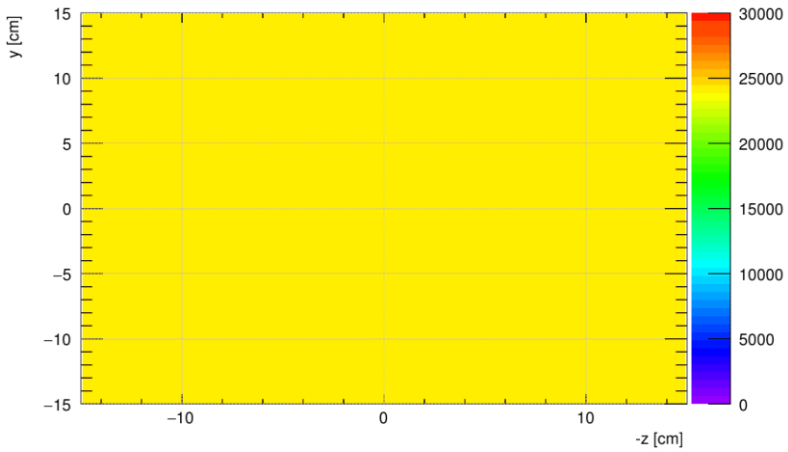

Figure 3.6 Electrostatic field map inside RPC at 23kV

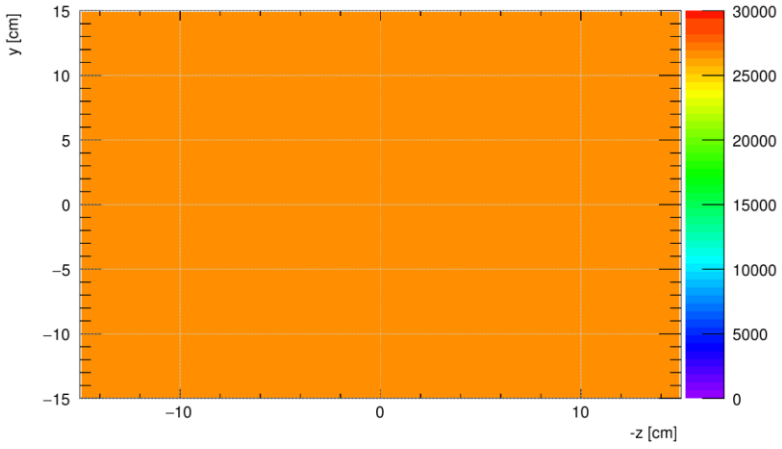

Figure 3.7 Electrostatic field map inside RPC at 30kV

It was considered that an constant electric field exits in between the 2 electrodes. And the field was varied from 10kV/cm to 30Kv/cm. Garfield++ has its own library to analytically calculate the electric field when the detector geometry can be decomposed in equi-potential planes, wires and tubes without intersections. For more complicated geometries, the program provides interfaces with different field solvers. Considering only the electrostatic fields, the trajectory of an electron or ion would be such that the position as a function of the time. The electric field configuration of the RPC is a key factor for operation of the detector as all the physical processes happen like a cascade starting from the movement of primary charges to signal induction on the read-out signal pick up panel is dependent on it. From Shockley-Ramo theorem , the induced signal depends on the amount of moving charges & their drift velocity and the weighting field. For the device , complete amount of charge contributing to the signal generation is created through avalanche multiplication which depends on the charge transport properties in the gas mixture. Transport properties, like, Townsend, attachment, diffusion coefficients and the drift velocity associated with charges depend on the value of applied field along with the properties of the mixture of gas . The value of weighting field at any point for a specific read-out is calculated by finding the value of electric field at that point keeping the read-out of interest at unit potential with all other read-outs grounded.

3.5 CALCULATION OF IONIZATION PRODUCED INSIDE THE GAS VOLUME

The amount of ionization occurred in the gas enclosed volume of a detector provides information about the charge and velocity of the traversing particle. To simulate the originating signal in a gas detector, we use a program that gives us how individual ionizations are produced and distributed throughout the path or track of the particles & their energies. The HEED was needed to calculate the initial positions of the electrons, their initial energy and their number at the locations of ionizations. It is a MonteCarlo Simulation package . The HEED program calculates the primary ionization parameters. It simulates the atomic relaxation processes. This takes place when an atom emits fluorescence photons & sometimes auger electrons. HEED also utilizes tracking of the emerging δ-electrons. It can simulate the ionization effects such as the cluster density, the primary electron distribution etc. inside the gas volume of the detector chamber.

The primary ionizations created by 2 GeV muons while passing through 2 mm gas chamber containing 95% C2H2F4, 5% i-C4H10 were calculated . The HEED was used & the distribution of different related parameters are displayed in figures

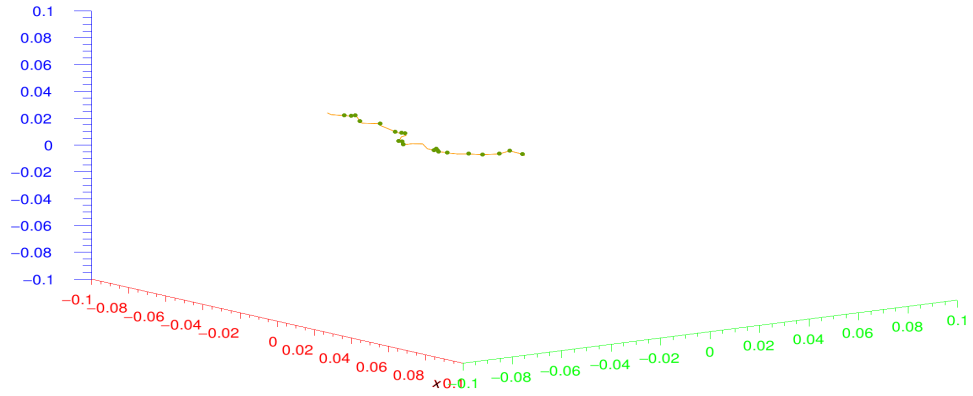

Figure 3.8 Formation of avalanche due to ionisation of muon inside RPC gas volume at 10kV

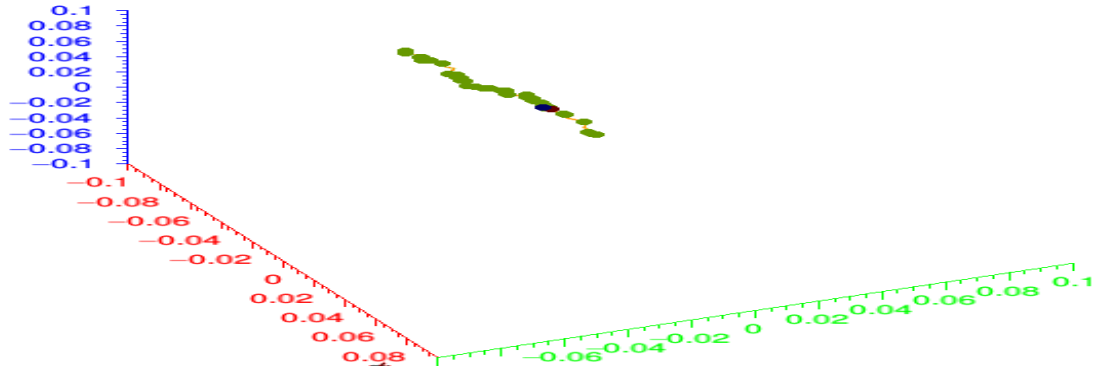

Figure 3.9 Formation of avalanche due to ionisation of muon inside RPC gas volume at 13k

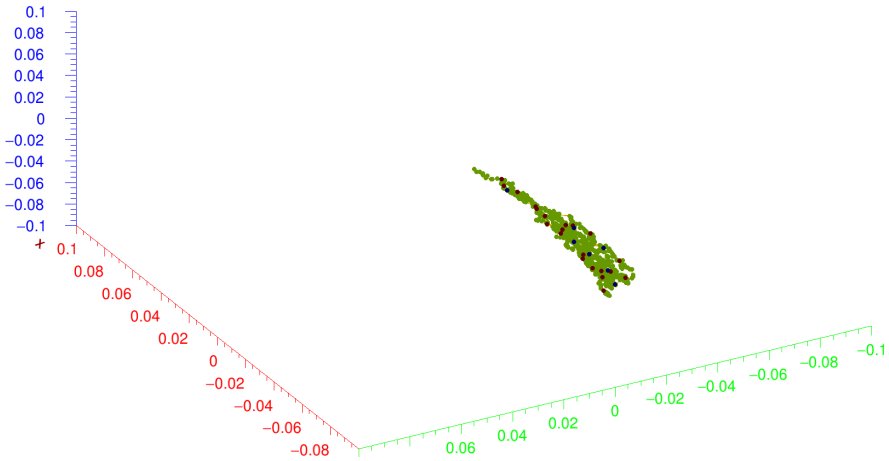

Figure 3.10 Formation of avalanche due to ionisation of muon inside RPC gas volume at 15kV

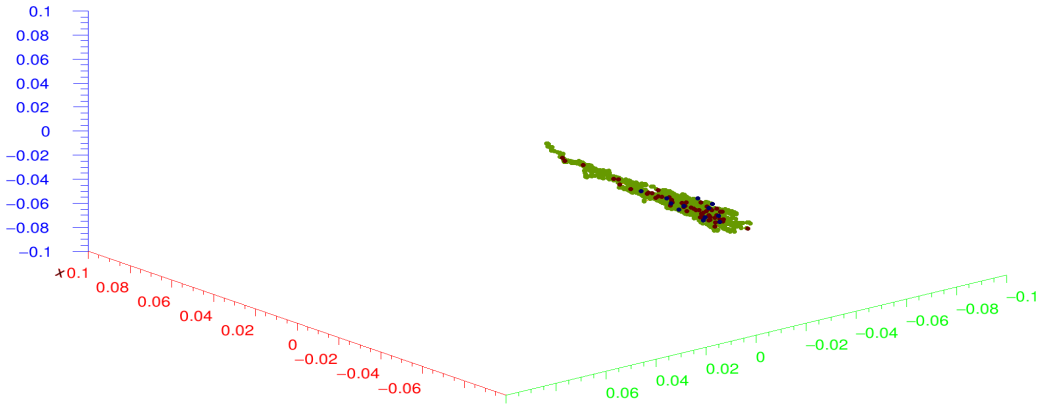

Figure 3.11 Formation of avalanche due to ionisation of muon inside RPC gas volume at 19kV

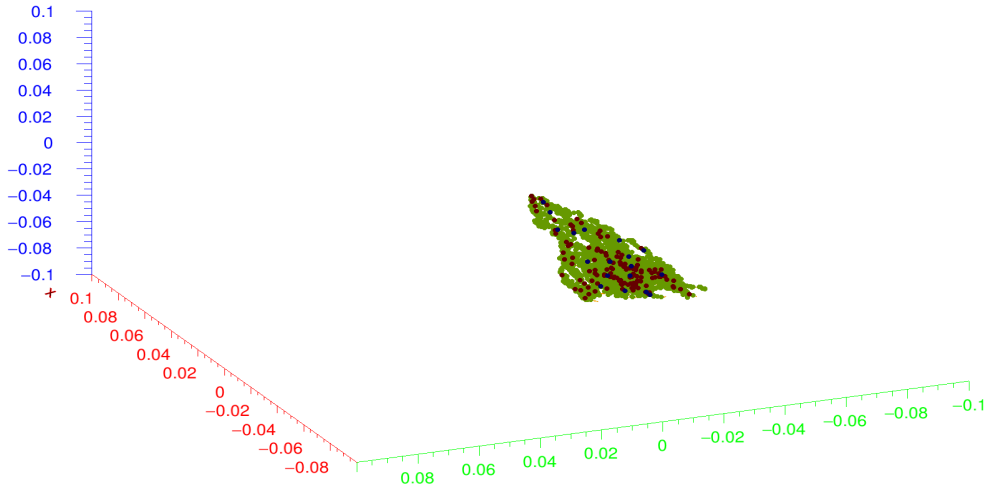

Figure 3.12 Formation of avalanche due to ionisation of muon inside RPC gas volume at 20kV

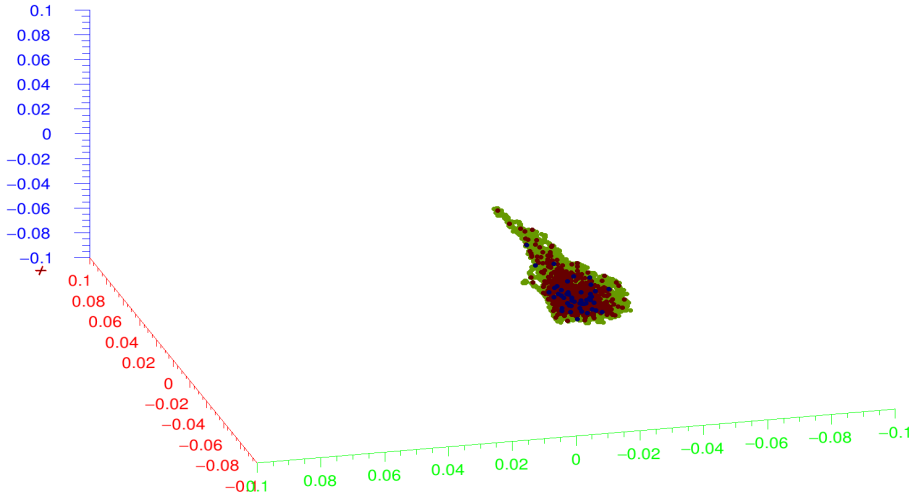

Figure 3.13 Formation of avalanche due to ionisation of muon inside RPC gas volume at 24kV

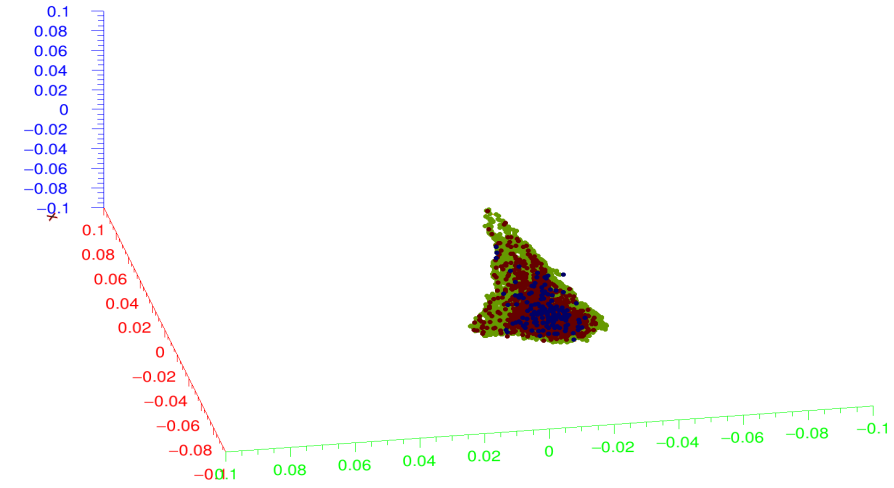

Figure 3.15 Formation of avalanche due to ionisation of muon inside RPC gas volume at 26kV

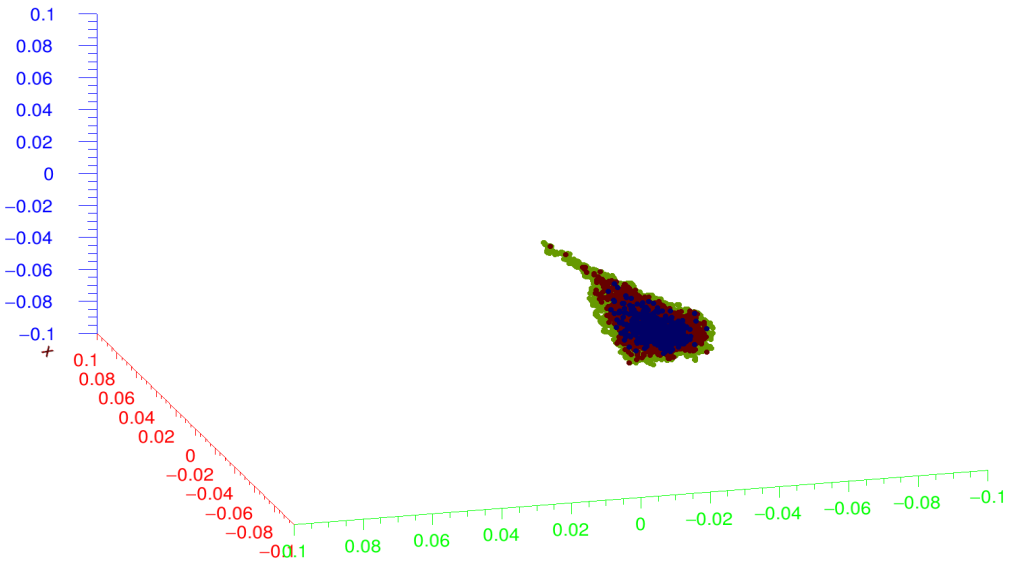

Figure 3.15 Formation of avalanche due to ionisation of muon inside RPC gas volume at 28kV

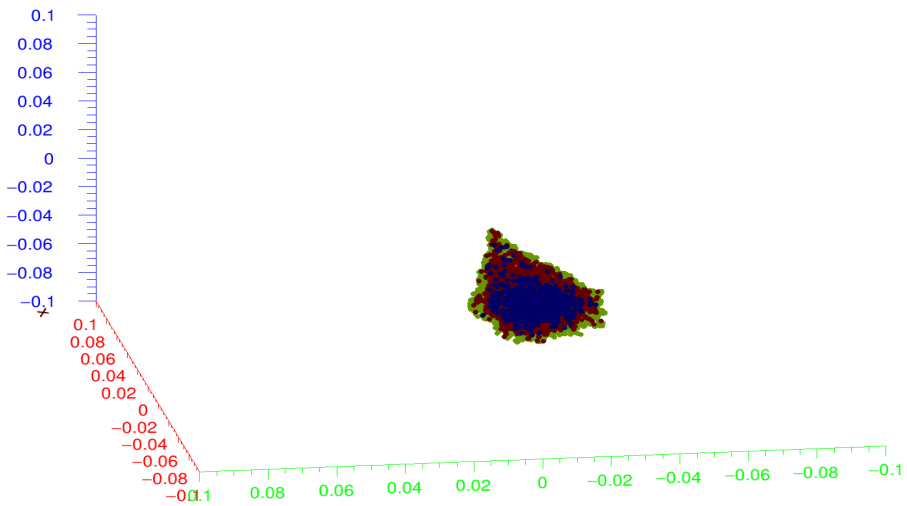

Figure 3.16 Formation of avalanche due to ionisation of muon inside RPC gas volume at 30kV

3.6 SIGNAL GENERATION

The amplitude of signal increased with the rise in the field for obvious reason. The rise in the Townsend coefficient or the gain in kinetic energy of the electrons with the field caused release of larger number of electrons through further ionization of the gaseous molecules that contributed to the rise in the induced current. The signal rise time was improved with the increase in the field as the electrons moved faster in higher fields as an effect of higher drift velocity and lower diffusion. The effect of a trace amount of highly electronegative SF6 in the gas mixture was a reduction in the signal amplitude. This was caused due to a fall in electron numbers owing to their attachment with the SF6 molecules . Also a larger rise time of the signal could be observed as SF6 is in the gas mixture. This is caused by the electrons, having longer time of flight due to an increase in the diffusion. Nevertheless, for the same gas mixture, the rise time improved with increase in the electric field due to faster movement of the electrons as was explained earlier. To study the effects of various operating & parameters of geometry on the induced signal systematically, the average signal amplitude was estimated for 1000 events for different cases from the mean of the distribution regarding signal amplitudes.

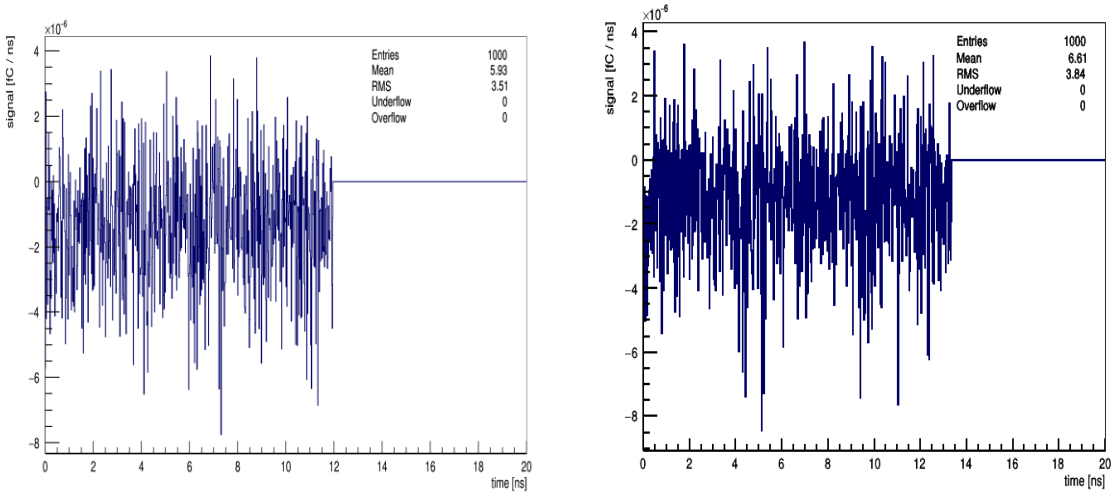

Figure 3.17 Signals of RPC at 10kV and 13kV

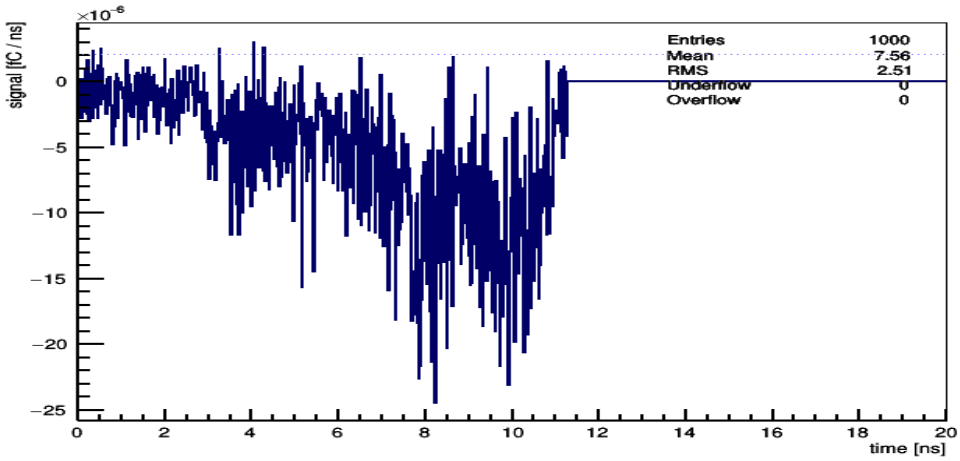

Figure 3.18 Signal of RPC at 15kV

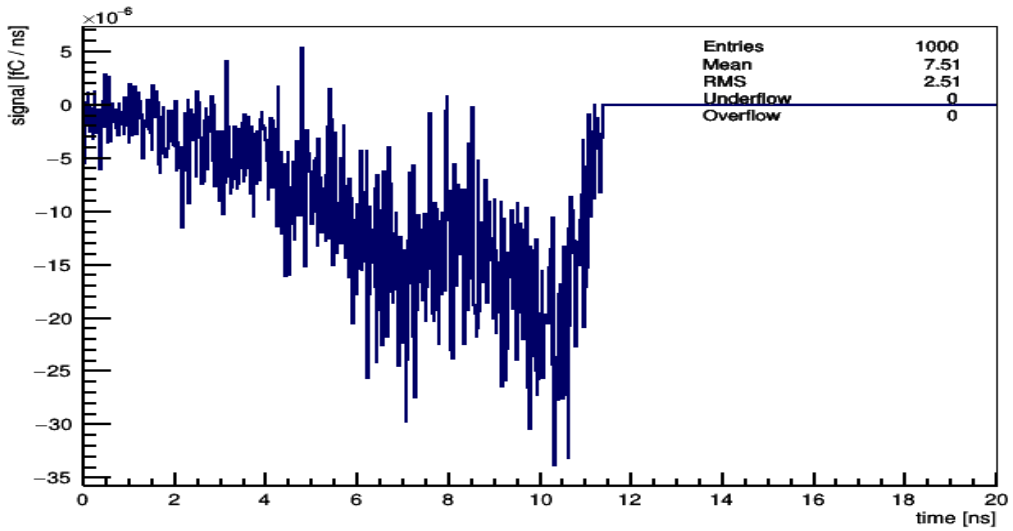

Figure 3.19 Signal of RPC at 17kV

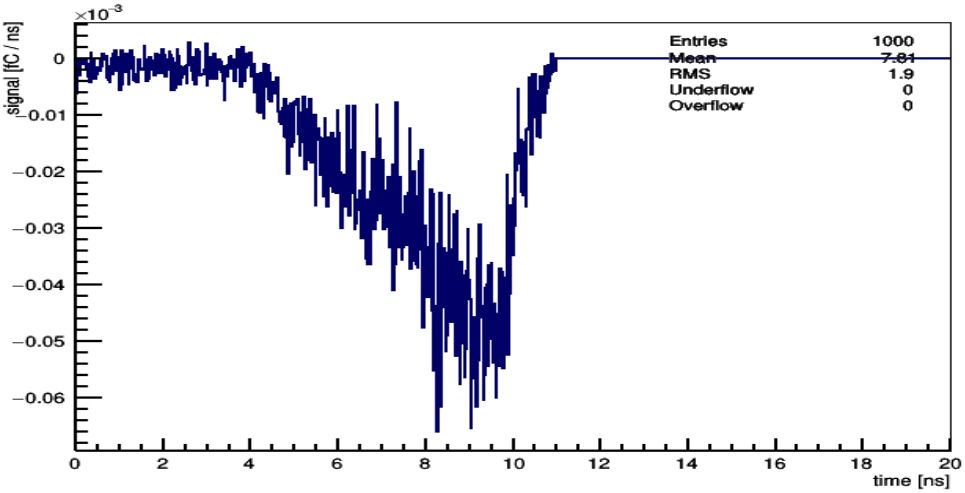

Figure 3.20 Signal of RPC at 19kV

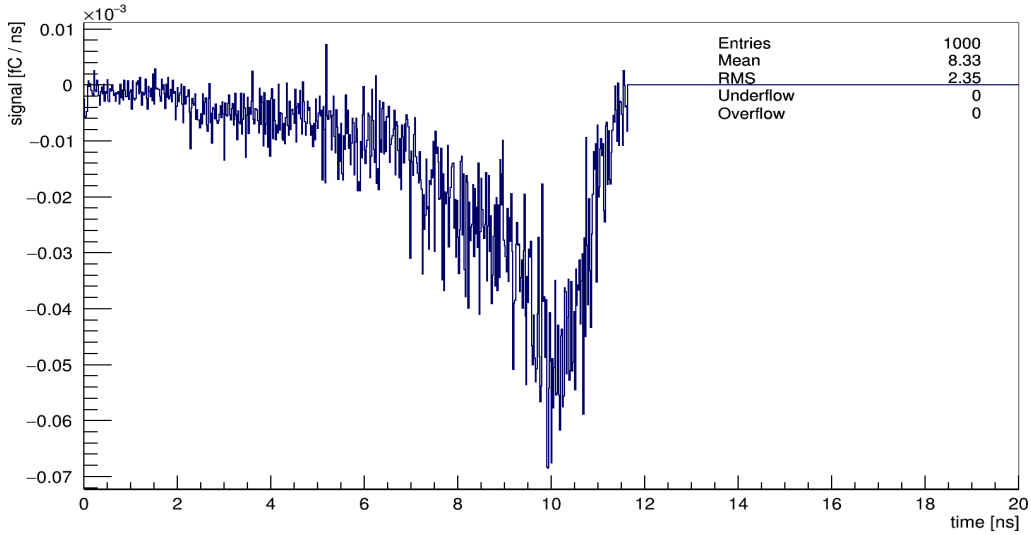

Figure 3.21 Signal of RPC at 24kV

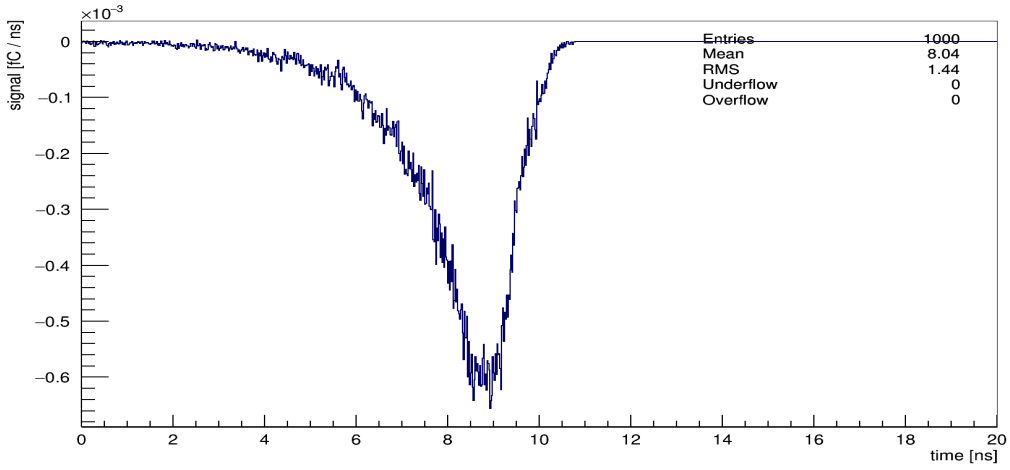

Figure 3.22 Signal of RPC at 24kV

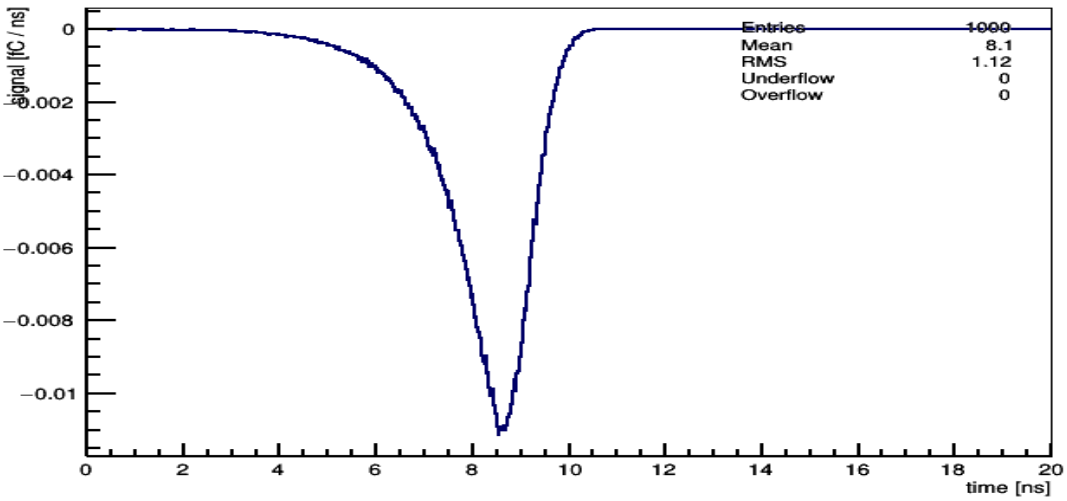

Figure 3.23 Signal of RPC at 26 kV

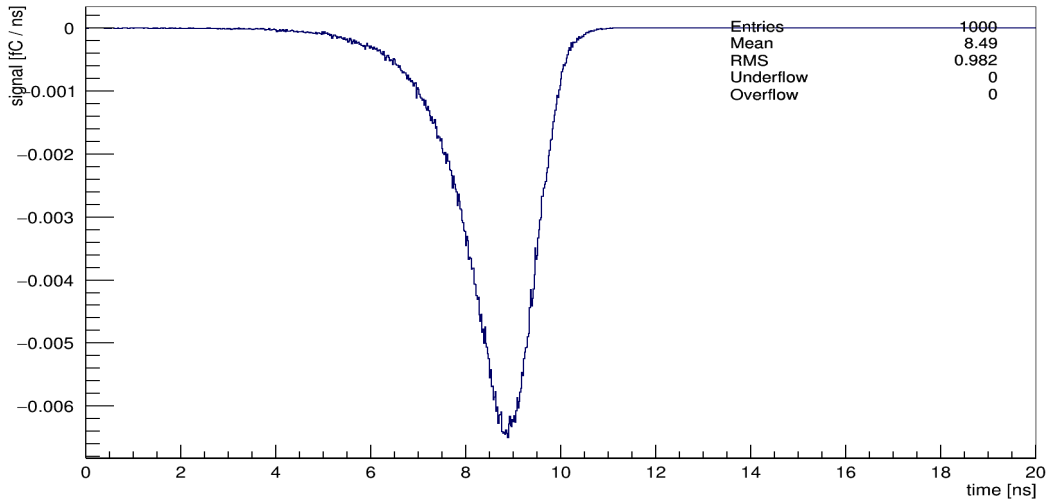

Figure 3.24 Signal of RPC at 30kV

CHAPTER 4

FABRICATION AND CHARACTERIZATION OF RPCs

4.1 Fabrication of RPCs

The task of prototype fabrication involves construction of three major components, (a) the gas chamber, (b) the resistive electrodes and (c) the read-out panels, to be followed by their assembly. Each of these steps are discussed separately in the following.

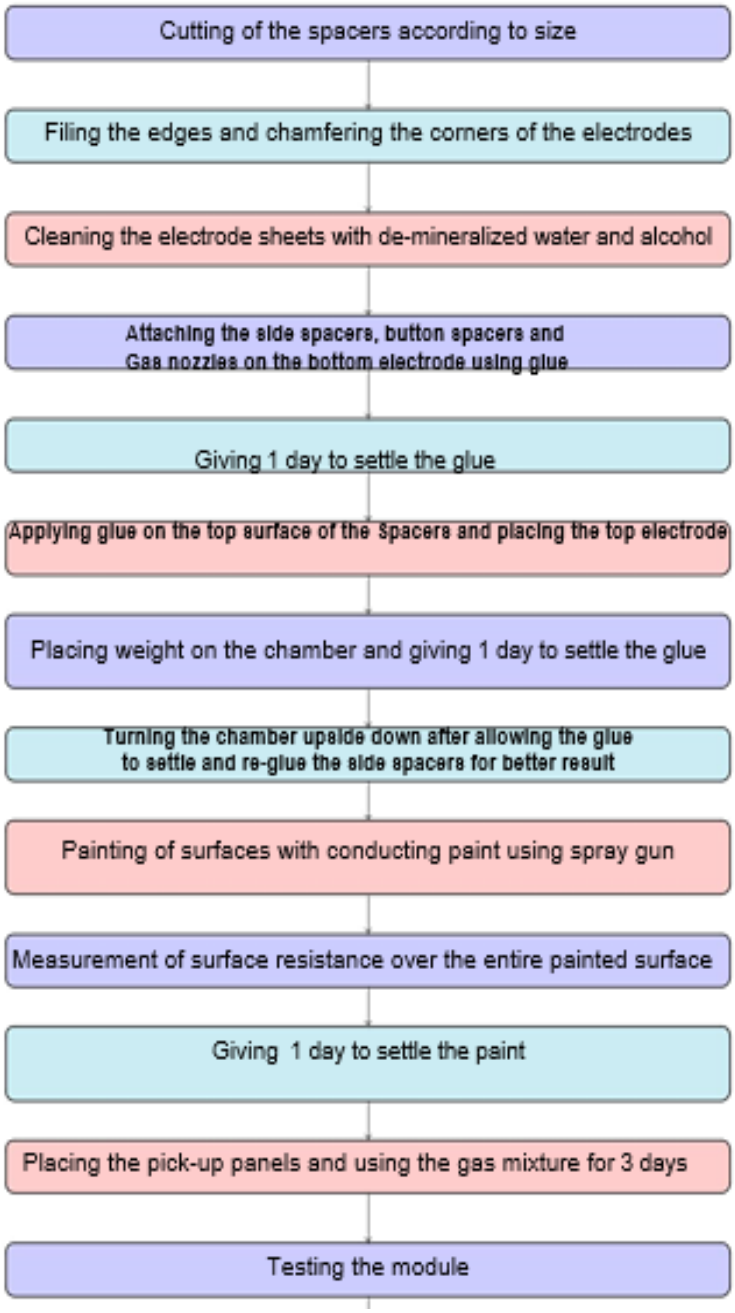

Figure 4.1 Flow chart of fabrication of RPC

4.1.1.Fabrication of gas chamber

The following steps describe the building of the gas chamber of the prototype with a height of 2 mm which acted as the active volume for detection. The mechanical structure of the gas chamber with all the components is schematically shown below

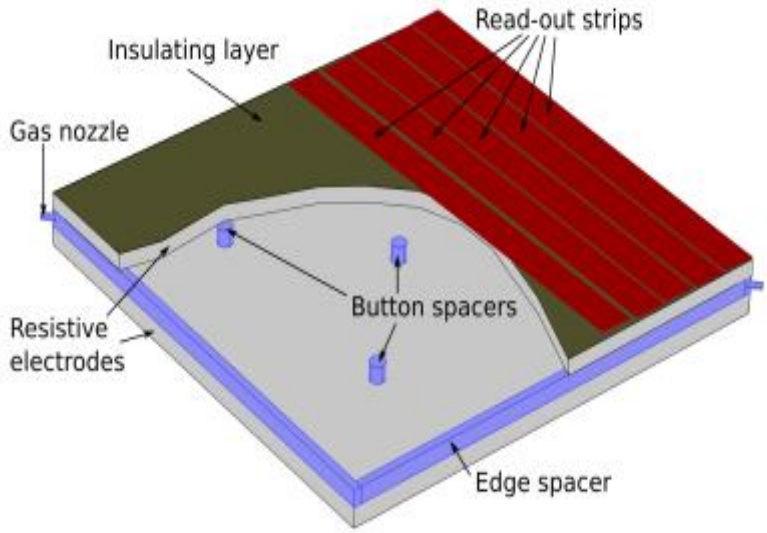

Figure 4.2 Schematic diagram of RPC structure

The electrode material (glass or bakelite) are cut in the VECC Workshop in appropriate size .A jig of right dimension is used to chamfer the four corners. This was done to make a perfect the 45^0 angle. Then the material, side spacers, polycarbonate made button spacers, gas nozzles (act as corner spacers) are cleaned with utmost care using alcohol. Four pieces of straight edge spacers along with four corner pieces with a width of 8 mm and a height of 2 mm, same as that of the gas chamber, were fabricated using polycarbonate material. They were used for enclosing the gas chamber between the electrodes and holding the bakelite plates at a separation of 2 mm.

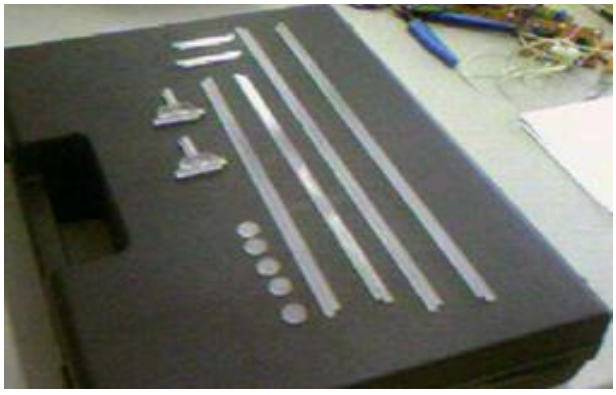

Figure 4.3 Spacers used in fabrication

Five polycarbonate button spacers of diameter 1.1 cm and thickness 2 mm were made in addition which were fixed inside the gas chamber to maintain the uniformity of the gap between the bakelite plates. A specific arrangement was followed to place them in order to maintain a proper gas flow. In figure 3.2, all the spacer components used to build the gas chamber are displayed along with their mechanical drawings.

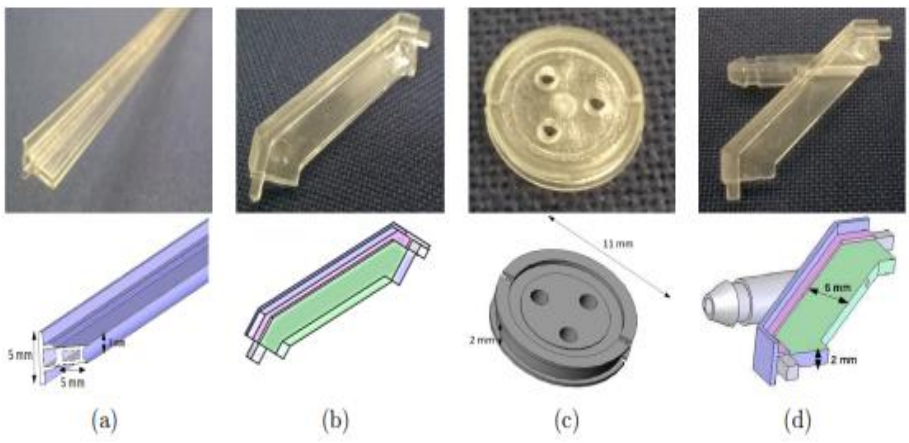

Figure 4.5 Different type spacers and their mechanical drawing (a) side spacers, (b) corner spacers, (c) button spacers , (d) gas nozzle

The spacers are glued on to the electrodes by making the glue of Dobeckot 520F Resin and Hardener 758 in a ratio 10:1 Then the other electrode plate is placed on this arrangement of polycarbonate made spacers. This created the 2mm gas gap of the RPC.

Figure 4.6 Placement of side and button spacers

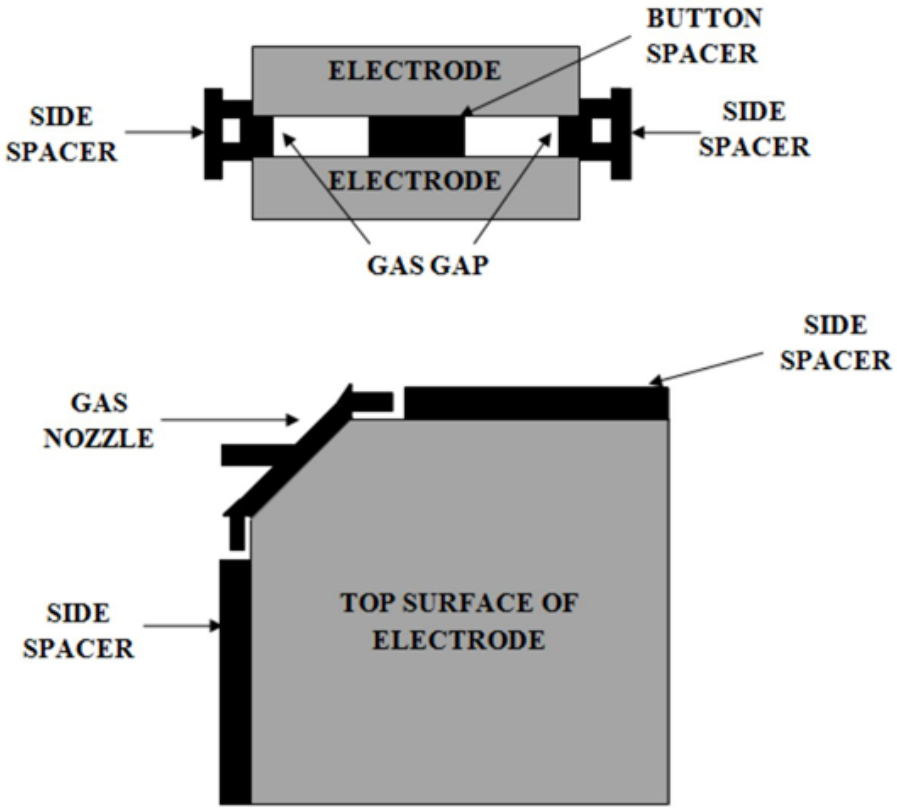

Figure 4.7 Diagram showing the position of different spacers during RPC fabrication

. To put a uniform weight throughout the area, the whole set up is sealed by using clippers and weights. The set-up is left for six hours to fix the spacers.

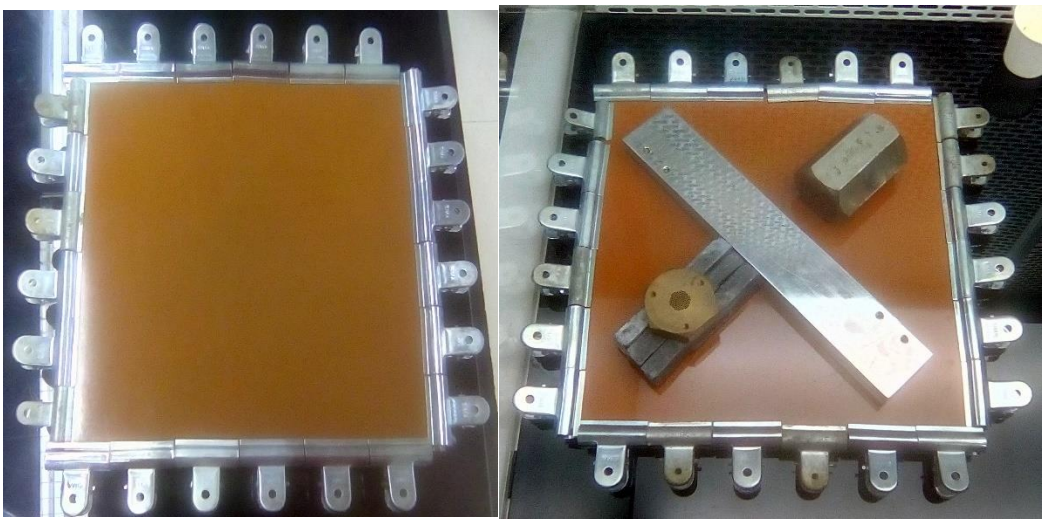

4.8 Weight kept on the upper plate of the RPC

4.1.2. PREPARATION OF RESISTIVE ELECTRODES

Preparation of resistive electrodes In the following, the steps to prepare the resistive electrodes of the prototype are described. The bakelite plates were converted to electrodes by coating them with conductive layers in order to supply high voltages to them. After cleaning the outer bakelite surfaces of the gas chamber with isopropyl alcohol, they were coated with a conducting paint. The electrode material used is highly insulating and in order to make a uniform electric filed inside the gap, a conducting layer (graphite paint) is coated over the outer surfaceA mixture of dry colloidal graphite and Industrial lacquer in a ratio of 1:1 is used and applied on the chamber by using a spray gun. Once the surface is coated, the tapes are removed and the resistivity of both surfaces is measured using a resistance measurement jig. It is desirable to obtain the average resistance value over the surface of ~1MOhm. Before applying the paint, the electrode edges are taped over (~1cm) with masking/kapton tape to prevent the conductive coating to be painted right up to the edge of the glass so that leakage of high voltage does not take place through the edge spacers. To ensure that the detector is leak proof, gas (any of our choice) is flowed through the chamber and the leak is checked by ensuring that the bubbles are produced in the isolation bubbler. If the leak is detected, then re-gluing is done on the edge spacers.

Figure 4.9 Pictures of RPC after painting with graphite paint and covering the surfaces with Myler sheets.

4.1.3 PREPARATION OF PICK UP PANELS

Pick-up panels, for signal collection are kept on the outer electrodes of RPCs . The charges produced inside the detector volume are result of passage of a charged particle induces signal on the strips of the pickup panels. Pick-up panels are designed using a dielectric medium between two metallic layers. We have used pick-up panel (30cm x

30cm) made up of copper strips of dimension 2.3 cm x 30 cm with a gap of 2mm in between them . Kapton sheets are used between the graphite coated electrodes and pick-up panels to avoid the direct contact between the two.

Figure 4.10 Different steps of fabrication of readout strips

The avalanche multiplied electron signals are induced on the external pickup strips. Each pick-up strip has dimensions (30cm x 2.3cm). Itching is being done with the anhydrous iron chloride (FeCl3) solution to maintain the gap of 0.2cm between the copper strips in the pick-up panel. Figures above illustrates different steps taken in the itching process and figure below shows the actual image of the pick-up strips.

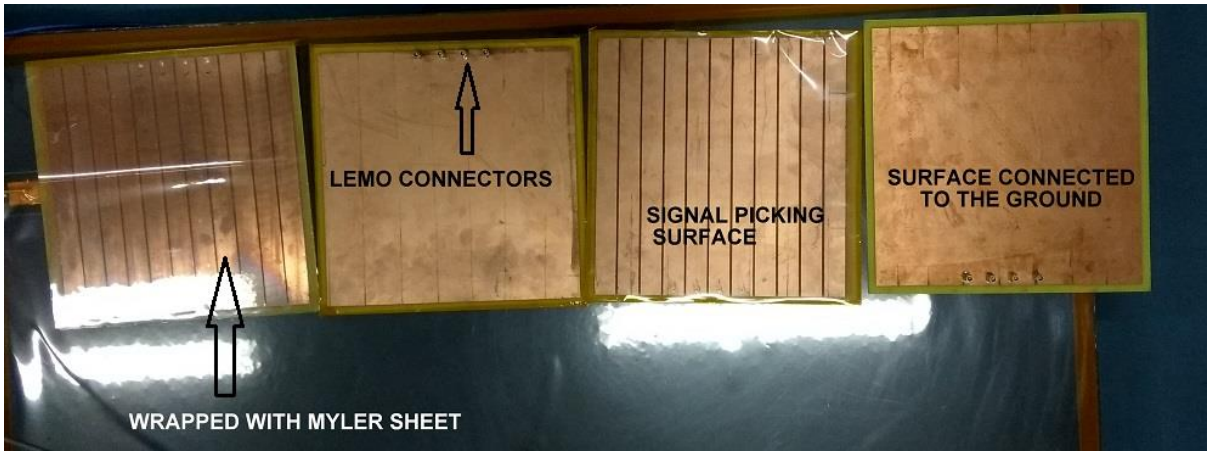

Figure 4.11 Fabricated readout strips

4.2 Basic Characterization of RPCs

After fabrication of six identical bakelite RPCs it is required to characterize them .

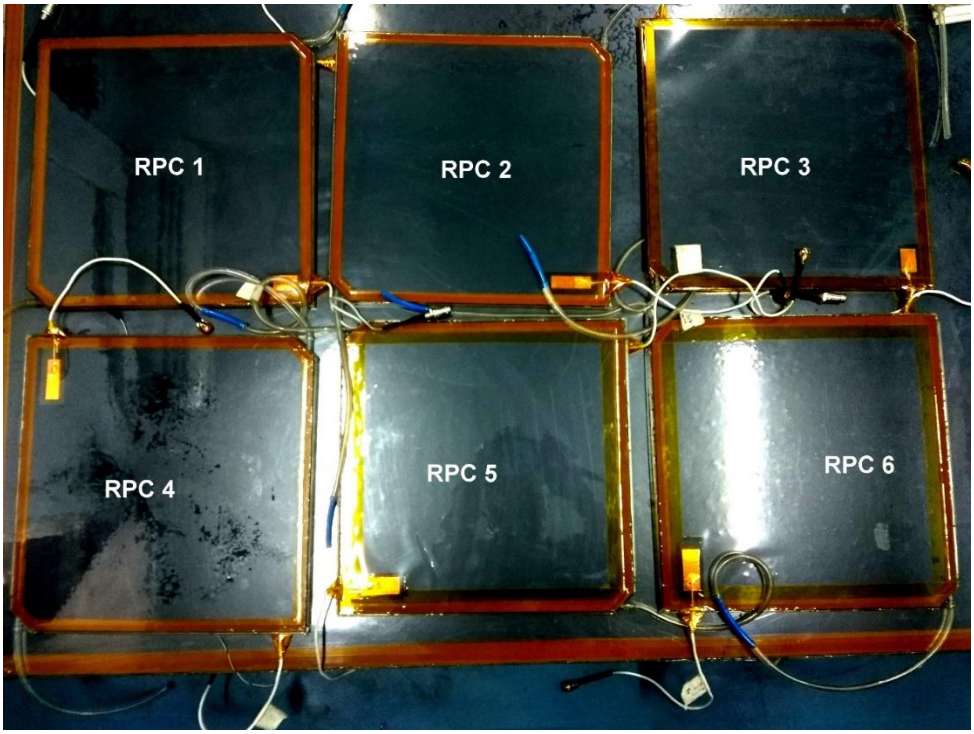

Figure 4.12 six bakelite RPCs after fabrication

4.2.1 Gas Leak Test: After gluing the spacers and the gas nozzles, leak test is performed to ensure against the leakage of gas through the detector. This test is performed by flowing a gas (freon or isobutane) at slightly higher pressure then the atmospheric pressure using gas leak detector. Wherever there is a leak, re-gluing is done on those areas.

Figure 4.13 Safety bubblers showing no bubble implies that the chamber is leak free.

4.2.2 SURFACE RESISTIVITY

The setup used while measuring surface resistivity is illustrated in figure below. Two electrodes are placed keeping contact with the surface of the graphite coated bakelite at a known distance apart (in this case, it was 5cm). A potential difference is then applied & the corresponding current is measured. The surface resistivity is measured by factoring in the width of the electrode (w) and the distance of separation between the electrodes

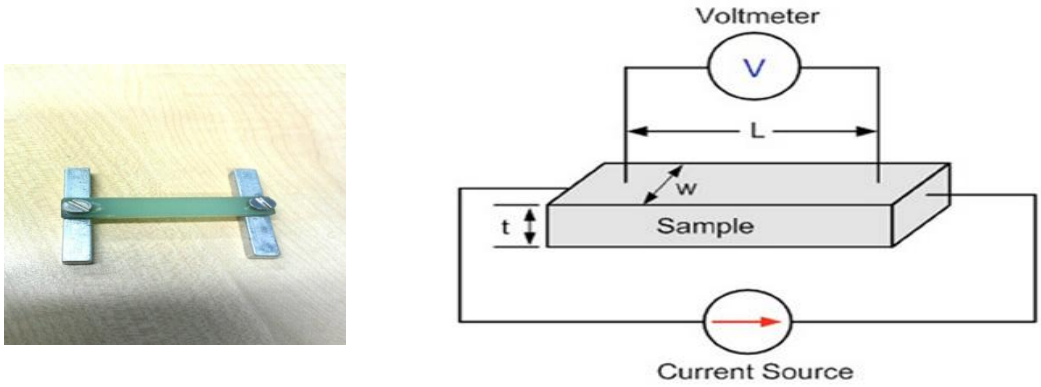

Figure 4.14 Picture of the jig used in measurement and schematic diagram of surface resistance measurement set up.

Surface resistance profile are plotted for all the surfaces of the six RPCs. The plots are given below From fig-4.15 to fig 4.25.

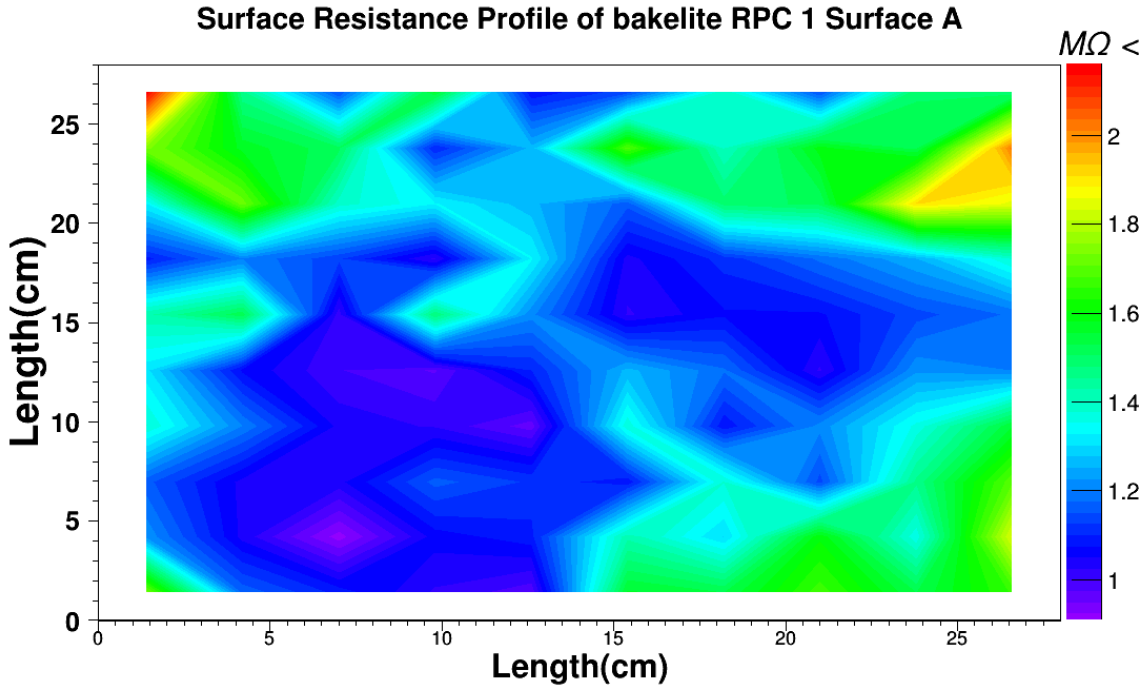

Figure 4.15

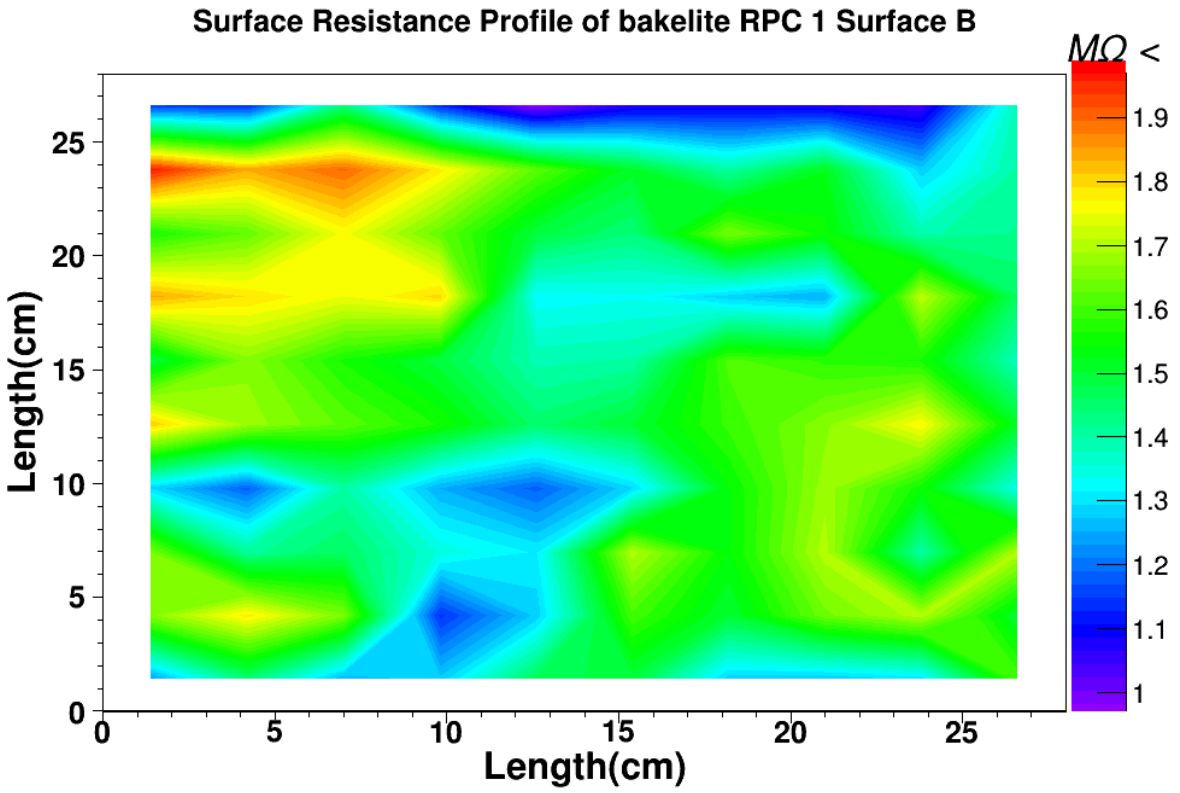

Figure 4.16

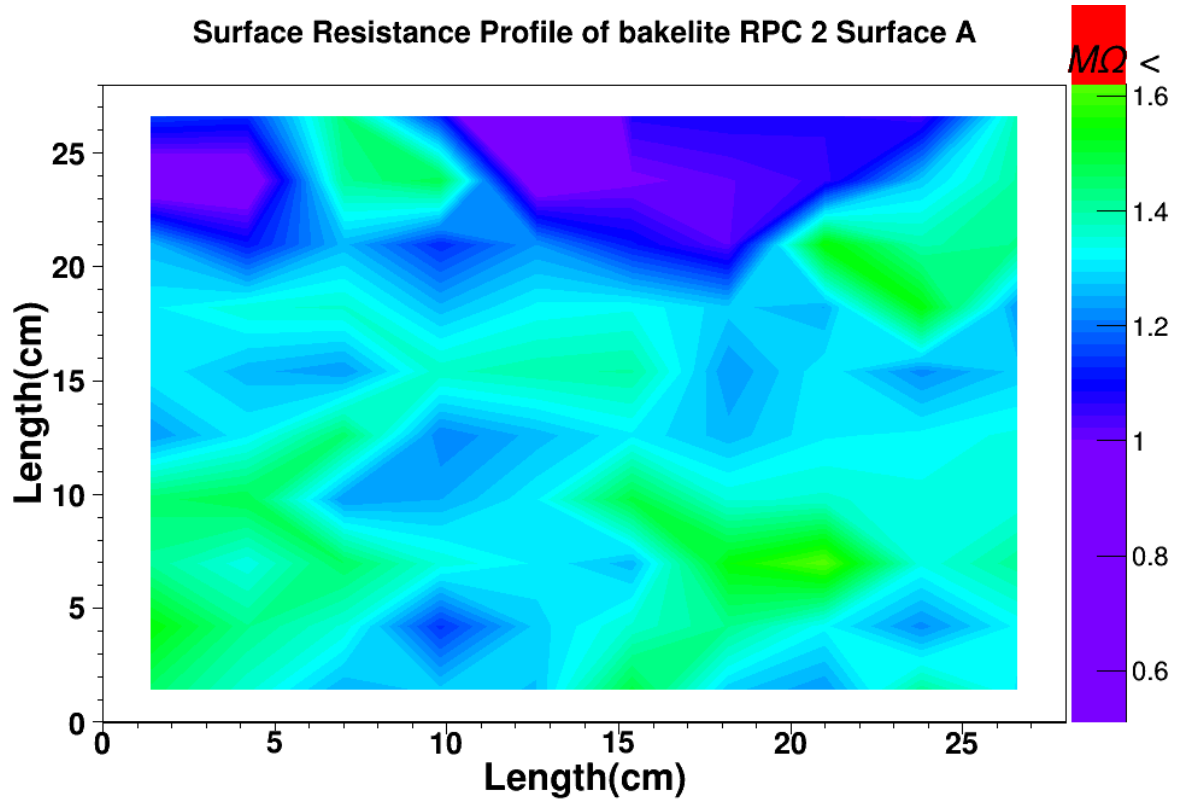

Figure 4.17

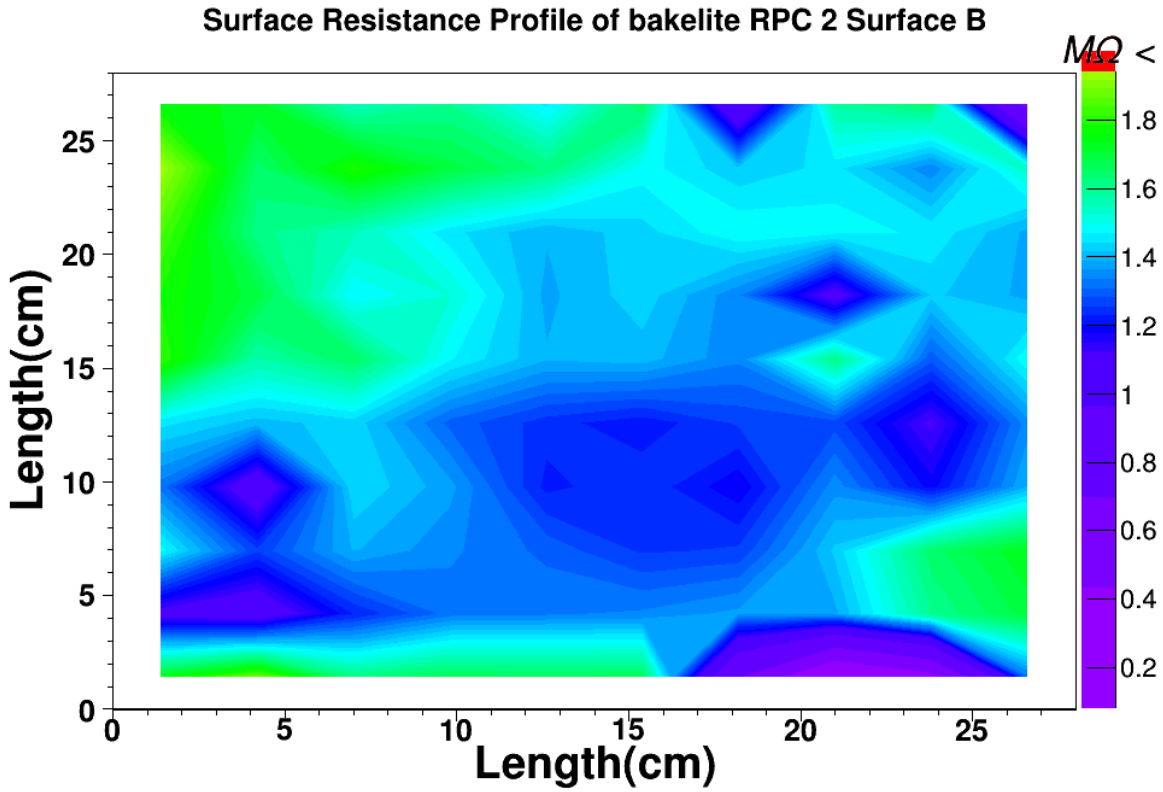

Figure 4.18

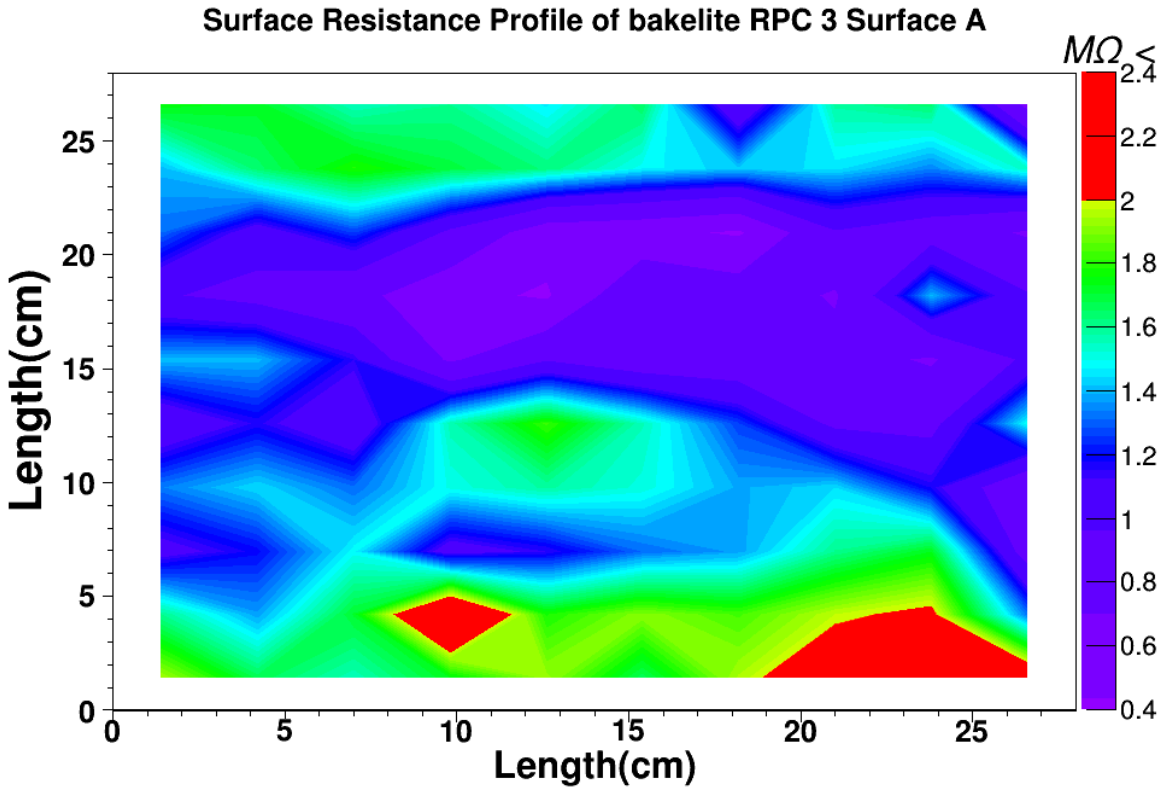

Figure 4.19

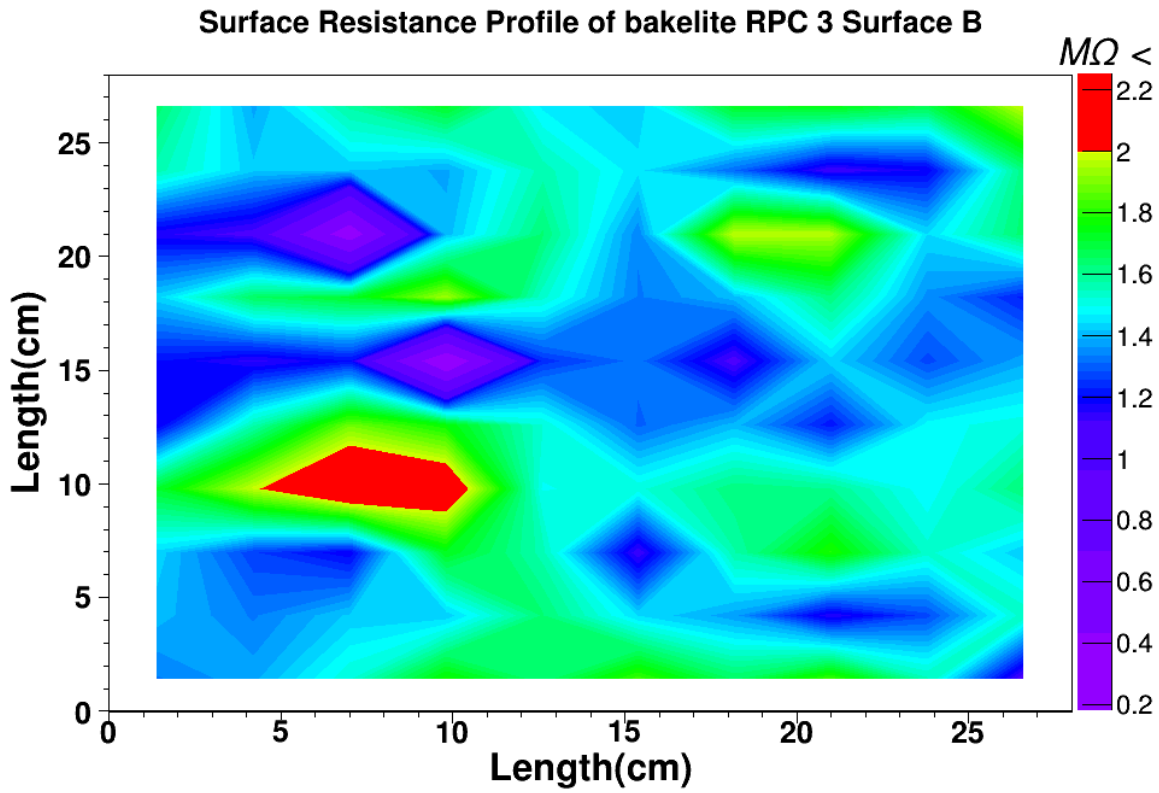

Figure 4.20

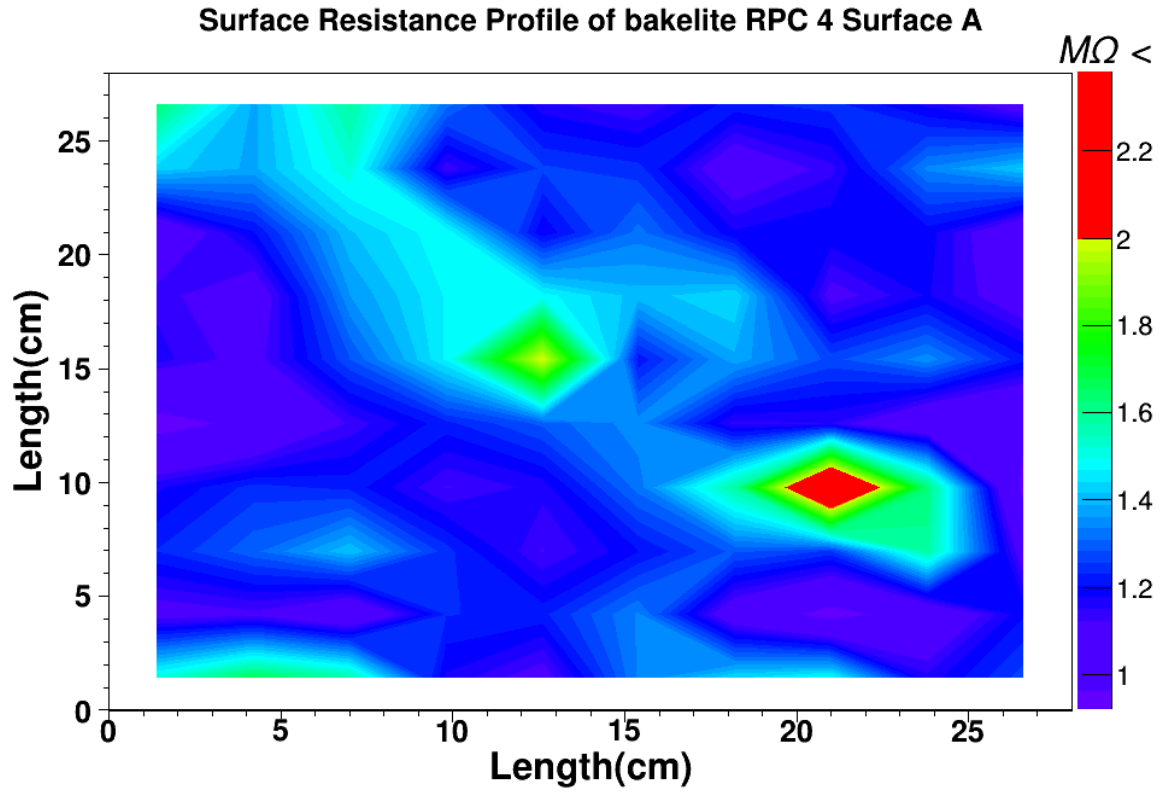

Figure 4.21

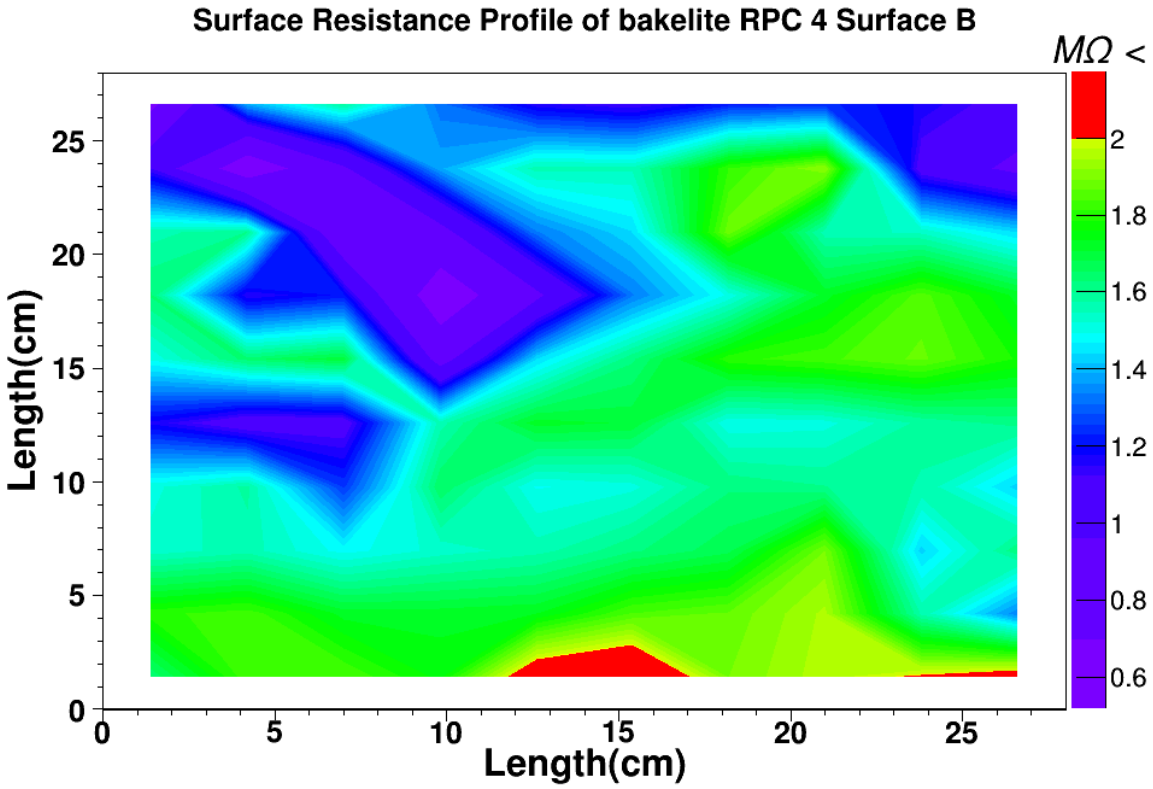

Figure 4.21

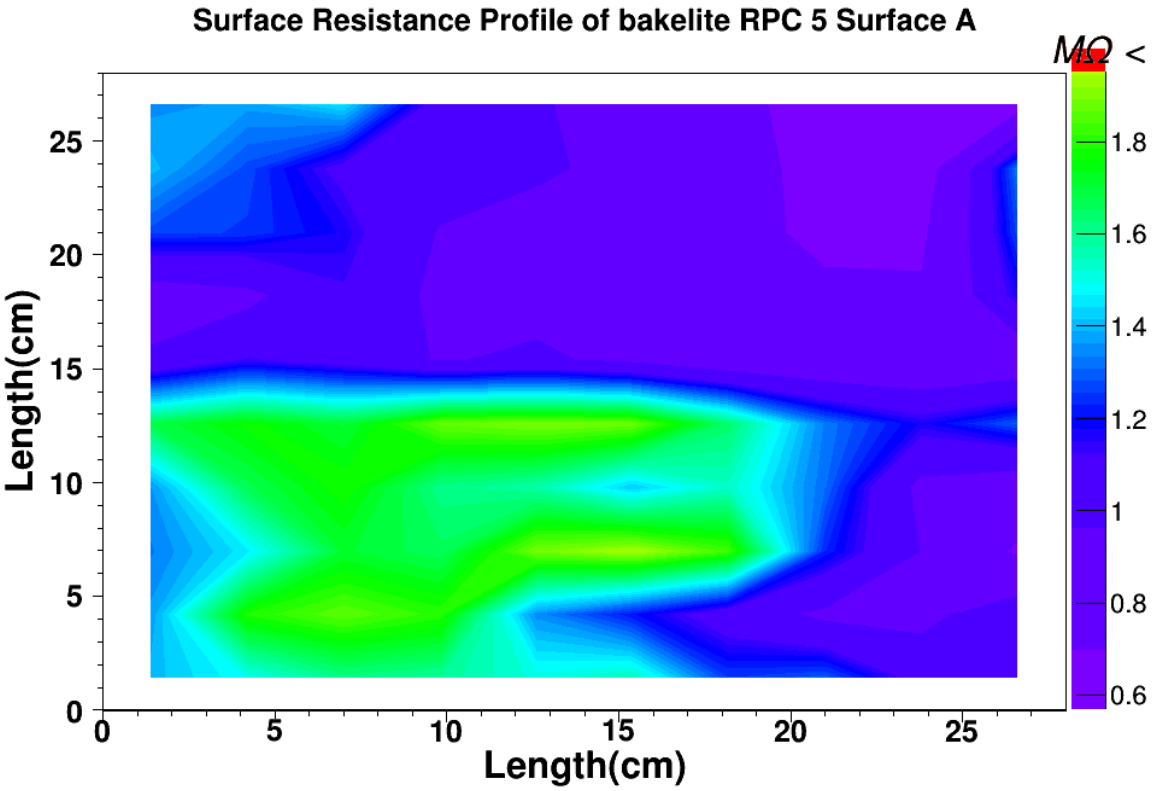

Figure 4.22

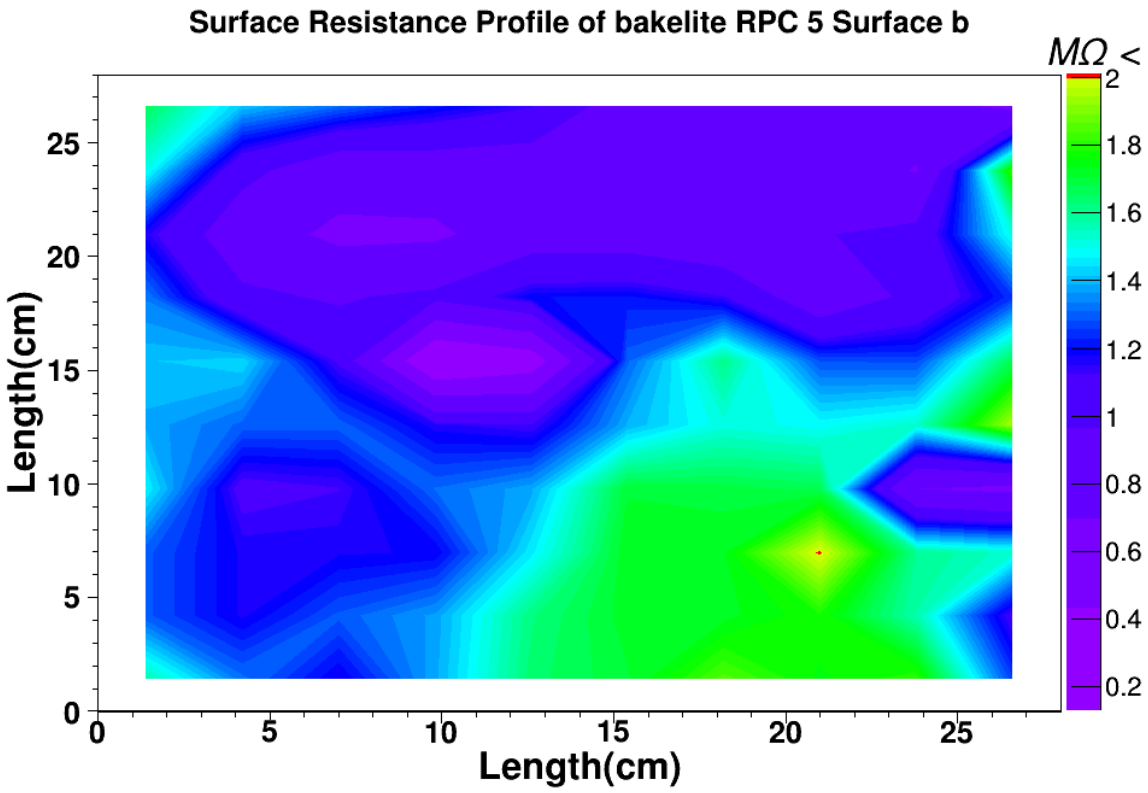

Figure 4.23

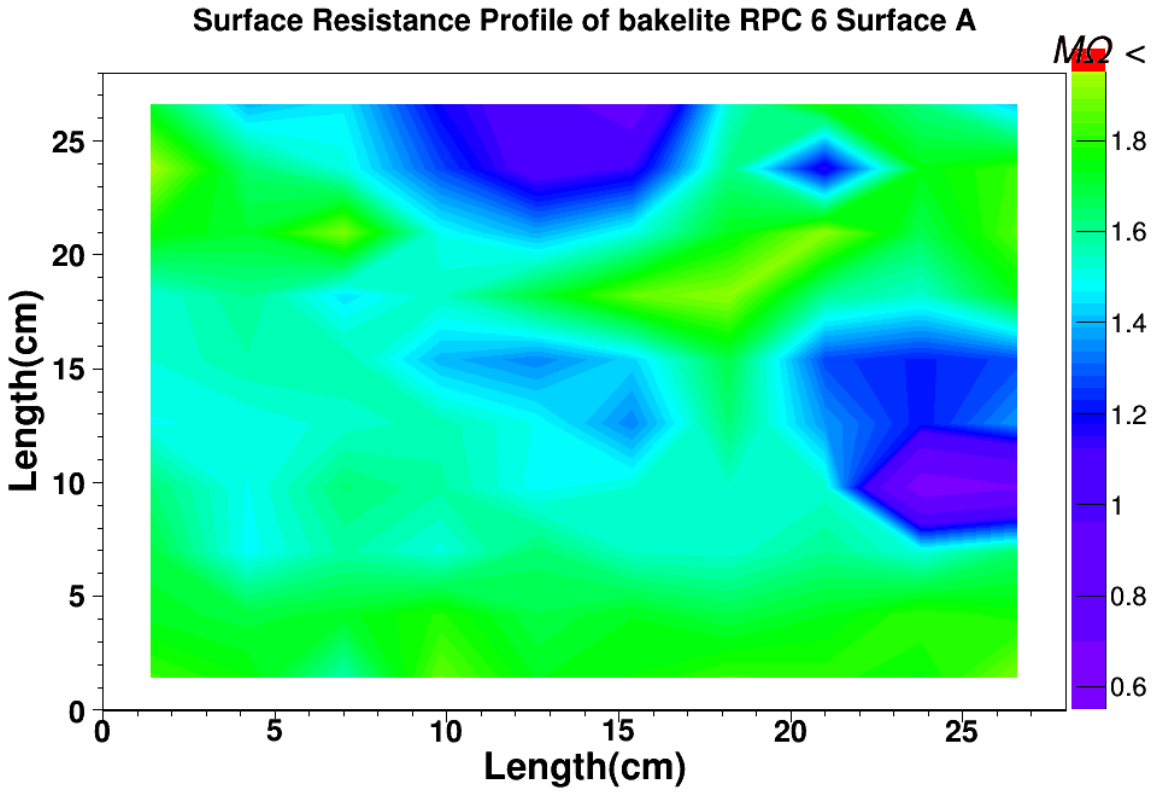

Figure 4.24

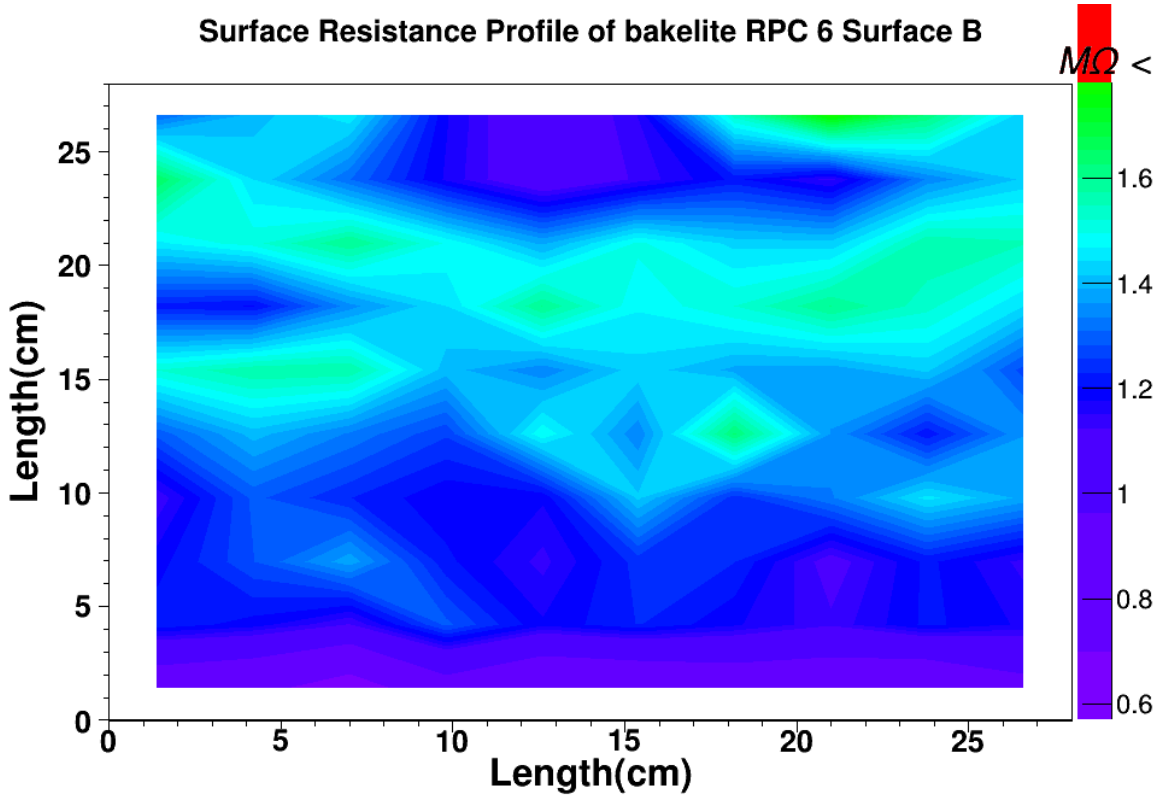

Figure 4.25

4.2.3 I-V CHARACTERISTICS

A severely important parameter for testing the required performance of the gaseous detector is to know about the leakage current of the detector at varying voltages. Leakage current is the rate of flow of discharge that develops and flows through the gas-gap of Multi-gap RPC. Figure 3.10 shows an equivalent RPC circuit. Any RPC gas-gap contains two primary resistive components i.e., highly resistive spacers (shows Ohmic behavior) and ionization gas (behaves as a Zener Diode), both of which are connected in a parallel combination.

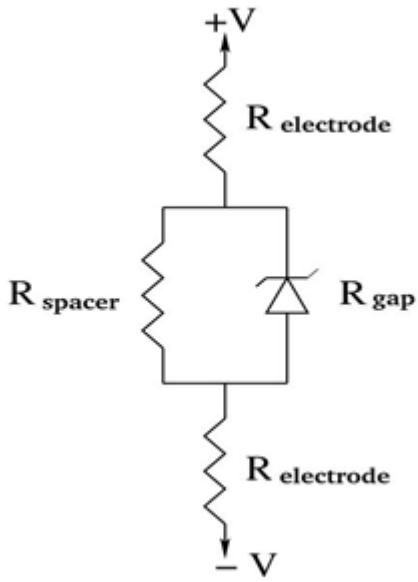

Figure 4.26 Schematic of RPC gas gap and its electric resistance

Since at lower voltages, primary ionizations don't develop any avalanches and discharge, gas-gap offers infinite resistance and the current passes through the spacers. Therefore the slope over this region gives the conductance of the polycarbonate spacers

$$R_{gap} \approx \infty,\ R_{spacer} >> R_{plate} \Rightarrow dV/dI = R_{spacer} \qquad (4.1)$$

Breakdown of the curve occurs where there is quick increment in the curve and current increases. This is because the ionization gas provides a conducting path to the current. So, in this case, the current which is flowing through the chamber is determined by the electrode resistance.

$$R_{gap} \approx 0 \Rightarrow dV/dI = R_{plate} \qquad (4.2)$$

IV characteristics of any detector mainly gives us information about the gas breakdown and the operating voltage upon which detector should be operated.

The I-V characteristics of the detectors are given below.

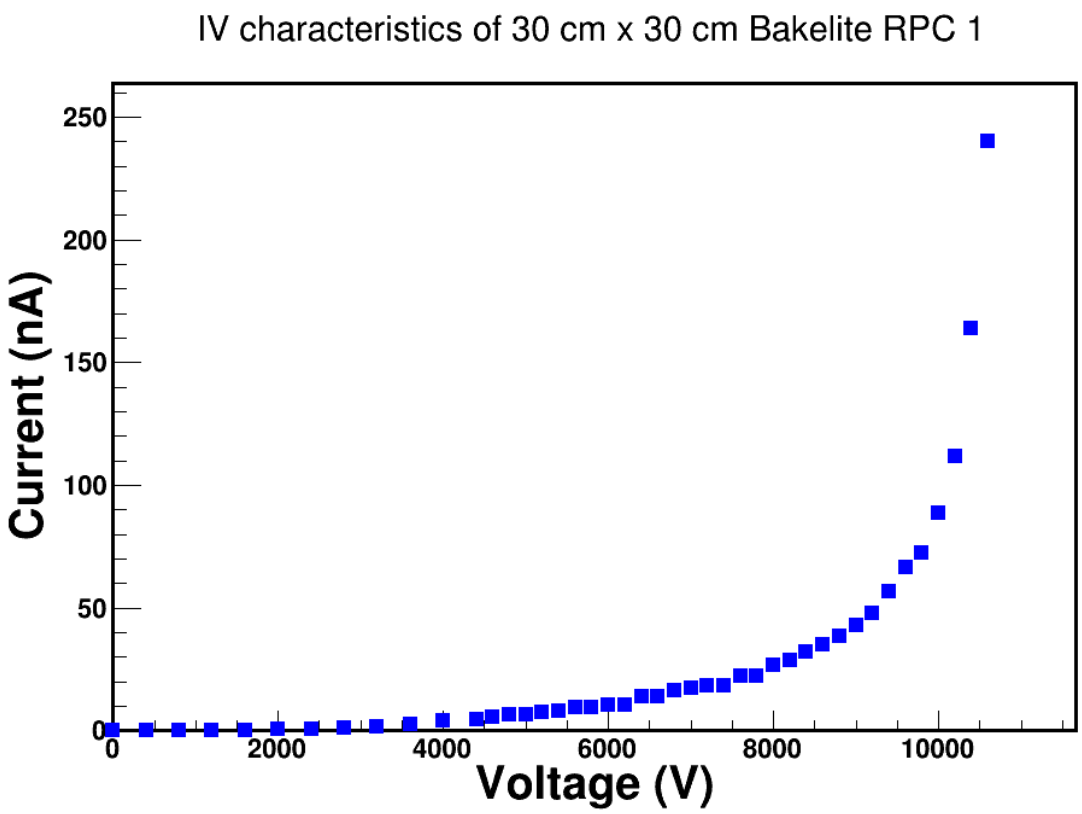

Figure 4.27 I-V characteristics of bakelite RPC 1

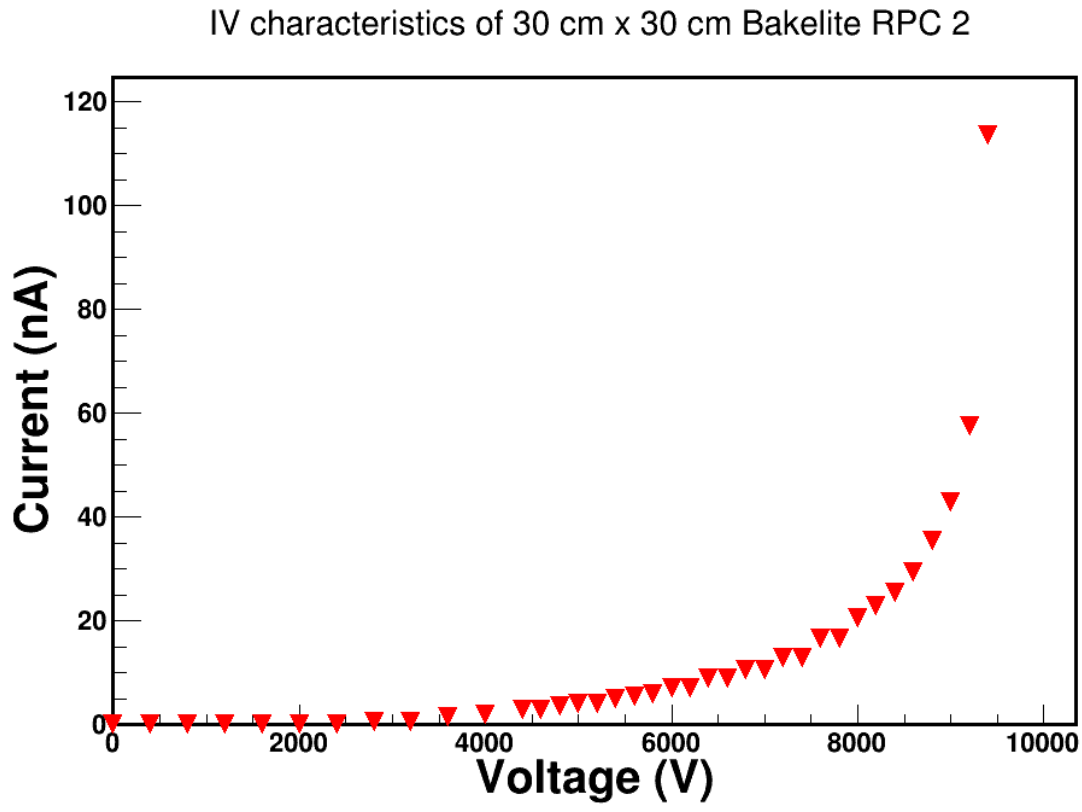

Figure 4.28 I-V characteristics of bakelite RPC 2

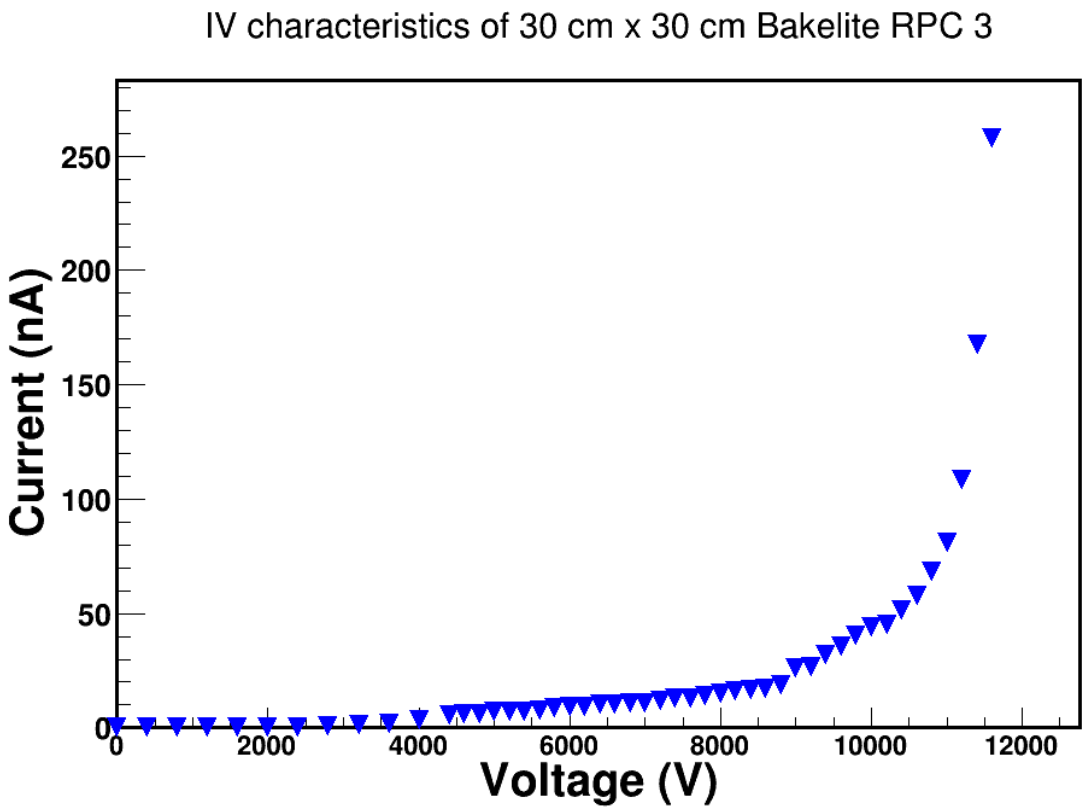

Figure 4.29 I-V characteristics of bakelite RPC 3

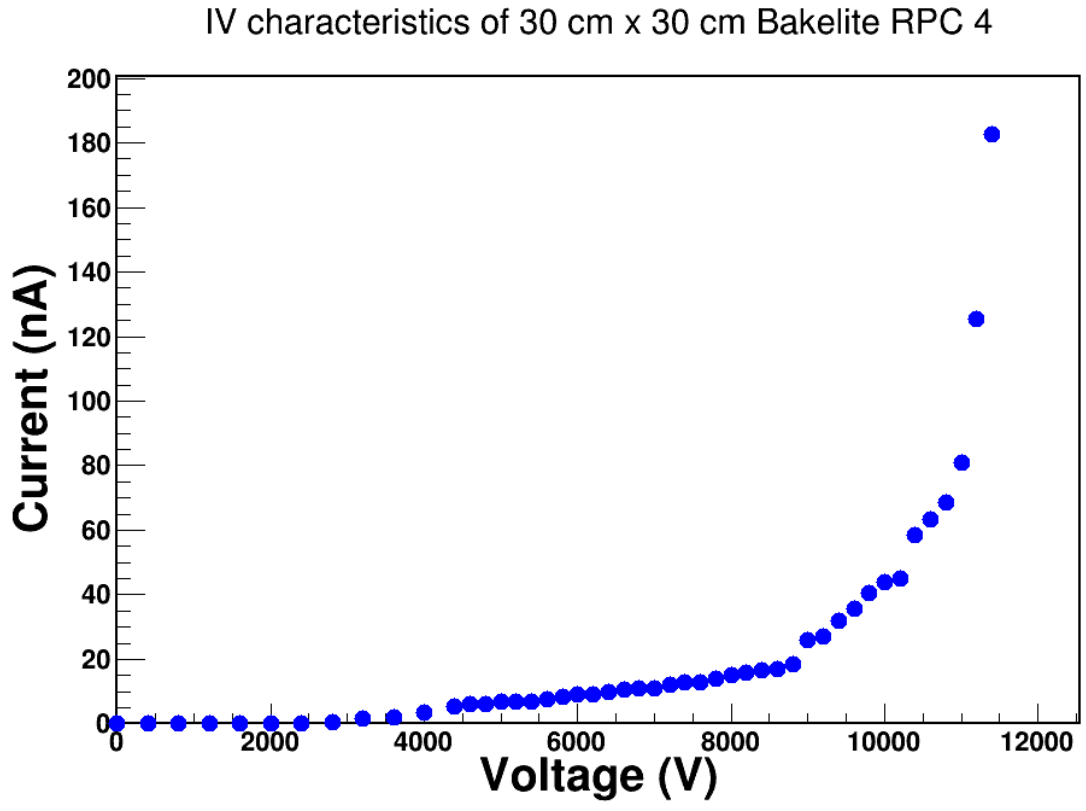

Figure 4.30 I-V characteristics of bakelite RPC 4

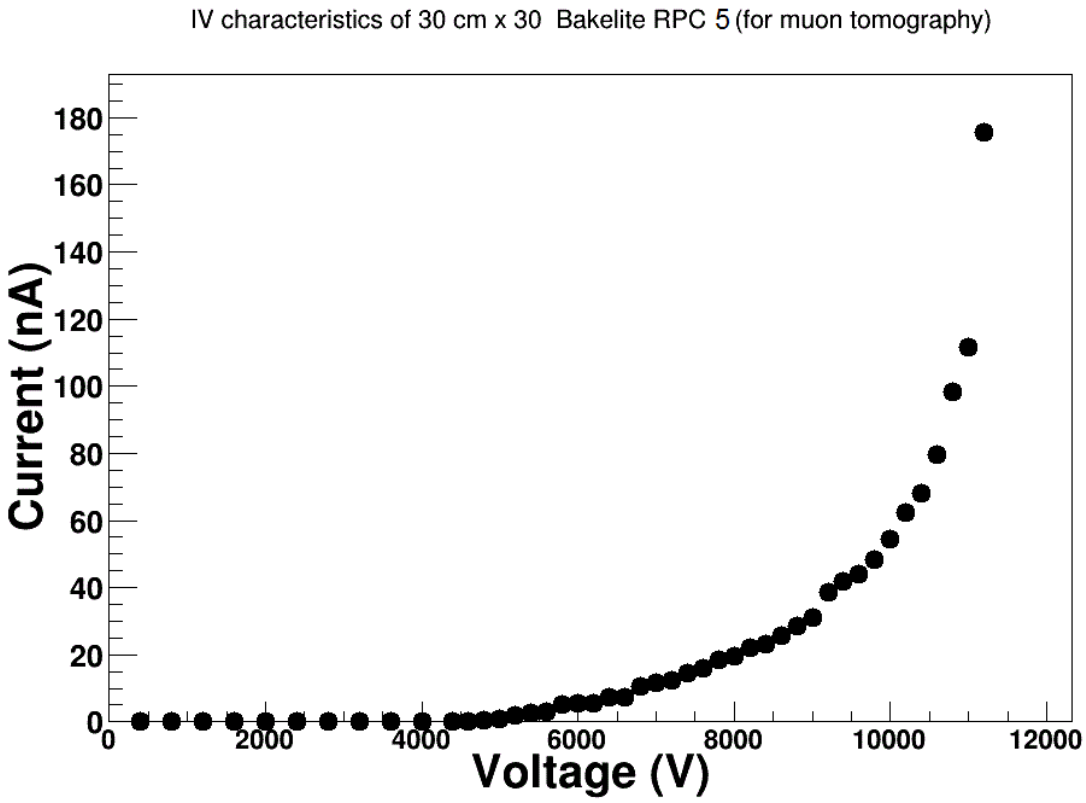

Figure 4.31 I-V characteristics of bakelite RPC 5

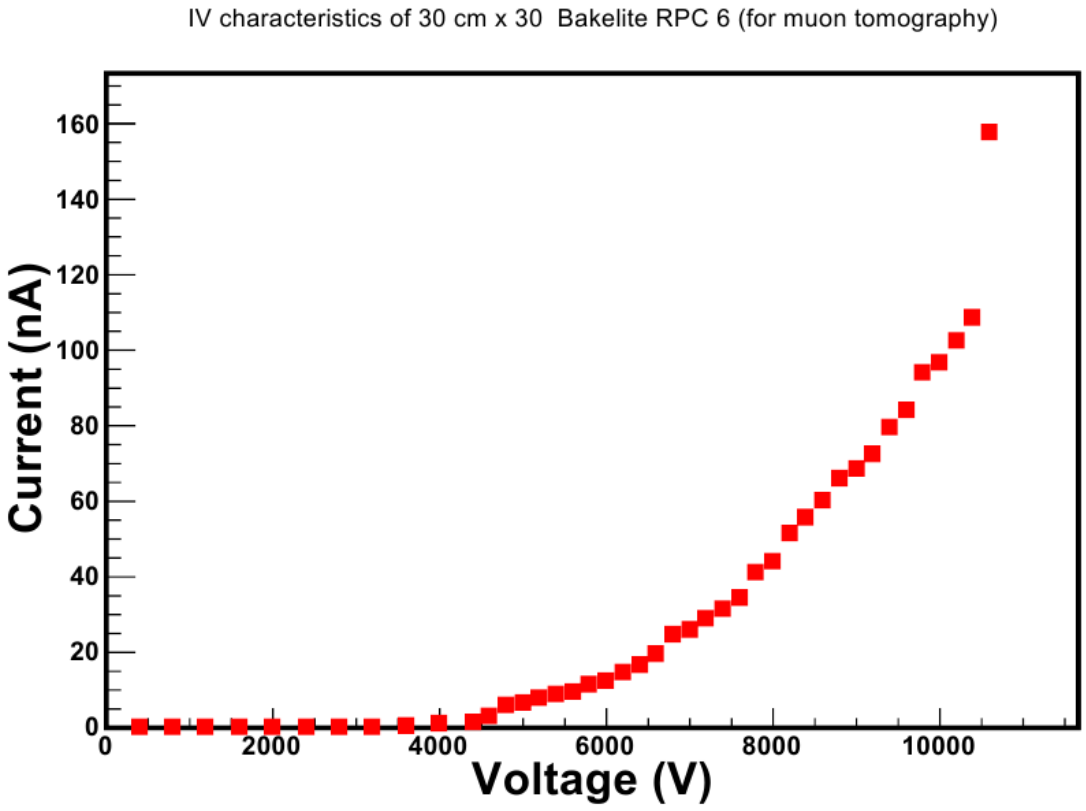

Figure 4.32 I-V characteristics of bakelite RPC 6

Observations from the plotted IV curve:

1. Firstly we get the Knee voltage from the plotted IV curve, i.e., the voltage at which current shows a sharp increase from its leakage (almost zero) value and in turn we get the **breakdown voltage** of the gases.
2. IV curve also gives us the information about the resistance. The slope of the plotted IV curve
   gives us the resistance.

$$\text{Slope} = \text{Current} / \text{Voltage} \qquad (4.3)$$

From Ohm's Law, we know that

$$V = IR \qquad (4.4)$$

Equation (4.3) and equation (4.4) says,

$$\text{Slope of IV curve} = 1/R = \rho \text{ (resistivity)} \qquad (4.5)$$

From the plotted IV curve, we find two regions: One is the region before the breakdown, i.e. low voltage region and the other region is the region after breakdown, i.e. high voltage region. So we need to find the resistance of both the regions separately.

In the region before breakdown, gases will not be conducting, so in that region, the resistance will be solely because of the spacers used.

$$\text{Slope} = 1/R = \rho \qquad (4.6)$$

Also,

$$\rho = (Rl)/A \qquad (4.7)$$

where,

R is the resistance we will get from the slope before the breakdown takes place.

l is the length of the spacer.

A is the total area of the spacer.

In the region after the breakdown, gas will start conducting. The resistance will be because of the gas as well as the thickness of the electrodes.

ρ (electrode) = ρ (overall resistivity of the chamber)= (R*l)/A
where,

R is the resistance we will get from the slope after the breakdown takes place.

l is the length of the electrode

A is the area

So, we can conclude that before the breakdown, the resistance will be the resistance of spacers and after the breakdown that will be of the overall chamber.

4.2.4 CURRENT STABILITY TEST

Resistive plate chambers were kept at a fixed voltage for 36 hours. The leackge current between the electrodes is measured . The detectors were connected to high voltage. The value was near to their breakdown voltage, which was obtained from the I-V curves.

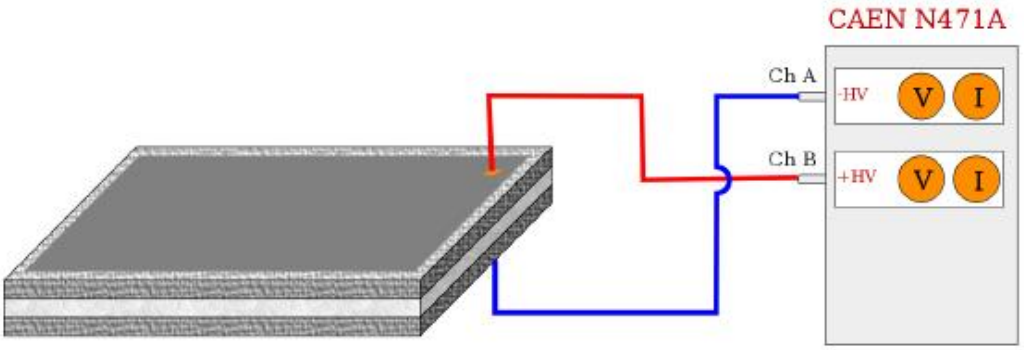

Figure 4.33 Schematic diagram of current stability set up with RPC and CAEN N71A high voltage module

Hourly readings were taken. Temperature and humidity was kept nearly constant during the experiment. The temperature of the laboratory was kept at 22 degree centigrade and the humidity was kept in between 40%-45%. The slight vaiation of current in the detectors is due to slight variation of humidity and temperature. The plots are given below.

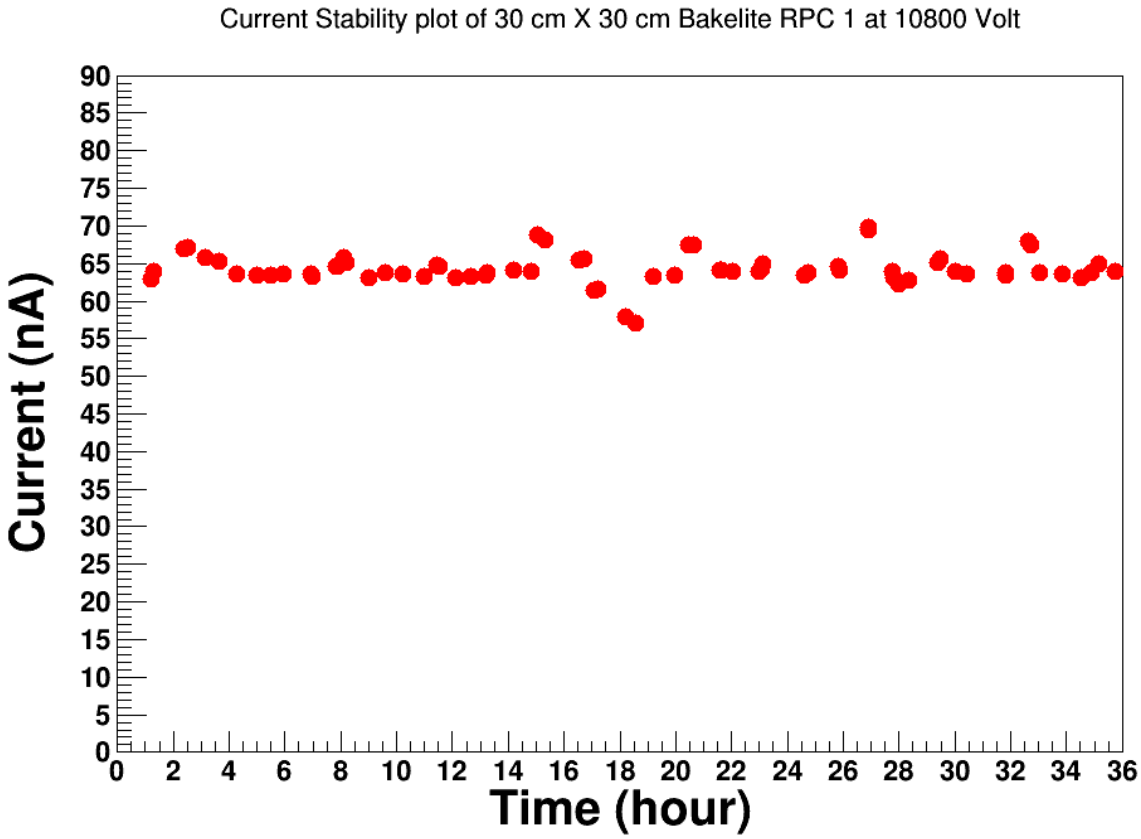

Figure 4.34 Current stability plot of RPC

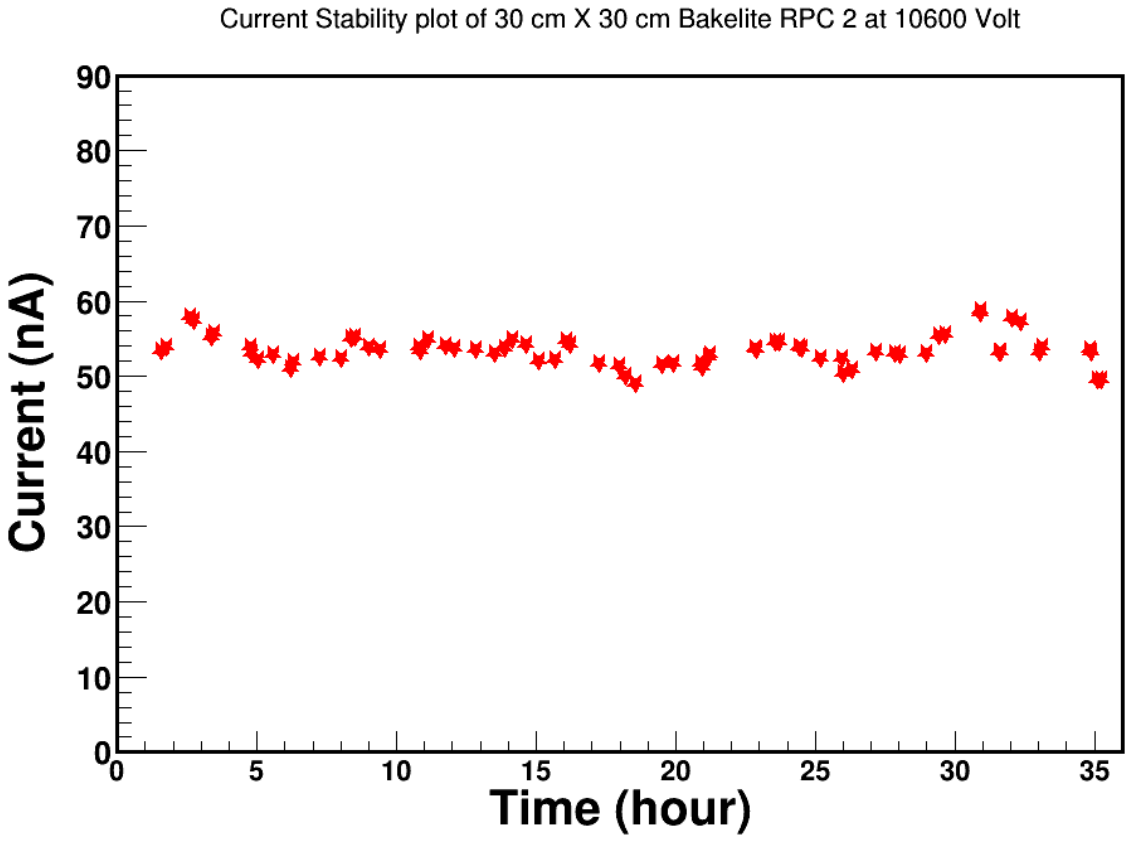

Figure 4.35 Current stability plot of RPC 2

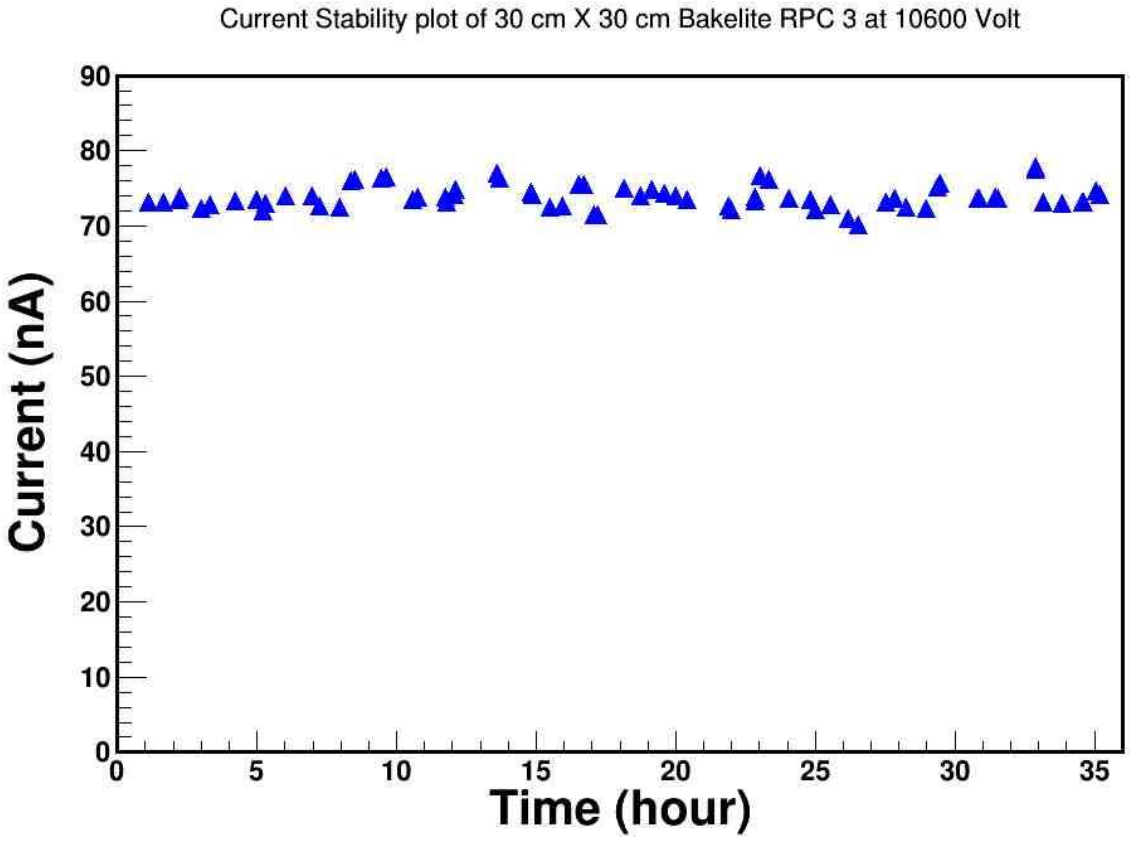

Figure 4.35 Current stability plot of RPC 3

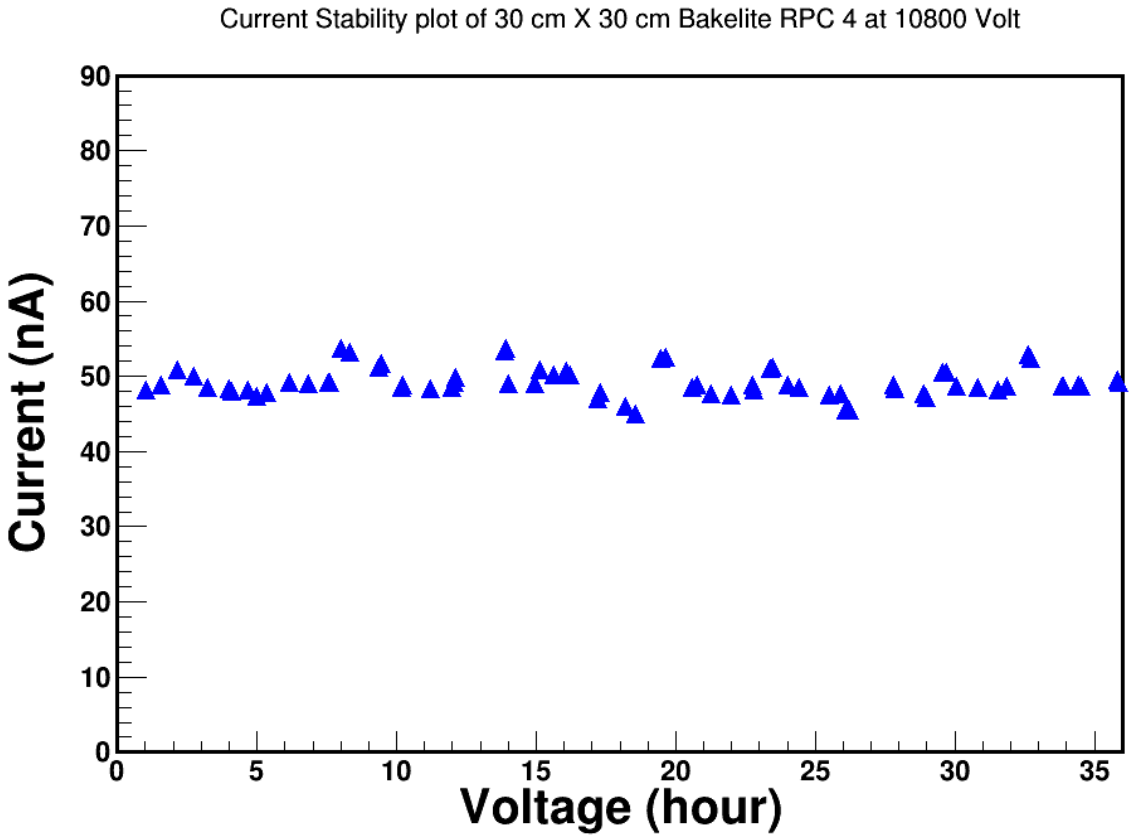

Figure 4.36 Current stability plot of RPC 4

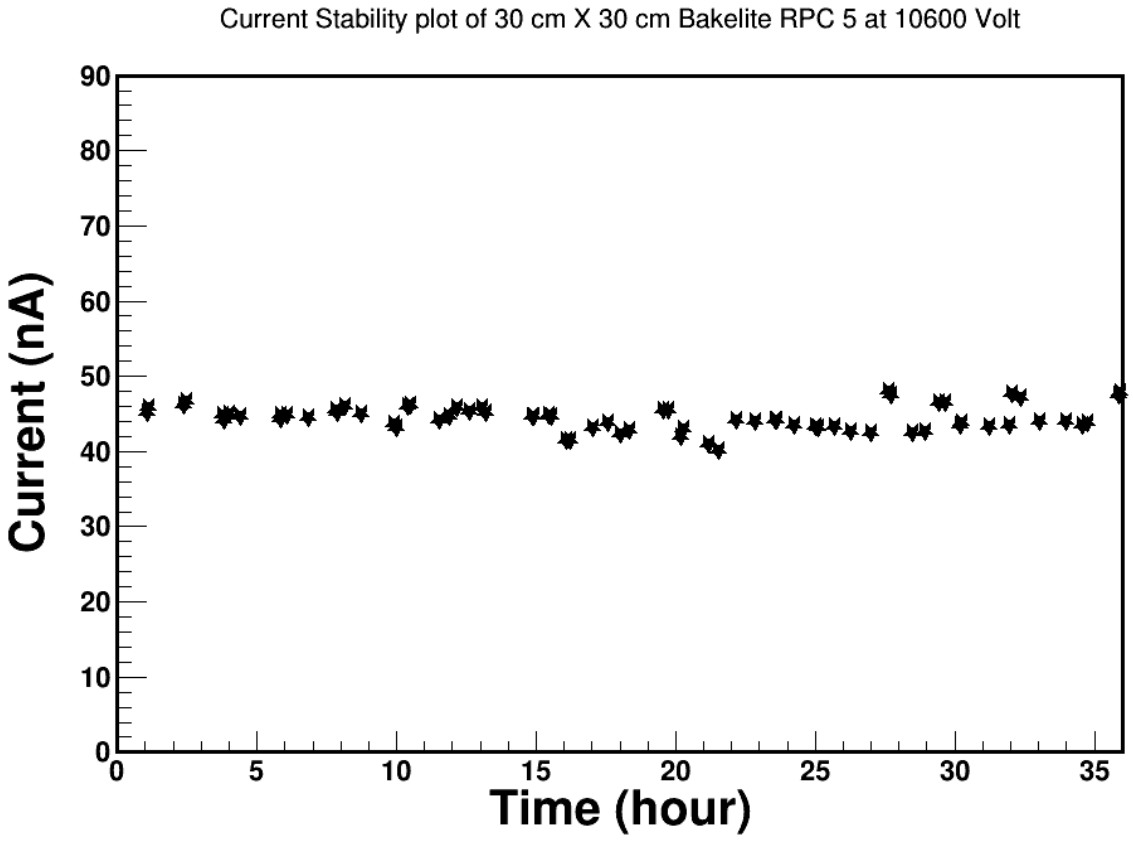

Figure 4.37 Current stability plot of RPC 5

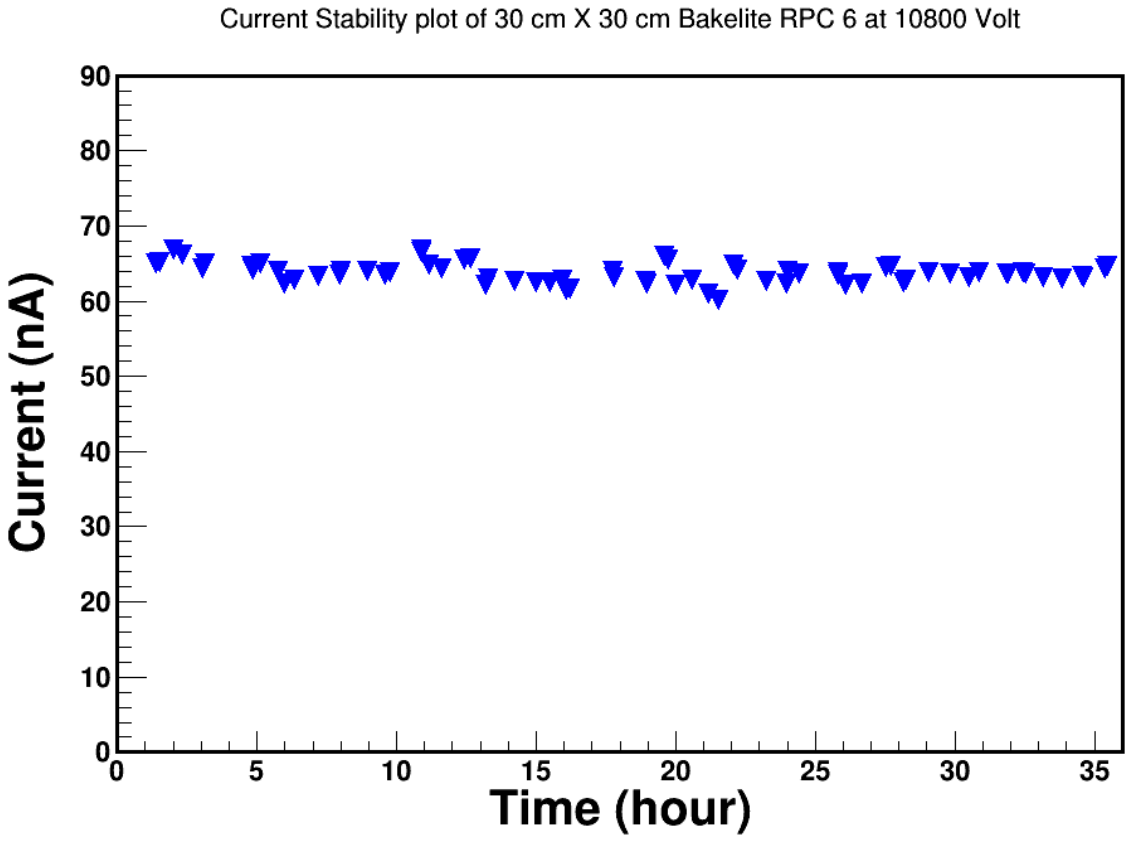

Figure 4.38 Current stability plot of RPC 6

4.3 FURTHER CHARACTERIZATION OF RPC USING DIFFERENT FRONT END ELECTRONICS

4.3.1 Testing of RPC-2 using PADI-ASIC front end electronics

Among the six detectors RPC-2 was taken to be tested with PADI-ASIC FEE. In the experiment CBMTOF, Front End ASIC PADI-6 is supposed to be used . PADI-6 does not have a pulse stretcher after the discriminator stage of the ASIC unlike NINO. Hence with very low input signals, digital output are not detected by conventional level translators like LVDS to LVTTL etc.

4.3.1.1 PADI-ASIC front end electronics

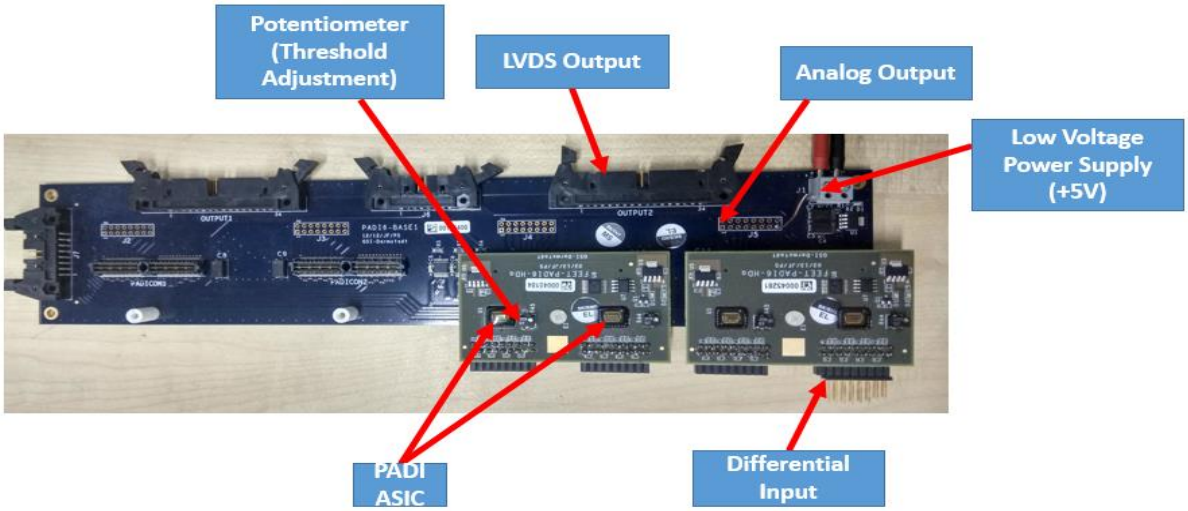

Figure 4.40 PADI-ASIC FEE board

GET-4 ASIC designed by CBMTOF group has this capability to detect such low signals but as at the time of this integration tests, GET-4 ASIC was not avilable at VECC. Apart from this, a test beam was planned to be taken at COSY-Juliech in Feb-18 where RPCs were planned to be tested with high particle rate. As the CBMTOF readout chain is too much complicated, we have built a custom made discriminator to feed the PADI output to further process the signal.

The ouput signal from this discriminator can be coupled by conventional electronics to find out efficiency and other basic parameters of RPCs in this test beam. Digital output from the PADI has been fed to a custommade fast Leading Edge Discriminator with adjustable delay and width output.

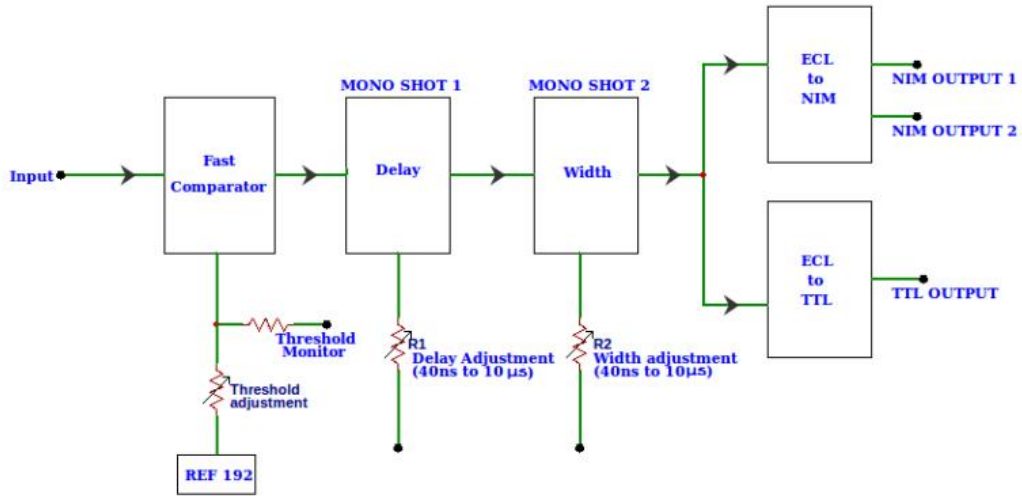

Figure 4.41 Schematic diagram of ustom made fast leading edge discriminator

It comprises of a fast ECL comparator, two monostables, to provide delay and width generation and subsequently gives two NIM standard outputs and a TTL output. In the heart of the unit,a fast comparator MAX9600 has been used. It has a maximum propagation delay of 500 ps, dispersion of 30 ps and also a tracking frequency of 4 Gbps.This IC also has a provision for hysterisis adjustment which is useful for preventing oscillation or multiple transitions due to noise. A voltage reference REF192 has been used to provide necessary voltage reference to the fast comparator with ultra low noise and good stability. This reference IC has a temperature coefficient of 5 ppm/ ◦C. The threshold of the comparator can be set from +50 mV to + 2.5V which can be adjusted by a multiturn trimpot. Both the delay and width of the output have a range of 10 ns to 40 µs adjustable via trimpots R1 and R2 respectively. The block diagram of the discriminator has been shown in fig4.41.

4.3.1.2 EFFICIENCY vs. VOLTAGE PLOT

Three paddle scintillators and one finger scintillator is used for trigger signal.A detector RPC-2 was selected randomly for testing with PADI-ASIC FEE and to compare the result after testing the same detector using NINO-ASIC FEE. The RPC-2 was connected with charge sensitive preamplifier the output of which is fed to the input of PADI-ASIC through a capacitive coupling of 820pF. The four coincidence signals from the scintillators are formed using leading edge discriminator and a logic unit. The four fold signal from these scintillators and 5 fold signal by adding discriminated RPC signal is used for efficiency measurement. The experimental set up is shown with block diagram.

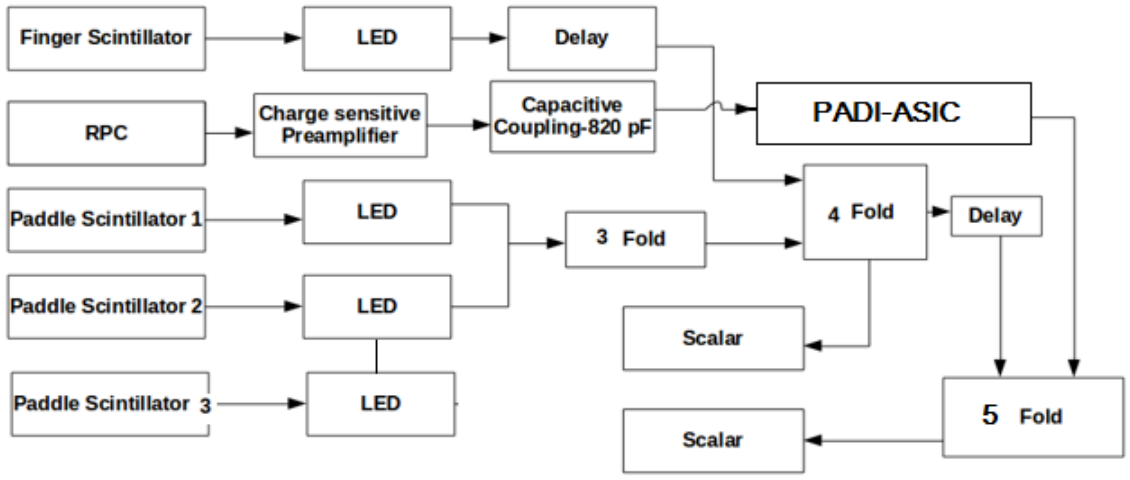

Figure 4.42 Block diagram of experimental arrangements for efficiency vs voltage and noise rate vs voltage measurement using PADI-ASIC FEE

The detector has shown promising results in avalance mode using PADI as FEE. It is seen from Fig4.43 that the efficiency plateau starts at 10500 Volt with above 90% efficiency at the dark count rate of 1.1 Hz/cm2 .

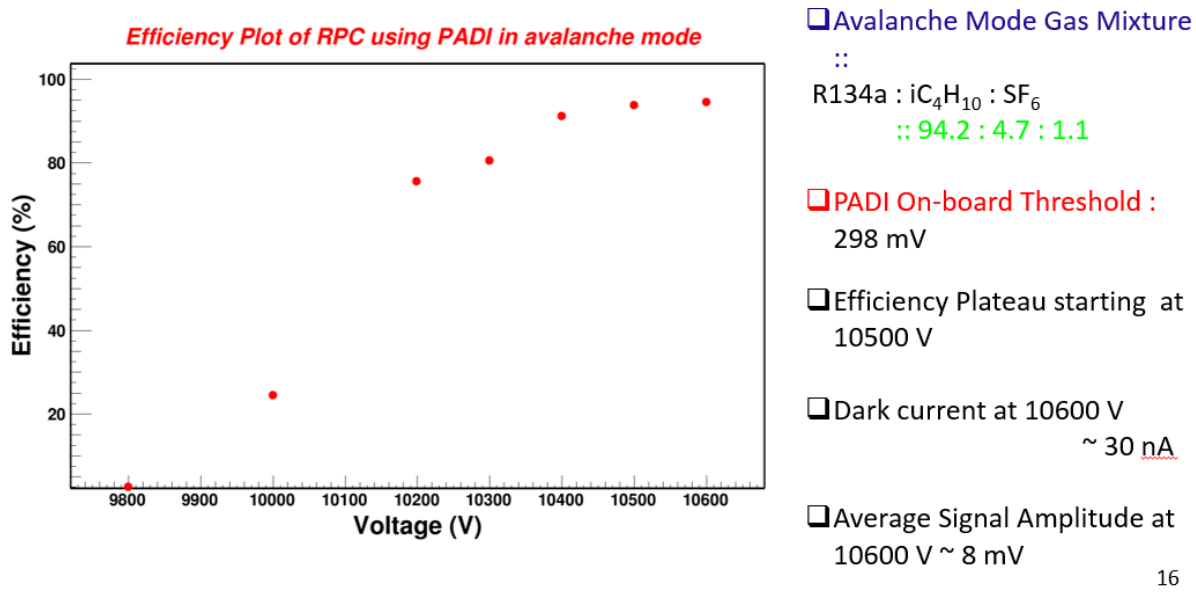

Figure 4.43 Efficiency vs Voltage plot of RPC-2 using PADI-ASIC FEE

4.3.1.3 NOISE RATE vs VOLTAGE

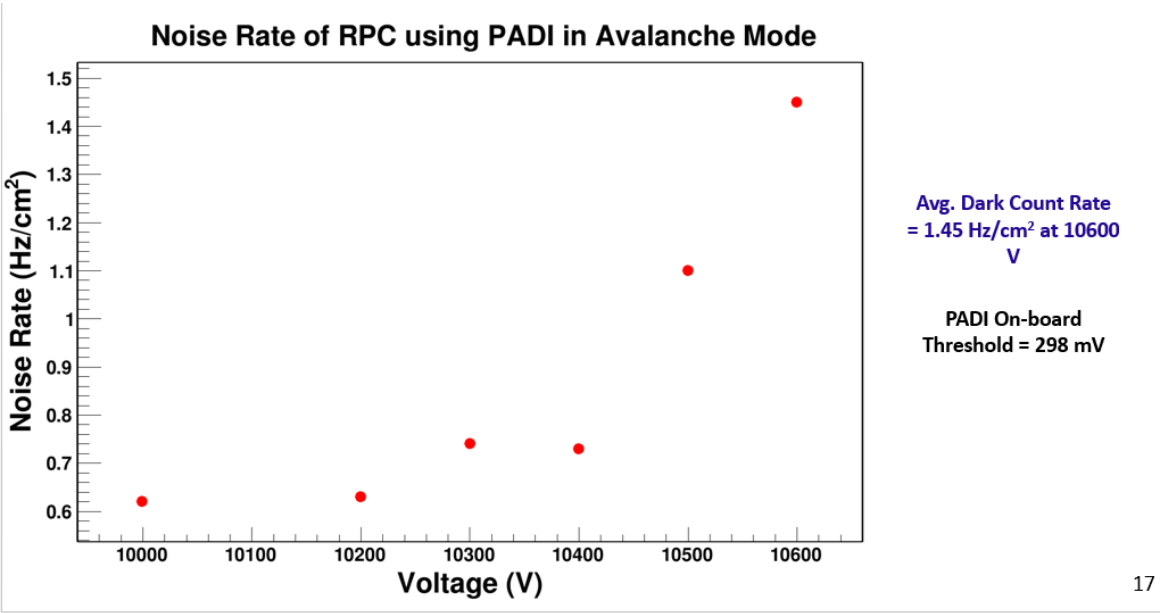

Figure 4.4 Noise rate vs Voltage plot of RPC-2 using PADI-ASIC FEE

The noise rate is within acceptable limit. It is evident from the fig4.44. Further study and optimization of detector parameters are required..

4.3.2 TESTING OF RPC-2 USING NINO-ASIC BASED FRONT END ELECTRONICS

CERN has created a front-end amplifier cum discriminator which consumes low power ASIC chip. This chip can be applied for electron and proton detection in the domain of medical imaging or tomography. This chip is named as NINO ASIC. It is also useful for CMS and ALICE experiment.

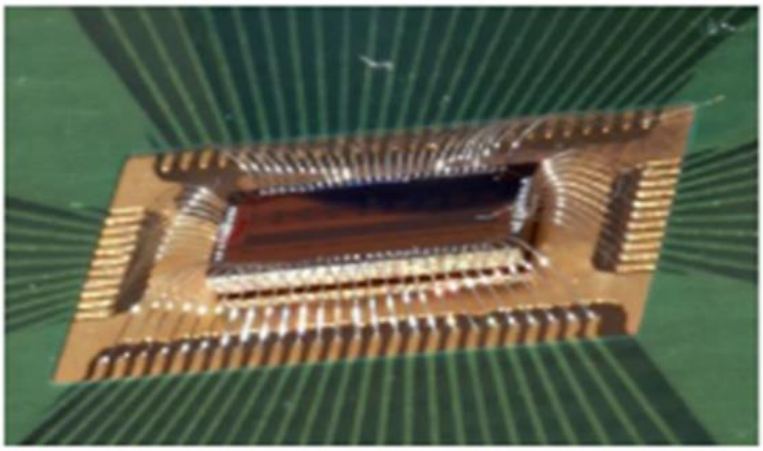

Fig 4.45 NINO- application specific integrated circuit chip

4.3.2.1 NINO-ASIC front end electronics

The NINO ASIC characteristics are : differential i/p, LVDS (low voltage differential signal) o/p, it is optimized to operate with 30pF i/p capacitance. The width of the NINO ASIC output pulse is dependent on the charge of i/p signal. It works as fast amplifier to curb the time jitter to its minimum. The discriminator threshold can be adjusted within the range of 10-100fC. NINO ASIC was first developed by CERN for ALICE-TOF. The FEE board accepts both polarity signal.

The voltage in which NINO ASIC is operated is ± 4 V. There are some integrated circuits present on the board which actually convert all the single polarity signals into differential input signals . The number of input channels is 8 in this board, i.e. J1 to J8. At first a front-end electronic board consisting NINO-ASIC as a component was used to test the RPC 2 . The detector was selected randomly.

The testing was done using cosmic muons. NINO-ASIC has 8-channels. It is in short a amplifier cum discriminator chip. . CMOS of 0.25 µm was required in fabrication of the ASIC. Nino has an attractive feature that is its low power requirement . It is calculated that only 40 mW/channel power is required.

Using a short transmission line , here a short LEMO cable the signal from the RPC was connected to the NINO ASIC input pin. The input impedance was a required criteria to be matched and open loop current to voltage conversion was used, with no feed back. The input current pulse was supplied to the NMOS(M1) transistor's source and then signal from drain of M1 is supplied to NMOS(M2) transistor's source. The emerging current pulse from drain of the later NMOS or M2 has a much larger impedance compared to input. The current is used up by charging capacitor on its drain. The signal rise time is dependent on the transistor's characteristics and the fall time depends upon the time that is required to recharge the capacitor C. The structural geometry and biasing of NMOS(M1) transistor is considered in such manner that the impedance becomes low and which can match the impedance attached to the transmission line of the input. C, a parasitic capacitance which determines the output voltage. The transistor M2 is designed in such a way that this capacitance is minimum.

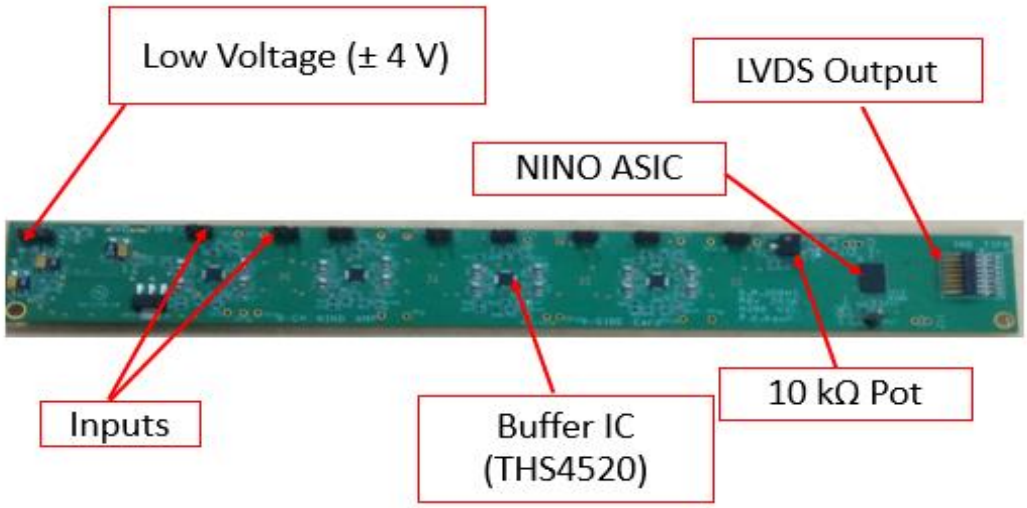

Figure 4.46 NINO-ASIC based front end electronics board

From the schematic of NINO it is clearly seen there are four stages after the input consisting low gain & high bandwidth differential amplifier. To keep the input stages properly biased, a slow feedback circuit provides current. This point has another role to play, which is by adding an offset here, threshold adjustment is done. To stretch the pulse within 2ns to 7ns a stretcher is present before LVDS o/p diver. HPTDC is used for measuring leading & trailing edges of i/p pulse having width greater than 6ns. The pulse stretcher can increase the width of the input . pulse by 10 ns. The measured bulk resistivity of the bakelite sample is ~ $9x10^{11}\Omega$cm. & surface resistivity is ~ 3 x 10^{12} Ω/cm. The RPC 2 was tested in standard cosmic ray set up, the schematic diagram of which is given below. It was operated in avalanche mode. The gas mixture used is R134a : iC_4H_{10}:SF_6 :: 94.2 : 4.7:1.1.

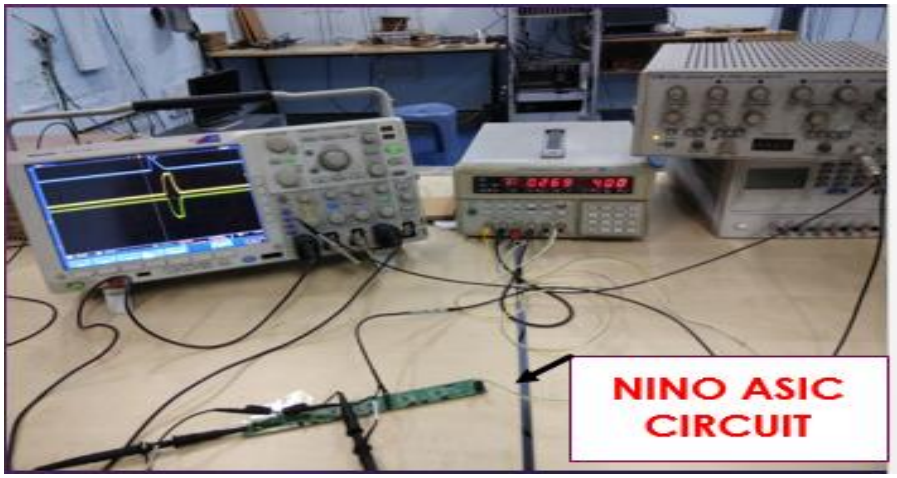

Figure 4.47 Experimental arrangement using NINO-ASIC FEE

Copper pick up panels having copper strips of dimension 30cm x 2.3cm is used to readout the signal. The laboratory temperature and humidity during the experiment was kept at 23 degree Celsius and 45%-55% respectively. The master triggering was done by 3 paddle scintillators & 1 finger scintillator of dimension 7cm x 1.5cm.

From the detector readout strip a negative signal, coming from the anode is used as the input of the FEE board. As other electronics module like scalar counter requires NIM pulses as input, the LVDS output given by the NINO ASIC based FEE board is converted into NIM signal. This required two converters. The LVDS signal is first converted into ECL signal by a converter and then the ECL signal is converted into NIM signal by a second converter. The NIM signal from the second converter is then feed into the other electronic modules.

4.3.2.2 EFFICIENCY vs VOLTAGE PLOT

The NIM logic pulse of RPC has been put in coincidence with the combination of scintillators signal and it formed the coincidence trigger. Ratio of coincidence trigger rates to master trigger rates gives us the efficiency of RPC and the threshold has been kept at around 2 mV. Plots below shows the variation of the efficiency with the applied voltage. The efficiency plateau has been observed at 10.6kV-11.4kV for different detectors.

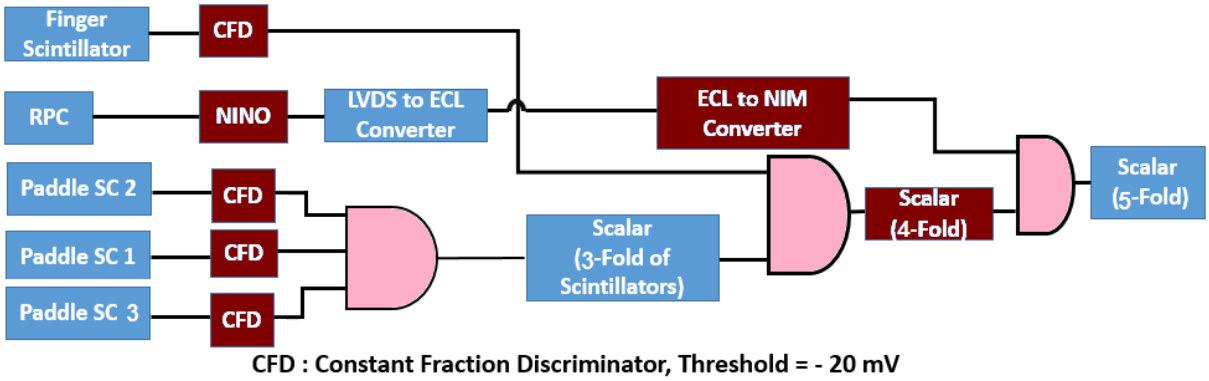

Figure 4.48 Block diagram of NINO-ASIC based FEE used for efficiency and noise rate measurement for RPCs

Test results of RPCs using NINO ASIC have been discussed.

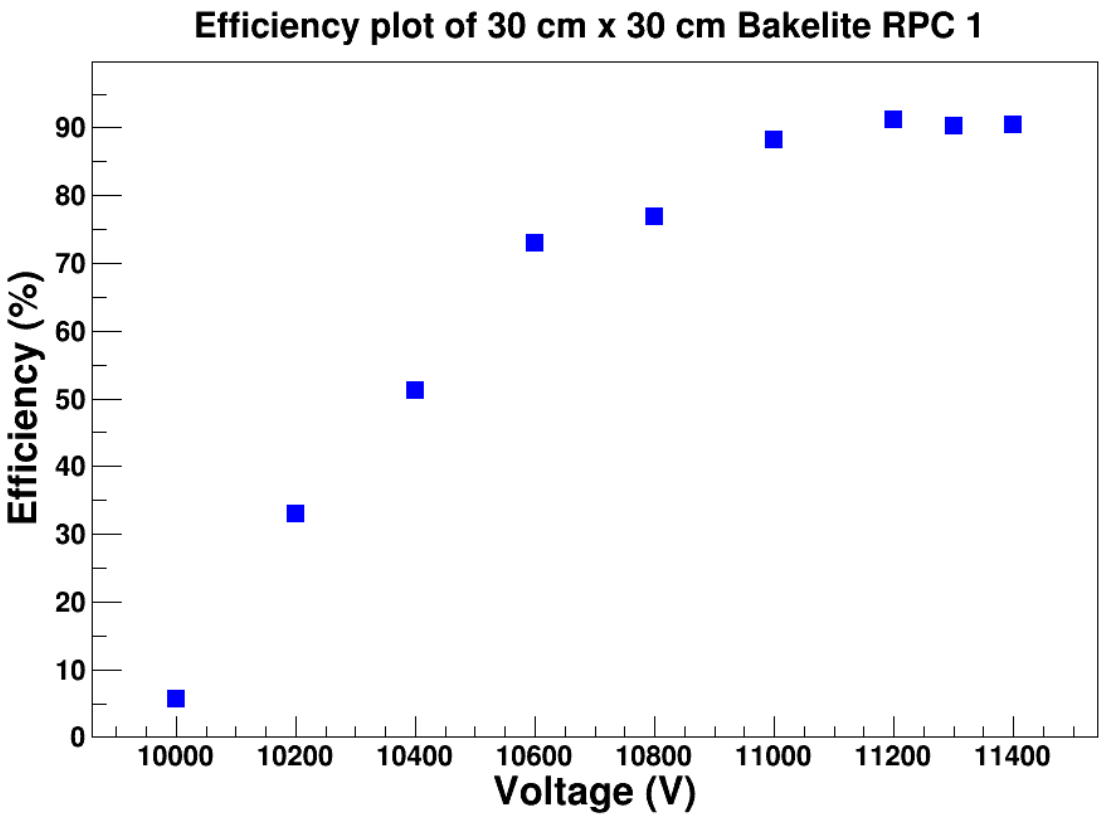

Figure 4.49 Efficiency vs Voltage plot of RPC-1

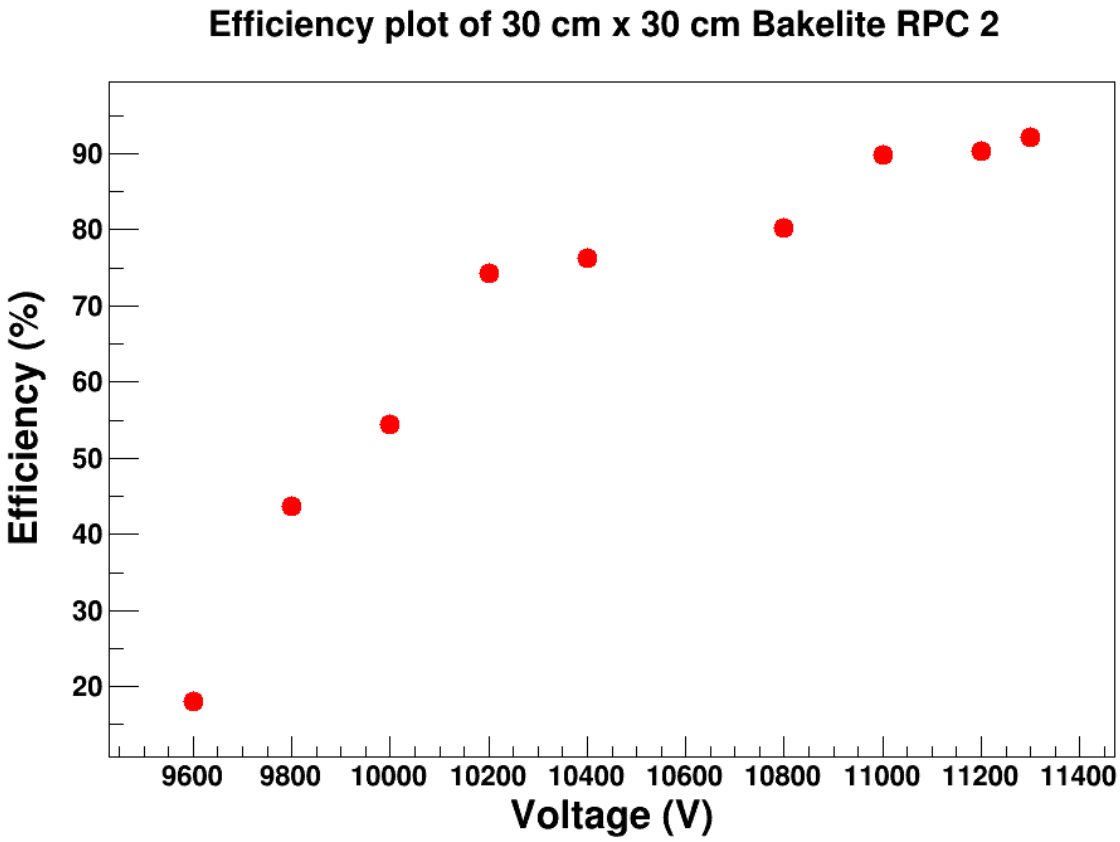

Figure 4.50 Efficiency vs Voltage plot of RPC-2

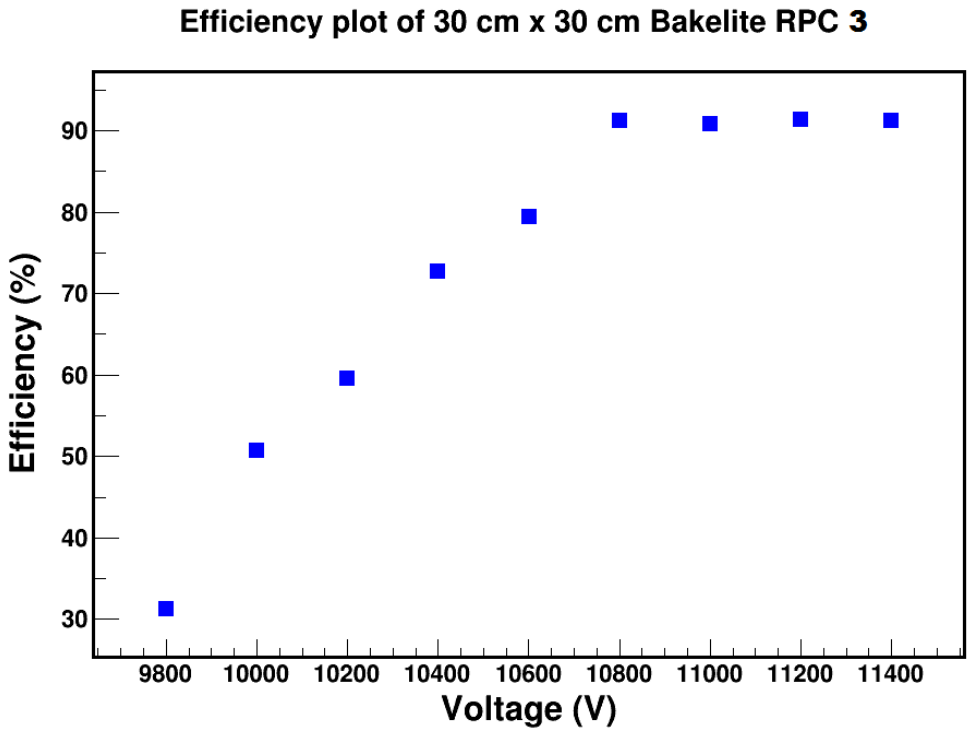

Figure 4.51 Efficiency vs Voltage plot of RPC-3

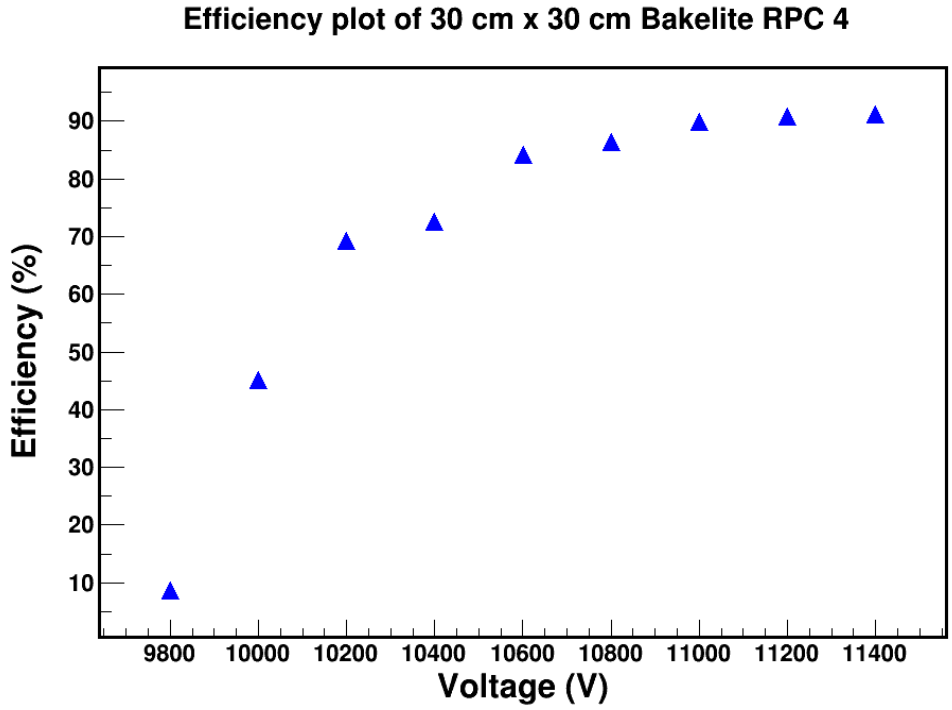

Figure 4.52 Efficiency vs Voltage plot of RPC-4

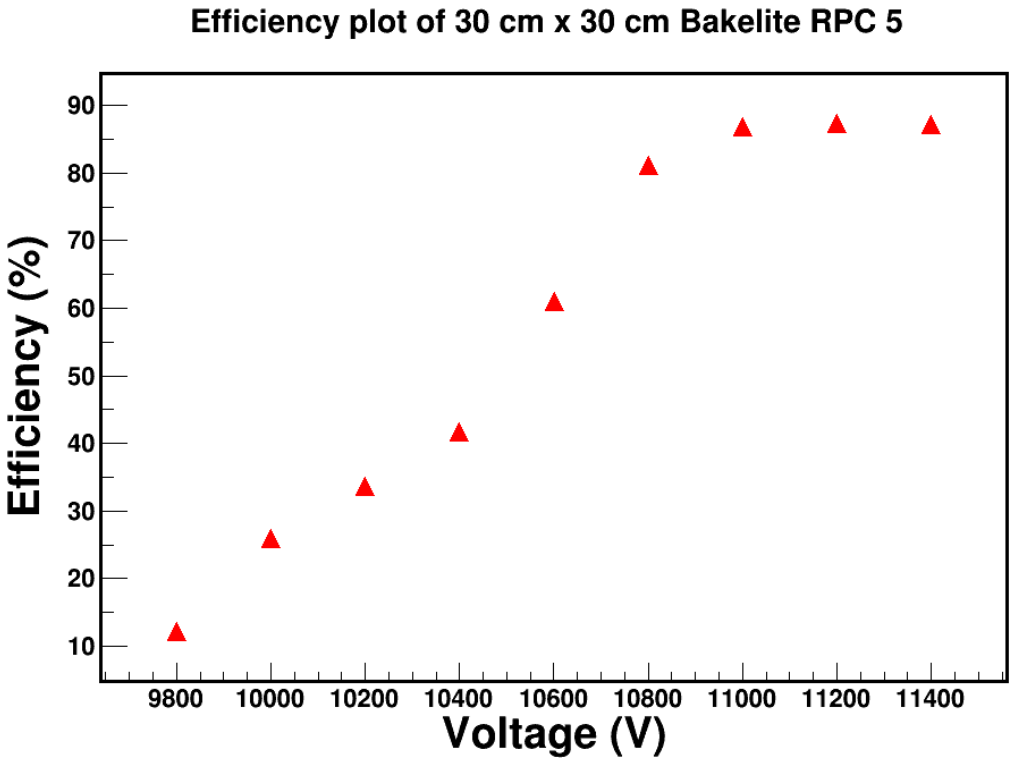

Figure 4.53 Efficiency vs Voltage plot of RPC-5

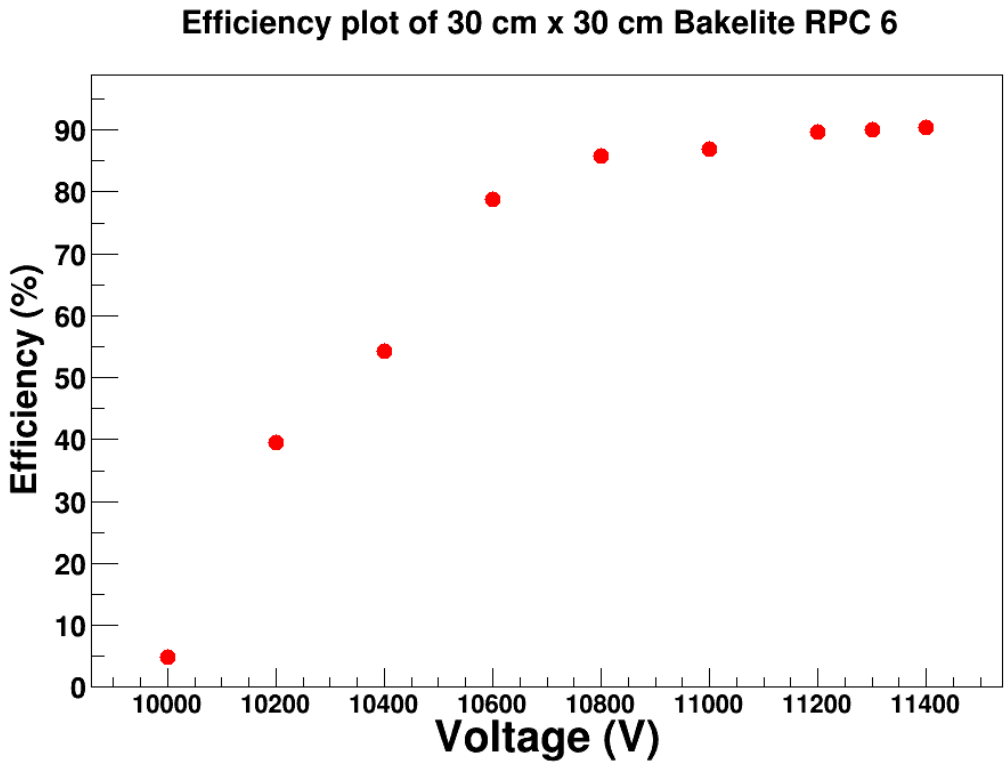

Figure 4.54 Efficiency vs Voltage plot of RPC-6

The RPCs shown good results while testing with the NINO FEE board. They have shown around 91-93% efficiency in detecting cosmic muons .

4.3.2.3 NOISE RATE vs VOLTAGE PLOT

The noise rate vs voltage was plotted for RPC-2 . This was done to compare the test results with PADI-ASIC. From fig. 4.44 it can be seen that the noise rate is around 1.44 Hz/cm^2 around 10.6kV. But while testing with NINO-ASIC FEE (fig.4.55) the noise rate is found to be near 0.7 Hz/cm^2

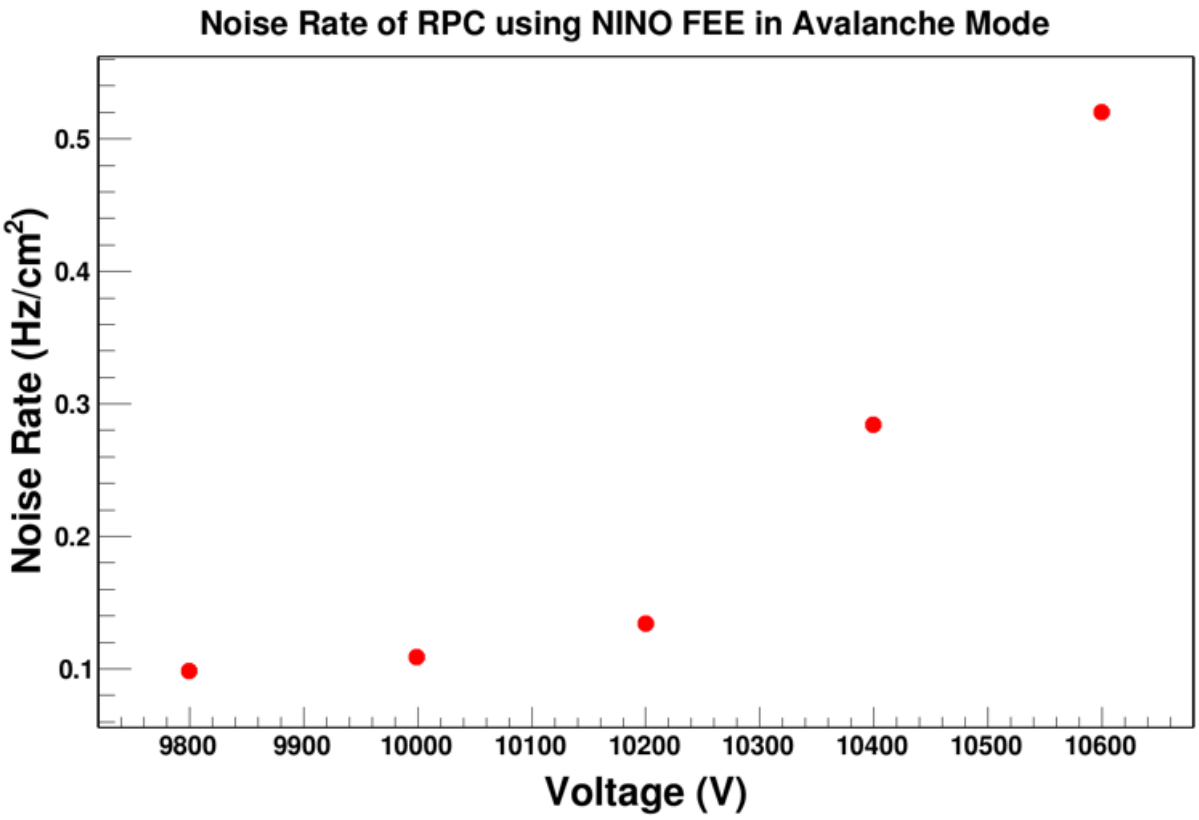

Figure 4.55 Noise rate vs Voltage plot of RPC-2

CHAPTER 5

DATA ACQUISITION SYTEM SETUP FOR RPC BASED MUON TOMOGRAPHY SYSTEM

5.1 PRINCIPLE OF COSMIC RAY MUON TOMOGRAPHY

Muons which have energy from 1GeV to 1000GeV interacts through matter in 2 ways. They cause ionization by losing energy to the electrons bound to the material atoms. In the second process muons interact with the nucleus of the atoms . It causes deflection in the track of the muons. This process of getting deflected multiple times is called multiple coulomb scattering. The energy loss mechanism of the muon is shown in the figure below.

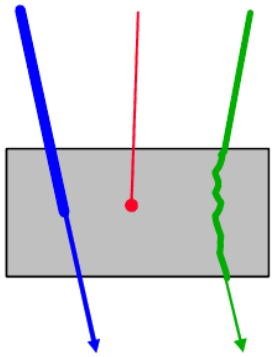

Muon interactions when passing through matter. Muons lose energy through ionization (left). If enough energy is lost, muons will stop (center). Muons are also deflected via multiple Coulomb scattering (right). These interactions are shown separately for clarity, although all three are applicable to any particle.

Figure 5.1 Interaction of muon while passing through matter

5.1.1 MULTIPLE COULOMB SCATTERING

In general it is seen that 2.2 GeV energy per g/cm^2 is lost by the 3Gev muons when they travel through matter. Muons can penetrate 10-100 meters of dense materials depending on

their energy. The cosmic ray muon's energy spectrum is found to be continuous & average of range is long. Hence for large objects differential attenuation is used to radiograph. But application of this technique is not suitable for small object muon tomography. Hence multiple coulomb scattering becomes important. The interaction of nucleus with an incoming charged particle deflects the original path of the particle. The particle comes out from the material at an different scattered angle.

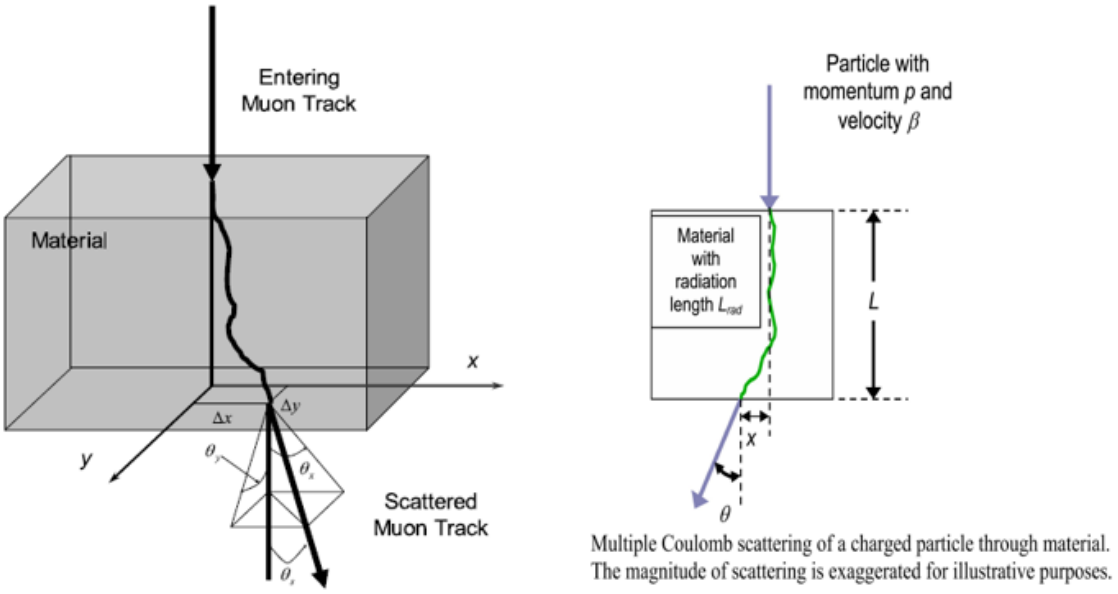

Figure 5.2 Multiple coulomb scattering of muon while passing through matter

The distribution of this scattered angle is found to be Gaussian .

$$f_{\theta_x}(\theta_x) \cong \frac{1}{\sqrt{2\pi}\sigma_\theta} \exp\left(-\frac{\theta_x^2}{2\sigma_\theta{}^2}\right) \tag{5.1}$$

And the standard deviation of this distribution is proportional to the square root of the ratio of depth of the material and radiation length. The standard deviation is given by

$$\sigma_\theta \cong \frac{15}{p}\sqrt{\frac{L}{L_{rad}}} \qquad (5.2)$$

Where, p = momentum of the particle.

L= depth of the material

L_{rad} = radiation depth of the material

5.2 BAKELITE RPC BASED MUON TOMOGRAPHY SYSTEM

A mechanical setup was created in VECC workshop to hold the detector in position for muon tomography. CAEN high voltage module is used to supply high voltage to the detetors. Three RPCs are kept above the target volume and three RPCs are kept below (fig.5.3). In this manner individual muon tracks before and after scattering can be detected.

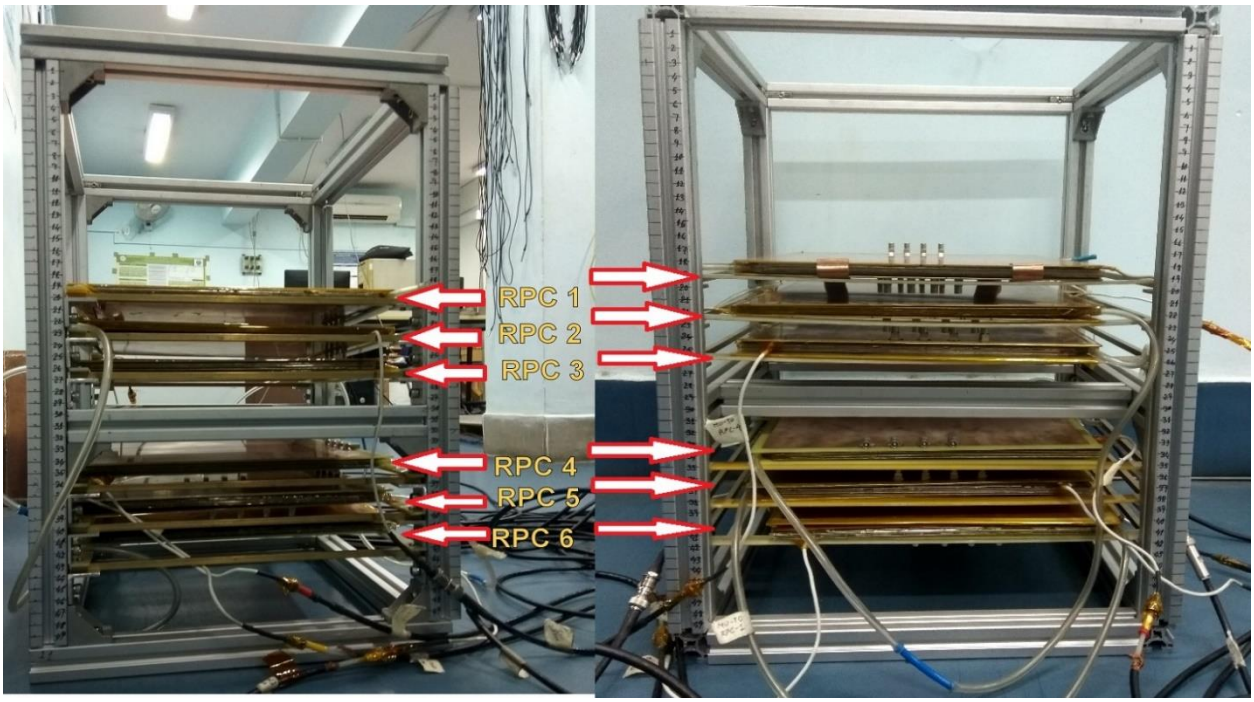

Figure 5.3 Bakelite resistive plate chamber based muon tomography system constructed at VECC, Kolkata

All of the six detectors measure the position of the muons in X coordinate and Y coordinate . The first three RPCs which are kept above measures the original track of the muons before they undergo deflection while passing through the test volume. The three detectors which are kept at bottom are kept there to determine the scattered track of the muons. As muons get more scattered while passing through high density material it is expected that scattering will be spotted if the test volume is filled with high Z material. Some of the incoming muons may not emerge from the test volume if they loss all of their energy. The detectors are expected to scatter the muons in a negligible amount. As their thickness is less and they are fabricated with low Z materials.

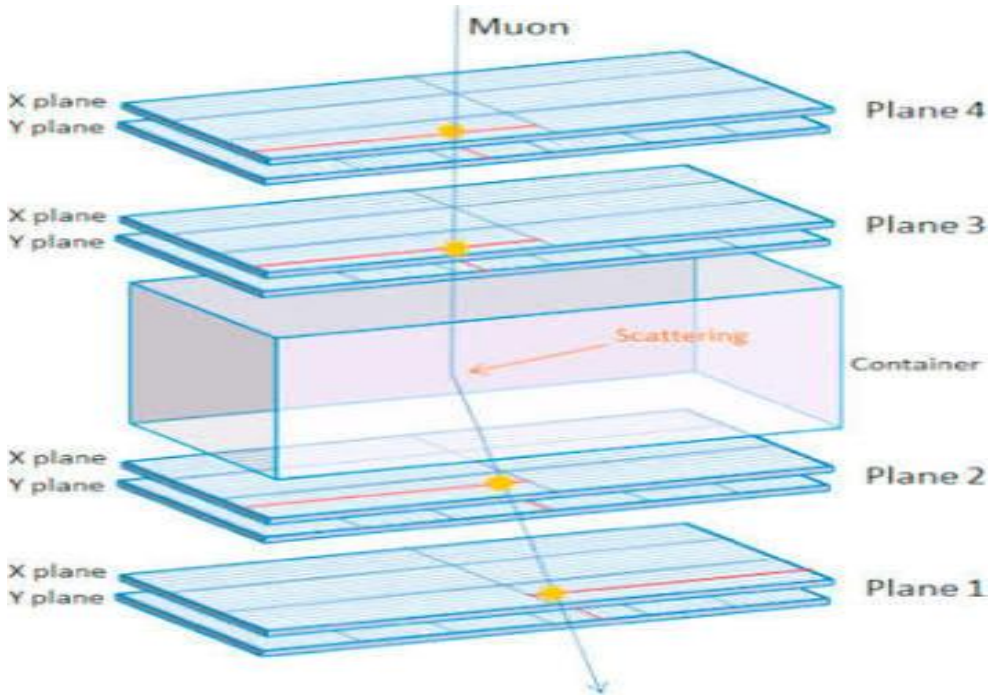

Figure 5.4 Schematic diagram of muon tomography principle and positioning of detectors

After calculating the scattering angle of each detected muon tracks an complete data set will be created . Reconstruction algorithms used in tomography is required in reconstructing the object placed in test volume. It is done by the data set from the detectors. Hence an data acquisition system which is compatible with bakelite RPCs is needed. For this data acquisition

purpose we have used MUCH-XYTER ASIC based system. The details of which is given in the following section.

5.3 DATA ACQUISITION USING MUCH-XYTER CHIP BASED ELECTRONICS

The MUCH-XYTER chip is dedicated for signal detection arising from the GEM based MUCH detector in the CBM environment. Some of the features provided by MUCH-XYTER chips are:

It has 128 analog front end channels for processing the charge pulses from the GEM detector. It also provides two test channels for testing the functionalities of the ASIC using test pulse. It is based on 180 nm CMOS process and uses radhard layout architecture. Power dissipation per channel is less than 10 mW. It can accept both polarity pulses Digital back-end with data transmission rate 320 Mbps.

5.4 MUCH-XYTER ASIC ARCHITECTURE

Like most of the other front-end ASICs used in HEP experiment internal architecture of MUCH-XYTER ASIC is divided into two parts: analog front end and digital back-end as shown.

Each of the channel in the analog front-end consists of charge sensitive amplifier (CSA), shaping circuit, high speed discriminator, peak detector, flash ADC and latch circuit. In the digital back- end there is a sequencer that will read each of the front end channel sequentially after digitization. Details architecture of the analog front-end

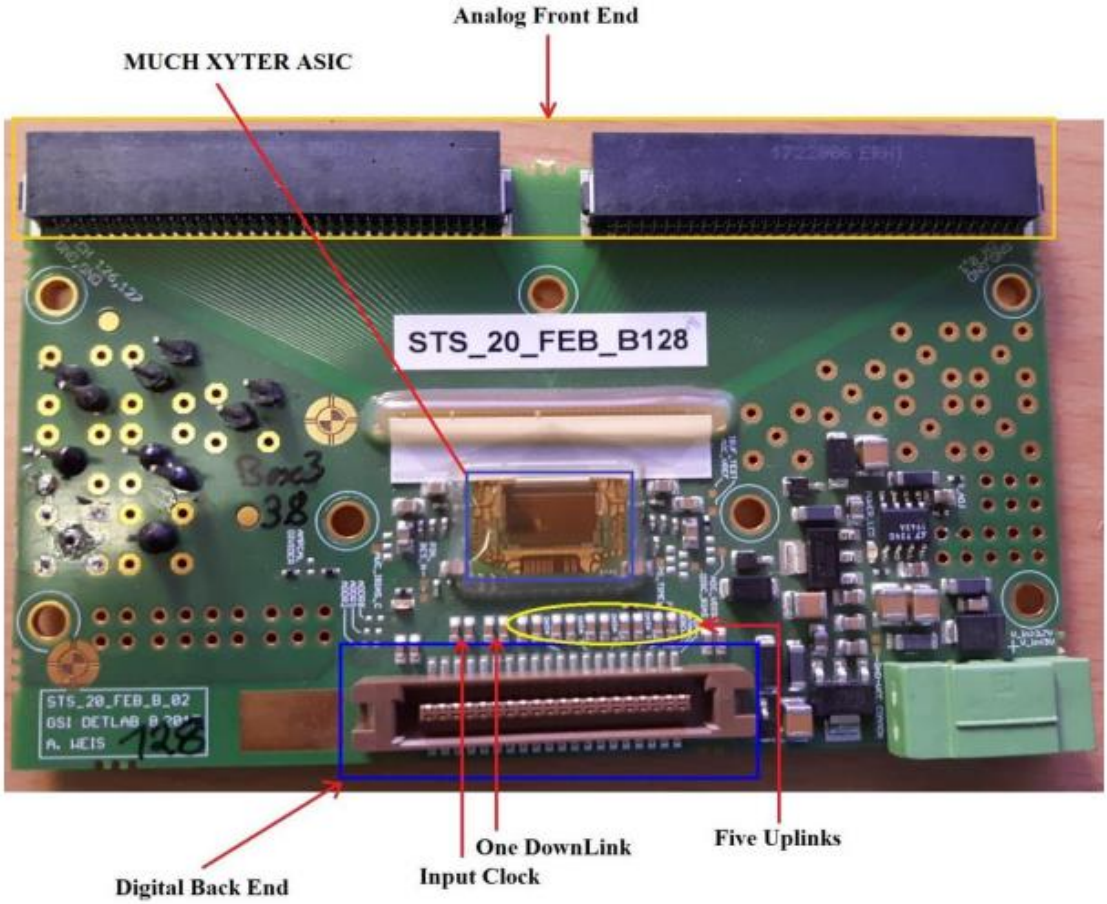

Fig 5.5 Top view of FEB containing MUCH-XYTER ASIC

All the channels in the analog front-end has charge sensitive amplifier , shaping circuit, high speed discriminator, peak detector, flash ADC and latch circuit. In digital back- end there is a sequencer that will read each of the front end channel sequentially after digitization. Details architecture regarding analog front-end channel is shown below. CSA in front of each channel receives the charge pulses directly from GEM detector for further processing. CSA circuit contains one operational amplifier with one resistance (RF), three capacitances (CF1, CF2, CF3) and reset circuit in feedback.

CSA is used for matching output impedance of detector & input impedance of FEB and it provides small gain to input pulses. By connecting or disconnecting the switches attached with

each feedback capacitor, gain of CSA can be varied. Output charge from the detector is integrated by feedback resistance and capacitance and gives voltage waveform at the output of CSA. Then output of CSA is fed into a polarity selection circuit (PSC) that helps to work MUCH-XYTER with pulses of both polarity. Output signal of PSC is divided into fast & slow path .Fast path comprising of fast shaper, fast comparator and time stamp latch circuit and responsible to provide timing information of the detected particle.

Slow path comprising of slow shaper, flash ADC and digital peak detector and provides energy of the detected particles. The CR-RC shaper in the fast path has shaping time of around 30 nanoseconds. Slow shaper is based on CR-(RC)2 filter architecture and has shaping time of around 80 nanosecond. As the slow shaper is responsible to provide energy information of the detected particles noise level should be low in this path. First comparator has three stages of processing the signal. In the first stage, it contributes further amplification useful for output signal of the fast shaper and converts it into differential signal. The second stage contains dynamic comparator with regenerative feedback. The third stage converts discriminator output signal into logic signal. Each channel has twelve-bit time-stamp generator that gives the timing information of the particles which are detected.

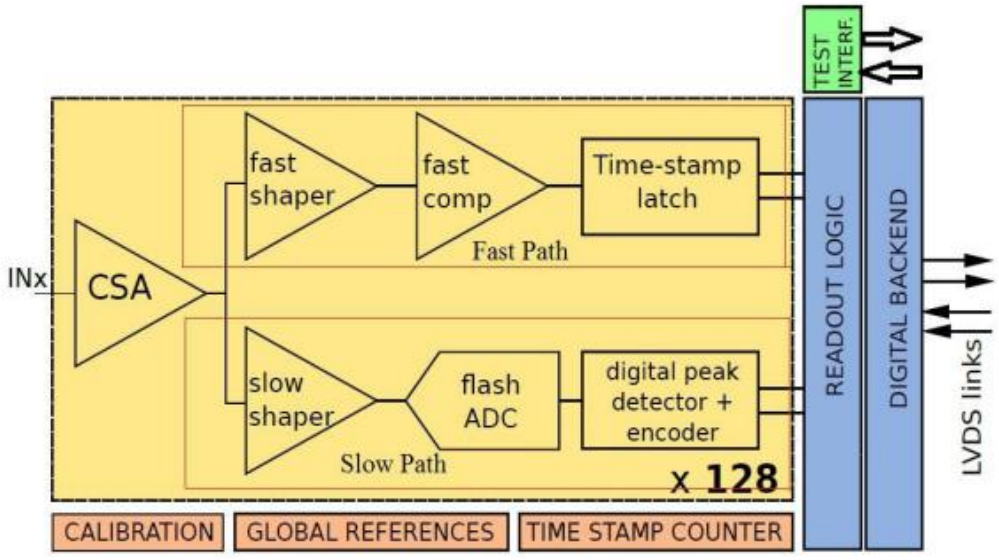

Figure 5.6 Internal architecture of each channel of MUCH-XYTER

Flash ADC based peak detector which is connected with slow shaper using AC coupling in each of the 128 channel consists of thirty one comparators and thirty two resistors. It provides information regarding energy of the detected charge particles. Details of the time stamp generation mechanism and function of the peak detector can be seen from [17]. MUCH-XYTER used here is a self-triggered ASIC, i.e. no trigger information will be transmitted from the back-end computing node to the front-end ASIC and it will accept the charge from the detector when the voltage level corresponding to the detected charge is above a threshold. MUCH is to detect muon particles (μ+ and μ -). In CBM experiment they will be generated from the J/ψ particles which are very rare in the density of other produced subatomic particles. Hence for the cosmic ray muons it can also be used.

5.5 Data Processing Board

AMC FMC carrier Kintex (AFCK) board shown in Figure 5.7 is used as a prototype development of DPB. AFCK board contains [12] Xilinx Kintex-7 325T FFG900 FPGA, Module Management Controller (LPC1764FBD100), 2 GB DDR3 SDRAM with 32-bit interface, 16020 kb BRAMs for high speed parallel access, SPI Flash, electrically erasable programmable read only memory (EEP- ROM) with unique MAC ID, mini USB UART and two high pin count (HPC) slots where each slots can handle maximum four GTx. Clock distribution circuit within the AFCK is compatible with the White Rabbit protocol (WR) [13] using CDCM61004RHBT and Si57x chip and jitter cleaner available in it helps to reuse the recovered clock from receiver as the reference clock of transmitter.

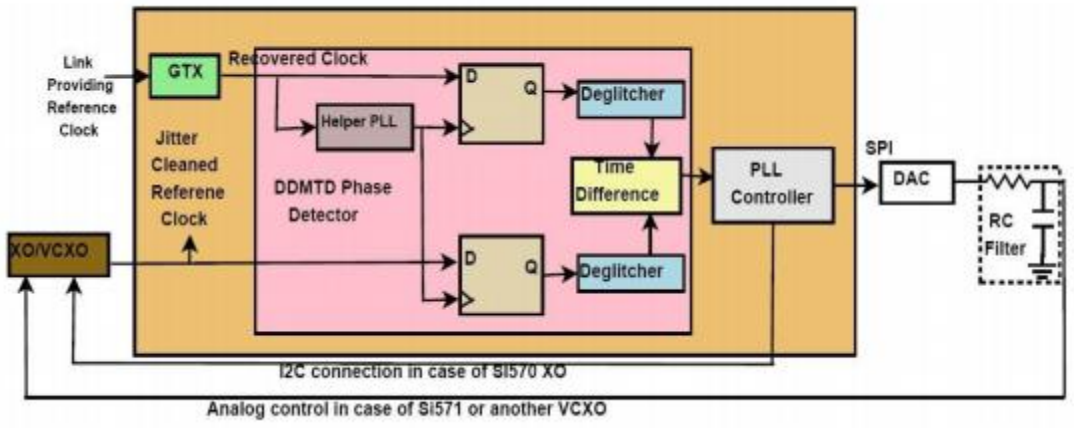

Fig 5.7 Clock Recovery and Jitter Cleaning Circuit of AFCK

Different clock domains are available within the AFCK board like120 MHz or 40 MHz for GBT FPGA interface, 125 MHz for 1 Gbps Ethernet used in WR core and 156.25 MHz for 10 Gbps Ethernet. Though AFCK board is developed to work with MTCA it can work in stand-alone mode also using 12V power supply, JTAG programmer, Ethernet and optical interface.

Data processing board acronymed as DPB is an intermediate layer between GBTx and FLIB and are placed in the moderate radiation zone. Hence, it uses COTS FPGA and perform the following activities:

1. It receives data from GBTx using long distance optical link having the data rate of 4.8 Gbps. The received data is aggregated, preprocessed and sent to the FLIB using very high speed optical link.
2. Timing & fast control (TFC) module in DPB provides reference clock for the whole read out chain and helps in the transmission of synchronous commands to the FEE. These are very helpful for synchronization between FEE and GBTx and implementation of flow control in the readout chain.

Fig 5.8 Top View of AFCK Board used as DPB

3. Control system attached with the DPB helps to conjure die rent registers that helps in controlling the analog front-end and digital back-end of FEBs.

The control system is attached with the DPB using some standard solutions like Ethernet with Transmission Control Protocol (TCP) or User Datagram Protocol (UDP).

To inject the charge to the 128 analog channels of the FEE Board, two charge injector boards has been made using copper pads. In this board, an ERNI 64 pin connector, 64 capacitors (1 pF), a Lemo connector and a 50 ohm termination resistor has been used.

Different amount of voltages are injected to the analog channels of the FEE Board using Lemo cables from the external pulse generator for calibrating the ADC comparators. For each

comparator of the Flash ADC of all 128 analog channels, a different linearly increasing amount of charge is being injected for calibration.

As mentioned there are some specifications for calibrating the 32 bit Flash ADC comparators and we have certain methods to check whether the comparators are properly calibrated or not.
1. Provided input voltage from the external pulse generator to the each capacitor to convert them into charge pulses and then injected the charge to each and every input analog channel of the FEE Board.

2. Two 1:10 attenuators are used which divides the input voltage by 10 since the capacitors are of 1 pF each to provide input pulses to the input analog channels.

Different amount of input voltage has been provided externally to check the corresponding calibrated comparators are firing or not for that particular input voltage & it will be then converted into charge using external capacitors.

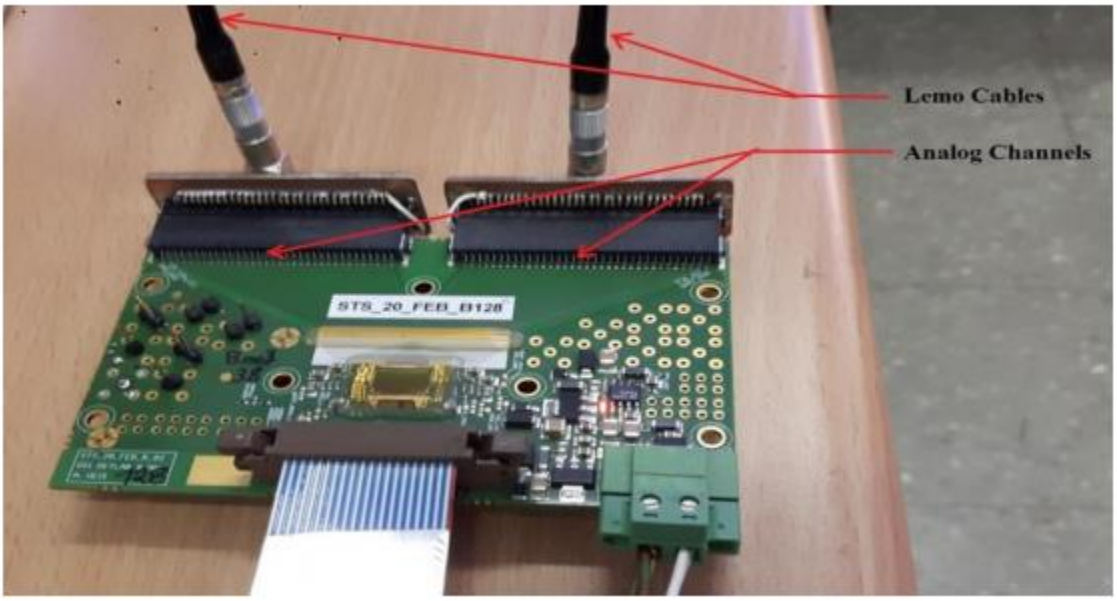

Figure 5.9 Charge injection from detector to the FEE Board using Lemo cables

5.3 PRILIMINARY DATA PLOTS

Four detector outputs were fed in the set up input. Input signal was taken from a pickup panel strip. The dimension of the strips were 30 cm x 2.3 cm. Different plots are shown below.

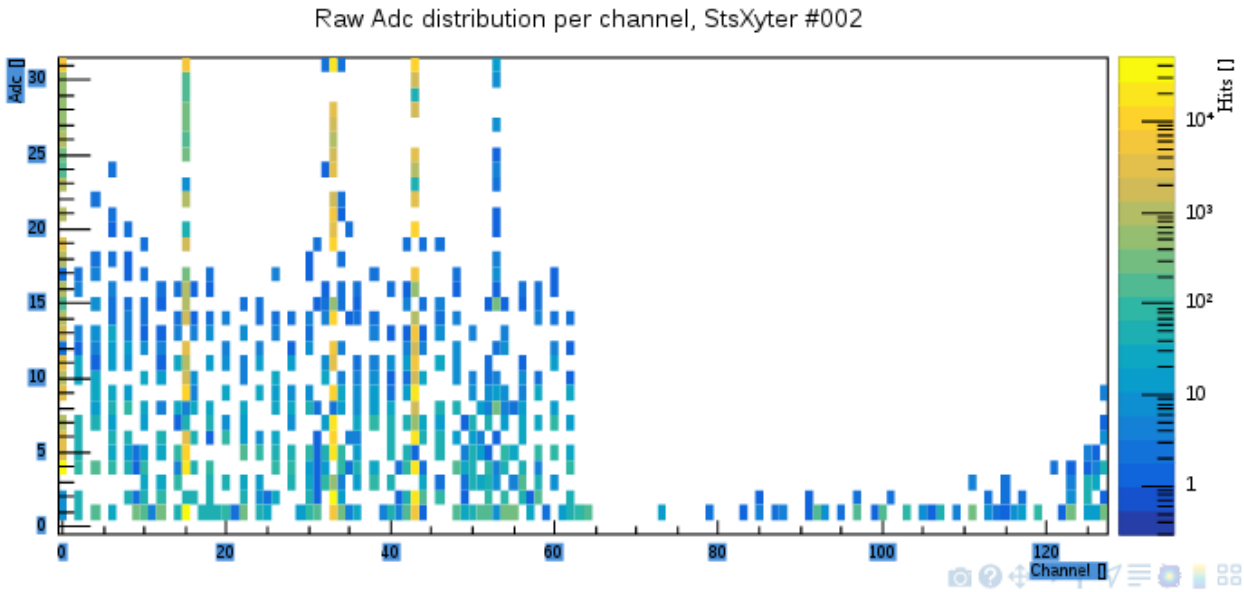

Figure 5.10 Raw Adc distribution per channel

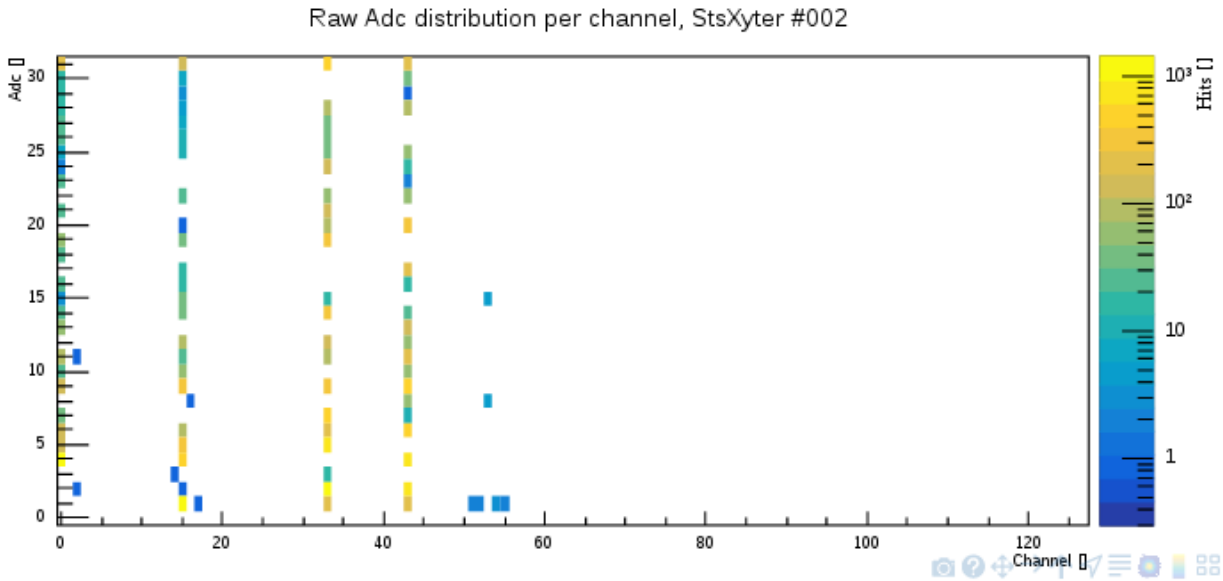

Figure 5.11 Raw time Adc distribution per channel using four channels only

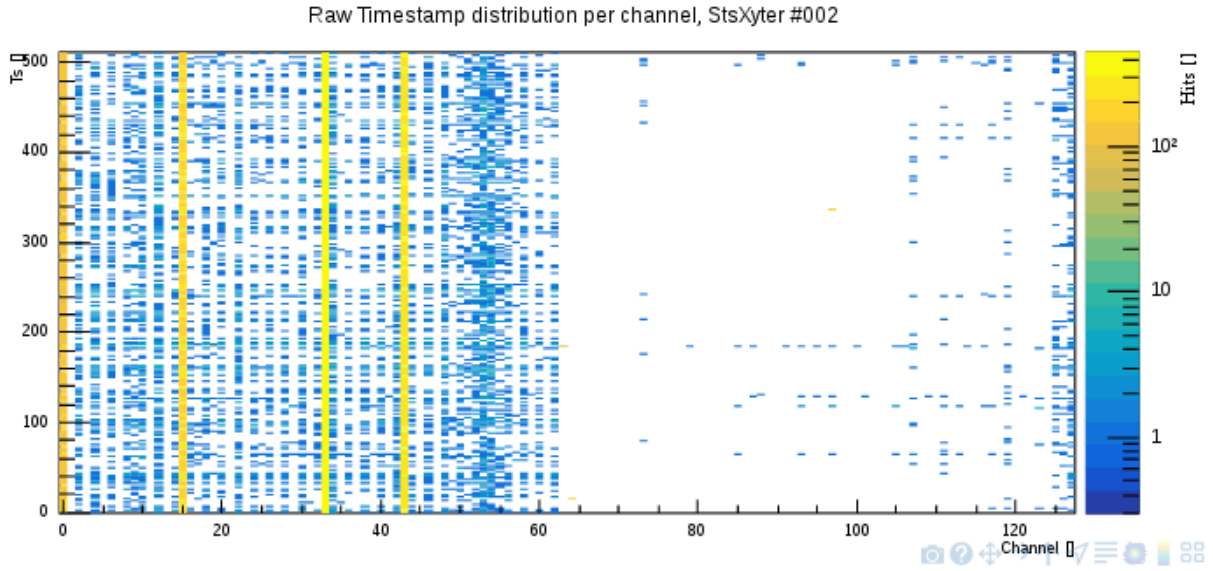

Figure 5.12 Raw timestamp distribution per channel

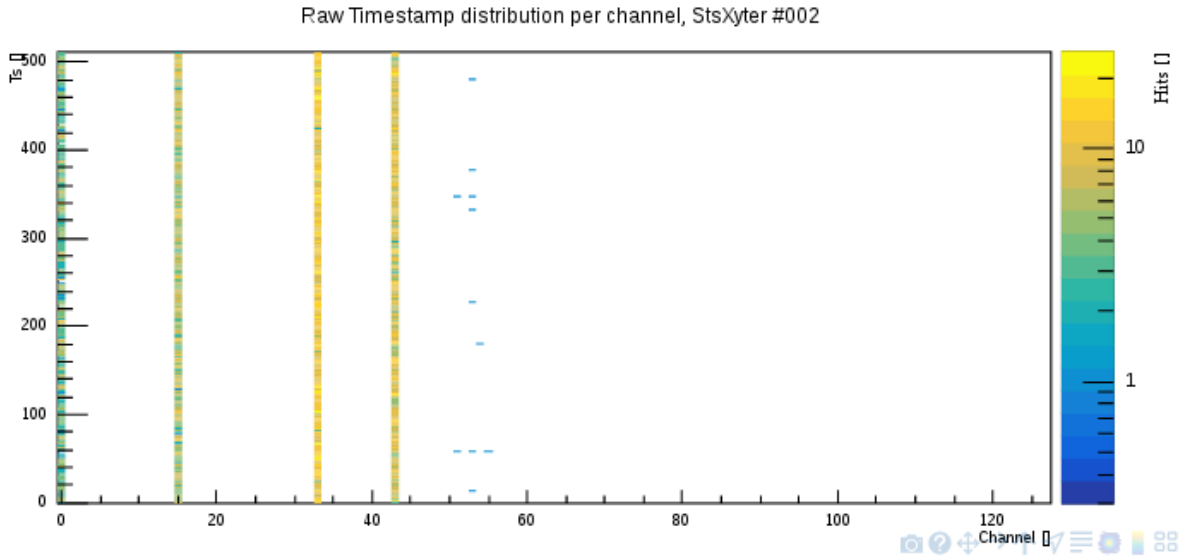

Figure 5.13 Raw time stamp distribution per channel using four channels only

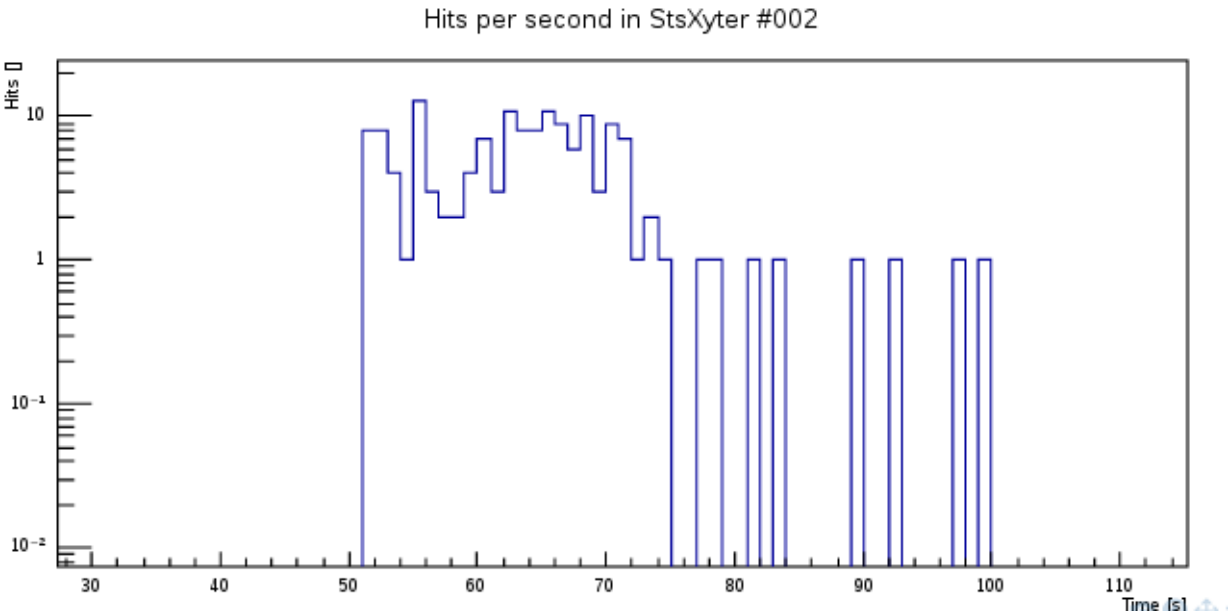

Figure 5.14 Hits per second in sts-XYTER

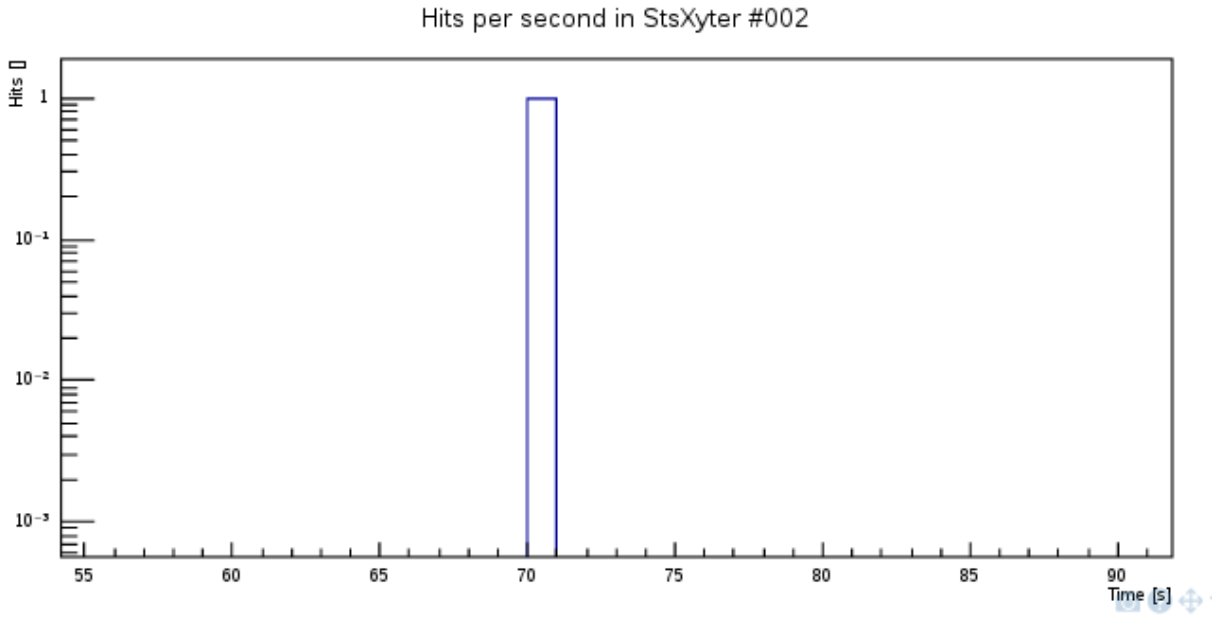

Figure 5.15 Hits per second in sts-XYTER using four channels

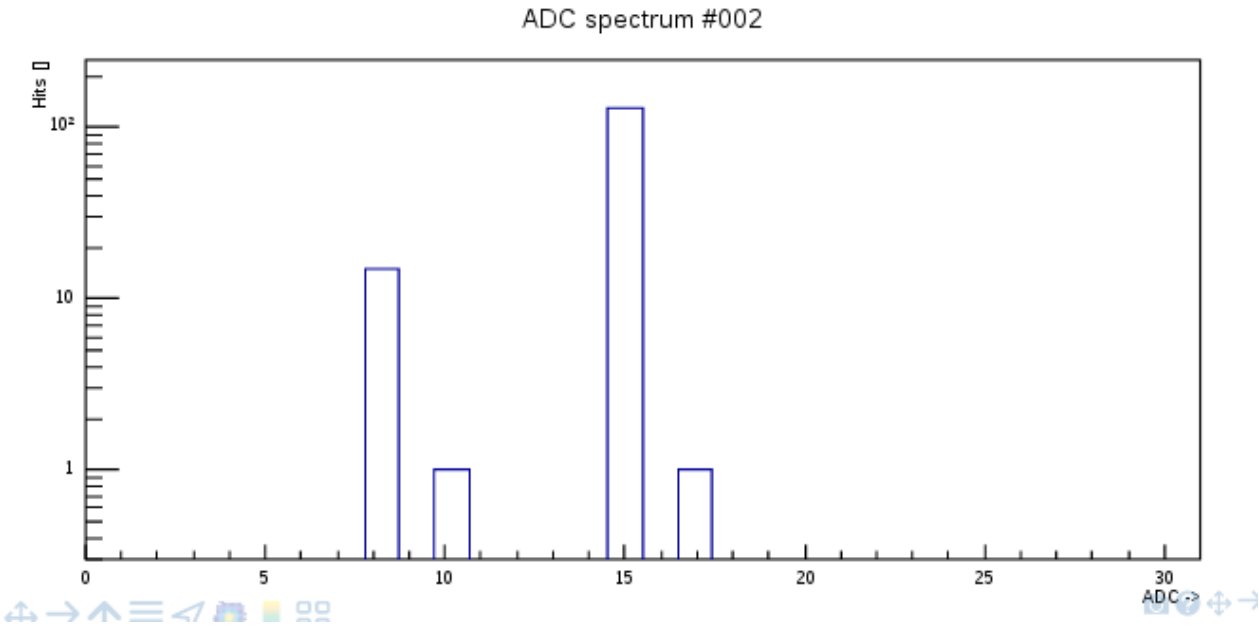

Figure 5.16 ADC spectrum

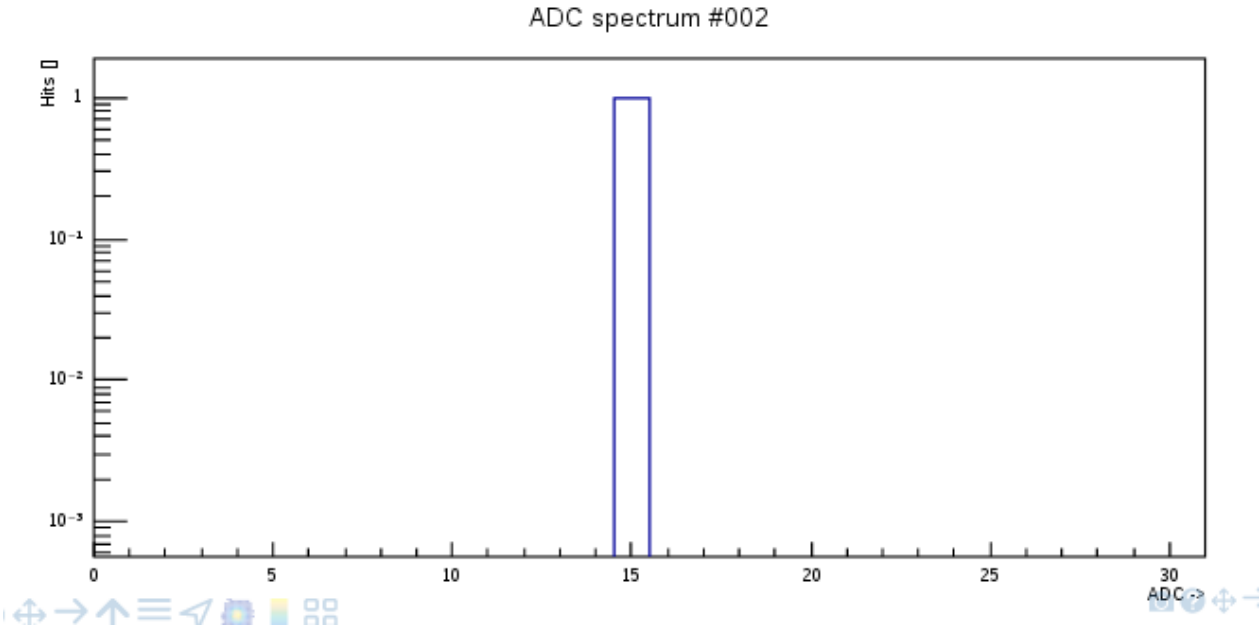

A difference in all channel data and using four channel only can be seen. Further analysis is on progress to implement the data acquisition system and reconstruction algorithm.

CHAPTER 6

CONCLUSION AND FUTURE OUTLOOK

Resistive Plate Chambers (MRPCs) are widely used gaseous detectors in experimental high energy physics and are well known for excellent time and spatial resolution. In addition to their application in HEP, they can be highly beneficial in the field of muon tomography as well. It has been studied through experiment that bakelite RPCs are compatible for muon tomography. The required characteristics of detector is satisfied for muon radiography . The system for data acquisition is now ready. Bakelite RPCs can have a strong application in muon tomography. So far Gas electron multipliers , drift or multi-wire chambers are used for this purpose but bakelite RPCs are preferred over them because:

1. Good timing and spatial resolution.

2. Relatively cheap due to its minimal fabrication material cost.

3. Fabrication is easy and can be in any dimensions.

4. Possess simple read-out electronics.

5. Compatible with various front end electronics.

6. Have a very good cosmic muon detection efficiency.

We have fabricated 6 identical bakelite RPCs and tested them for muon tomography.

Future Outlook

The present other detector based muon topography provides material information .But image quality needs to be improved . Bakelite RPC is a suitable candidate having better field of view hence giving a clearer image with good spatial resolution. The electronics associated with bakelite RPCs is also simpler. MRPCs are also better suited for muon tomography as it can

be easily implemented over large areas resulting in better image resolution. The POCA based reconstruction algorithm needs to be implemented.

REFERENCES:

[1] R. Oerter. The Theory of Almost Everything: The Standard Model, the Unsung Triumph of Modern Physics. Penguin Group, 2006.

[2] D. J. Griffiths. Introduction to Elementary Particles. John Wiley & Sons, 1987.

[3] S. F. Novaes. Standard Model: An Introduction. arXiv:hep-ph 0001283, 2000.

[4] Francis Halzen and Alan D. Martin. Quarks and Leptons: An Introductory Course in Modern Particle Physics. John Wiley & Sons, 1984.

[5] Y. N. Pestov. Status and future developments of spark counters with a localized discharge. Nucl. Instrum. Meth. A, 196:45, 1982.

[6] C. Lippmann. Detector Physics of Resistive Plate Chambers. PhD thesis, CERN, 2003.

[7] W. Shockley. Currents to conductors induced by a moving point charge. Journal of Applied Physics, 9:635, 1938.

[8] S. Ramo. Currents Induced by Electron Motion. Proceedings of the IRE,27:584, 1939.

[9] H. Raether. Electron avalanches and breakdown in gases. London, Butter- worths, 1964.

[10] M. Yamaga et al. RPC systems for BELLE detector at KEKB. Nucl. Instrum. Meth. A, 456:109, 2000.

[11] S. F. Biagi. Magboltz - transport of electrons in gas mixtures. mag-boltz.web.cern.ch/magboltz/.

[12] N. Majumdar and S. Mukhopadhyay. Simulation of 3D electrostatic con-figuration in gaseous detectors. Journal of Instrumentation, 2(09):P09006,2007.

[13] N. Majumdar and S. Mukhopadhyay. neBEM - A nearly exact Boundary

Element Method. nebem.web.cern.ch/nebem/.

[14] COMSOL: a multiphysics simulation tool. www.comsol.co.in.

[15] W. Riegler. Induced signals in resistive plate chambers. Nucl. Instrum. Meth.A, 491(1):258–271, 2002.

[16] W. W. M. Allison and J. H. Cobb. Relativistic Charged Particle Identification by Energy Loss. Ann. Rev. Nucl. Part. Sci., 30:253–298, 1980.

[17] B. Friman. The CBM Physics Book. Springer,2011.

[18] T. Matsui and H. Satz. j/ψ suppression by quark-gluon plasma formation. Physics Letters B, 178(4):416_422,1986.

[19] Andrei Linde, Dmitri Linde, and Arthur Mezhlumian. From the big bang theory to the theory of a stationary universe. Phys. Rev. D, 49:1783_1826, Feb1994.

[20] Lyndon Evans and Philip Bryant. Lhc machine. Journal of Instrumentation, 3(08):S08001, 2008.

[21] S.Procureur, Muon imaging: Principles, technologies and applications, https://doi.org/10.1016/j.nima.2017.08.004

[22] S. Chattopadhyay. Technical Design Report for the CBM. CBMCollaboration, 2014. iv, 4, 5, 49

[23] Phd thesis , Rajesh Ganai

[24] Phd thesis , Abhik Jash

[25] Larry J. Schultz et. al. ,' Statistical Reconstruction for CosmicRay Muon Tomography', IEEE TRANSACTIONS ON IMAGE PROCESSING, VOL. 16, NO. 8, AUGUST 2007

[26] Zhifel Luo , 'Energy measurement and application on material discrimination in muon tomography 'DOI : 10.1109/NSSMIC.2015.7581957